Ganymede's Magnetosphere: Unraveling the Ganymede-Jupiter Interaction through Combining Multi-fluid Simulations and Observations

Carol S. Paty

A dissertation
submitted in partial fulfillment of the
requirements for the degree of

Doctor of Philosophy

University of Washington

2006

Program Authorized to Offer Degree:
Earth and Space Sciences

University of Washington
Graduate School

This is to certify that I have examined this copy of a doctoral dissertation by

Carol S. Paty

and have found that it is complete and satisfactory in all respects,
and that any and all revisions required by the final
examining committee have been made.

Chair of the Supervisory Committee:

_____
Robert Winglee

Reading Committee:

_____
Robert Winglee

_____
Robert Holzworth

_____
Ronald Merrill

Date:_____

In presenting this dissertation in partial fulfillment of the requirements for the doctoral degree at the University of Washington, I agree that the Library shall make its copies freely available for inspection. I further agree that extensive copying of the dissertation is allowable only for scholarly purposes, consistent with "fair use" as prescribed in the U.S. Copyright Law. Requests for copying or reproduction of this dissertation may be referred to ProQuest Information and Learning, 300 North Zeeb Road, Ann Arbor, MI 48106-1346, 1-800-521-0600, to whom the author has granted "the right to reproduce and sell (a) copies of the manuscript in microform and/or (b) printed copies of the manuscript made from microform."

Signature_____

Date_____

University of Washington

Abstract

Ganymede's Magnetosphere:
Unraveling the Ganymede-Jupiter Interaction through Combining Multi-fluid Simulations and Observations

Carol S. Paty

Chair of the Supervisory Committee:
Professor Robert Winglee
Department of Earth and Space Sciences

The Galilean moon Ganymede provides a unique case study in furthering our understanding of how space plasmas interact with planetary magnetospheres. Ganymede is the largest of Jupiter's moons and the only one to have its own magnetosphere, which is embedded within the large Jovian magnetosphere. In order to understand the complex interactions in this system, we have implemented a novel three-dimensional modeling technique that represents different ion sources as collisionless fluids that interact via electric and magnetic fields. The results from this multi-fluid treatment are well correlated with observations of aurora and magnetic fields, and demonstrate the important role heavy ions and their gyromotion play in governing the shape and dynamics of Ganymede's magnetosphere. Predictions for the morphology of Ganymede's tail-side aurora were made using these simulations, which were later validated by the Hubble Space Telescope.

The multi-fluid nature of the simulations also allows one to track the differential acceleration of heavy and light mass ions sourced from Ganymede's ionosphere and the Jovian magnetosphere. Thus, sampling the simulated ion energies, temperatures and densities for each ion species along Galileo's trajectory permits the representation of simulated data in a way directly comparable to ion energy spectrograms from Galileo. This enables new interpretations of the heavily debated ionospheric outflow

observations using a method based purely on the physics governing the magneto-plasma interactions of Ganymede's near space environment.

TABLE OF CONTENTS

LIST OF FIGURES

LIST OF TABLES

ACKNOWLEDGEMENTS

I wish to thank Professor Robert Winglee whose intellectual support, advice and mentorship has greatly helped to shape this work. I have learned so much from our discussions, and I have appreciated his suggestions, questions, and encouragement throughout my graduate career. I would also like to thank my committee, Robert Holzworth, Ron Merrill, Don Brownlee, and John Wilkerson, as well as William Paterson (of Hampton University), Michael McCarthy, Walt Harris, and Gonzalo Hernandez who have made many suggestions and had the patience to listen and read this work. Funding from NSF and NASA has made much of this research possible. I want to thank my fellow graduate students, especially Michael Kokorowski, Jeremy Thomas, Erin Lay, Louis Giersch, Toby Neef, Darci Snowden, Matt Fillingam and the rest of the amazing space physics group for all of their help during my time at the University of Washington. A special thanks to Dr. Erika Harnett, whose thoughtful advice and constant support has made much of this work possible, and to the seemingly constant supply of enthusiastic and dedicated undergraduates who have participated in this research (especially Laurel Rachmeler, Angela Stickle and Erin Bell). Finally, I want to thank my family (Charlie, Louise, Catherine 'Cat', and Rosemarie Paty) and Joe Dufek for their patience and support.

DEDICATION

To my family, for their unwavering support and for always believing in me. For my sister Cat who continuously follows her own unique drummer, my mother who inspired me through her dedication to going back to school, and my dad who taught me to follow my dreams, to enjoy math, and to believe in myself.

Chapter 1

INTRODUCTION

Interactions between space plasmas and magnetic fields abound in the universe. These interactions range for example from playing a role in stellar formation, defining the boundaries of solar systems, being responsible for solar activity from sun spots to coronal mass ejections to flares, and defining how planets interact with the solar wind. It is important to understand these processes, as the interaction of the solar wind with the Earth's magnetosphere has direct impact on everything from communications, satellite function and longevity, astronaut and aircraft safety, power grids, and pipeline erosion. At the planets these interactions are important in the formation of radiation belts and the loss of a planet's atmosphere, and at planetary satellites they can be responsible for the loss and/or creation of a moon's atmosphere and even surface erosion.

The dynamic and sometimes storm filled solar wind bathes planets in high doses of particle and electromagnetic radiation. For many of the planets, at least partial shielding is provided from energetic particles by an internally generated global magnetic field. The magnetic field creates a cavity that excludes the solar wind surrounding the planet, where the incident flow of magnetized plasma is slowed and deflected by the magnetic barrier. This magnetically shielded region is known as the planet's magnetosphere. The shape and internal structure of the magnetosphere is governed by internal sources of plasma, such as the planet's ionosphere or orbiting moons and rings, as well as the electromagnetic coupling of the solar wind to the magnetosphere (for further detail see Figure 1.1 and caption). The outer magnetosphere is controlled by solar wind processes. Magnetospheres are not limited to planets; moons in orbit around planets can possess magnetospheres, and the solar wind is a component of the sun's magnetosphere, known

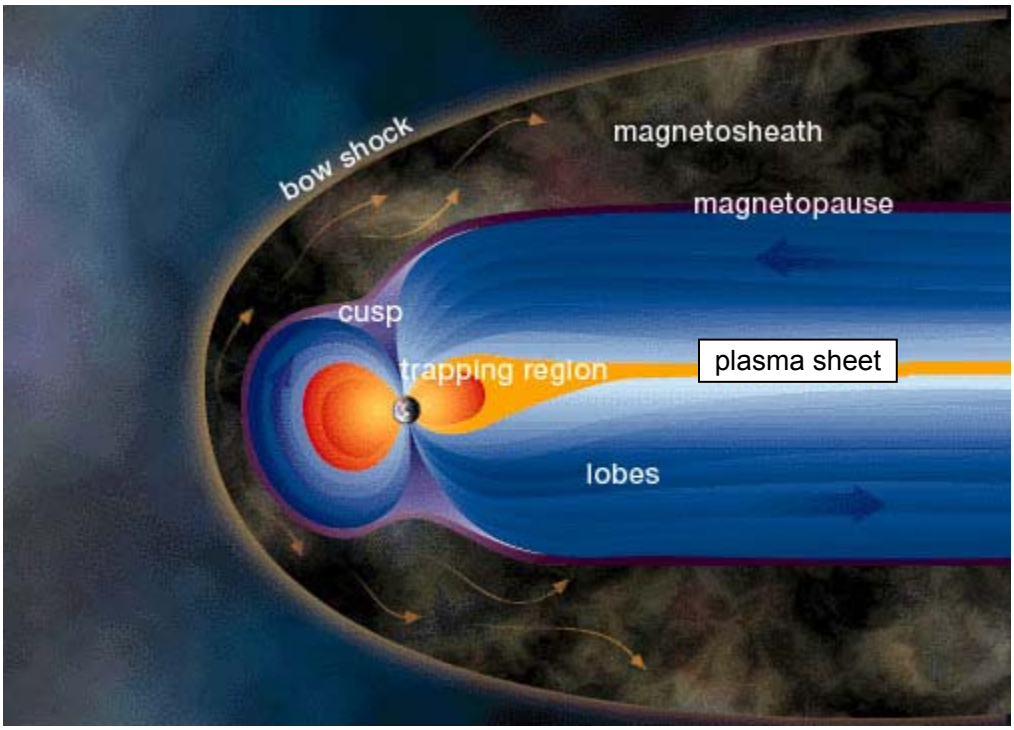

Figure 1.1: Cartoon of the Earth's magnetosphere [modified from the UCAR *Windows* website]. Notice the seven labeled regions: the **bow shock** forms upstream in the incident solar wind where the supersonic and super-Alfvénic flow slow down in response to the obstacle presented by the Earth and its magnetic field, the **magnetosheath** consists of the shocked solar wind that was compressed and heated, the **magnetopause** is where the plasma pressure from the solar wind and the magnetic pressure of the Earth magnetosphere are in balance marking the boundary between the solar wind plasma and the Earth magnetospheric plasma, the **plasma sheet** and **trapping regions** colored in orange represent areas of higher density plasma confined in the Earth's magnetosphere (within the trapping region lie the ***radiation belts***, ***plasmasphere*** and ***ring current*** not labeled here), whereas the **lobes** are areas of lower density plasma containing some convected solar wind plasma, lastly the **cusps** represent areas where solar wind can be funneled to and precipitate to the ionosphere if they are not mirrored back out into the lobe.

as the heliosphere, which shields the solar system from the magnetized plasma of the interstellar wind. Earth, the gas giants and the ice planets all possess magnetospheres, and so far Ganymede is the only moon known to have a magnetosphere supported by an internal magnetic field.

Planets and moons that do not possess internal magnetic fields may also be globally shielded via induced magnetic fields. These fields arise from changes in the incident magnetic field strength and/or orientation that induce currents in either the ionosphere or sub-surface conductive layers which then generate local magnetic fields around the planet or moon. While fundamentally different in structure from a global magnetosphere, these induced magnetospheres provide various levels of shielding from incident magnetized plasmas. Venus, Mars, Europa, Io, Titan and likely Enceladus are all examples of planets and moons with induced magnetic fields.

The direct exploration of Earth's magnetosphere began in the 1950s with a series of rocket launches conducted by J. Van Allen and others. Since then advances in technology from new satellites to advanced computer modeling capabilities have enabled researchers to broaden and deepen their understanding of the Earth's magnetosphere and its interaction with the solar wind. We observe this interaction in a variety of ways; using satellites like SOHO and TRACE to observe the surface of the Sun and measure solar activity, and spacecraft such as FAST, WIND, IMAGE and CLUSTER to monitor the Earth's magnetospheric response to Space Weather (variations in the solar wind and solar energy spectrum from solar activity) by measuring the magnetic and energetic environment of the Earth's magnetosphere and observing the aurora. Spacecraft missions have also been sent to other planets in order to study their magnetospheres, and space-based telescopes like the Hubble Space Telescope are used to remotely observe the interaction of the solar wind with other planetary magnetic fields through imaging the ultra-violet aurora.

While the study of the Earth's magnetosphere has been extensive over the last several decades, it is important to remove the blinders of our local environment in order to more completely understand the interactions of magnetic fields and plasmas. In order to further

our understanding of the interactions of plasmas and magnetic fields it is necessary to qualitatively appreciate and quantify the roles of wind speed, density, magnetic field strength, and plasma composition. In studying other planets in the solar system and their interactions with the solar wind or other local magnetized plasmas we broaden our understanding by dispelling the assumptions used at Earth that rely heavily on the local boundary conditions provided by the Earth's magnetosphere and incident solar wind. Moons embedded within large planetary magnetospheres provide an example of objects subjected to a flow of magnetized plasma with properties that differ significantly from those of the solar wind; they are shielded from the effects of the solar wind by a planetary magnetosphere, but interact with the magnetized plasma provided by the planet's rotating magnetosphere. Ganymede, the largest moon in the solar system, provides an example of a magnetosphere within a magnetosphere. It is the only moon known to have an intrinsic dipole magnetic field that provides it with its own magnetosphere, and it possesses the only magnetosphere in the solar system embedded within a sub-Alfvénic magnetized plasma flow (the Jovian rotating magnetosphere). This phenomenon will be described in detail later in the thesis.

This chapter details the environment of Ganymede, embedded deep within the Jovian magnetosphere. It further explores the parameter space that defines Ganymede and its magnetosphere as both a unique case study and an important end member in our attempt to fully understand the interaction of magnetic fields and space plasmas, specifically the interaction of planetary magnetospheres and magnetized plasma flows. The contents and direction of the rest of the thesis will be outlined at the end of this chapter.

1.1 The Jovian Magnetosphere

With an equatorial radius of 71,600 km Jupiter is the largest planet in our solar system. It has a rotational period of 9.92 hours, and at a distance of 5.2 AU from the Sun its orbital period is 11.86 years. The Jovian magnetosphere is also the strongest and the largest in the solar system; the magnetic moment is 1.6×10^{20} Tm^3 which gives an equatorial field

strength at 1 R_J of 428,000nT [*Ness*, 1994]. The magnetosphere extends to roughly 85-100 Jovian radii (R_J) into the solar wind, and to greater than 7,000 R_J down tail [*Scarf et al.*, 1981; *Kurth et al.*, 1982]. Figure 1.2 shows a schematic cartoon of Jupiter's magnetosphere from both a side view (top) and a view looking down on the northern hemisphere (bottom) [from *Bagenal et al.*, 2004]. While the picture is not completely to scale, important characteristics and boundary layers have many similarities to the terrestrial magnetosphere. Notice that the rotation axis, labeled Ω, and the magnetic axis, M, are offset by ~10°.

Despite the similarities, the Jovian magnetosphere morphologically and functionally differs from terrestrial magnetosphere for many reasons. Most obviously is the presence of the volcanic moon Io which acts as an energetic source for heavy ions and neutrals into the magnetosphere. Io orbits Jupiter at ~6.1 R_J and experiences extreme tidal forcing from interacting with the gravitational pull of Jupiter and the harmonically orbiting icy Galilean moons of Europa, Ganymede and Callisto. This tidal forcing generates internal heat which makes Io the most volcanically active object in the solar system. Constant volcanic eruptions provide Io with a relatively thick and energetic atmosphere, which escapes to the Jovian magnetosphere through hydrodynamic neutral expansion producing an outwardly expanding neutral torus that is visible by telescopes from Earth as shown in Figure 1.3 [*Schneider and Trauer*, 1995].

Io's neutral atmosphere and neutral torus can become ionized through several processes, the three main ones are: photoionization from solar radiation, impact ionization from energetic electrons in Jupiter's magnetosphere, and charge exchange with ions from the Jovian magnetosphere. Once ionized, these particles can be picked-up and trapped by Jupiter's rapidly rotating magnetic field and energized as they are accelerated to rotational speeds of up to 200 km/s. This process of picking up newly ionized particles from Io's atmosphere and neutral torus is a substantial source of mass loading for the Jovian magnetosphere, and creates a plasma torus surrounding Io's orbital track around Jupiter.

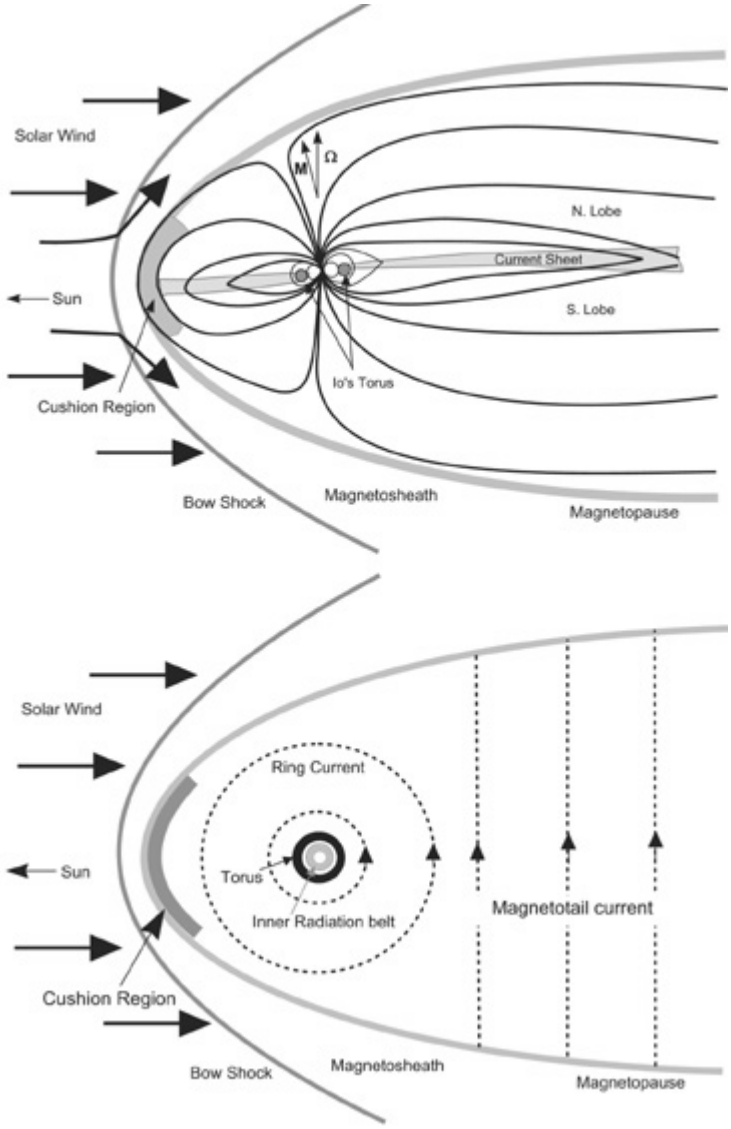

Figure 1.2: Schematic of the Jovian magnetosphere from *Bagenal et al.* [2004] with features and boundary layers labeled. The top figure shows a side view of the magnetosphere interacting with the solar wind, while the bottom figure shows a view looking down on the northern hemisphere and indicating some of the major current systems within the magnetosphere.

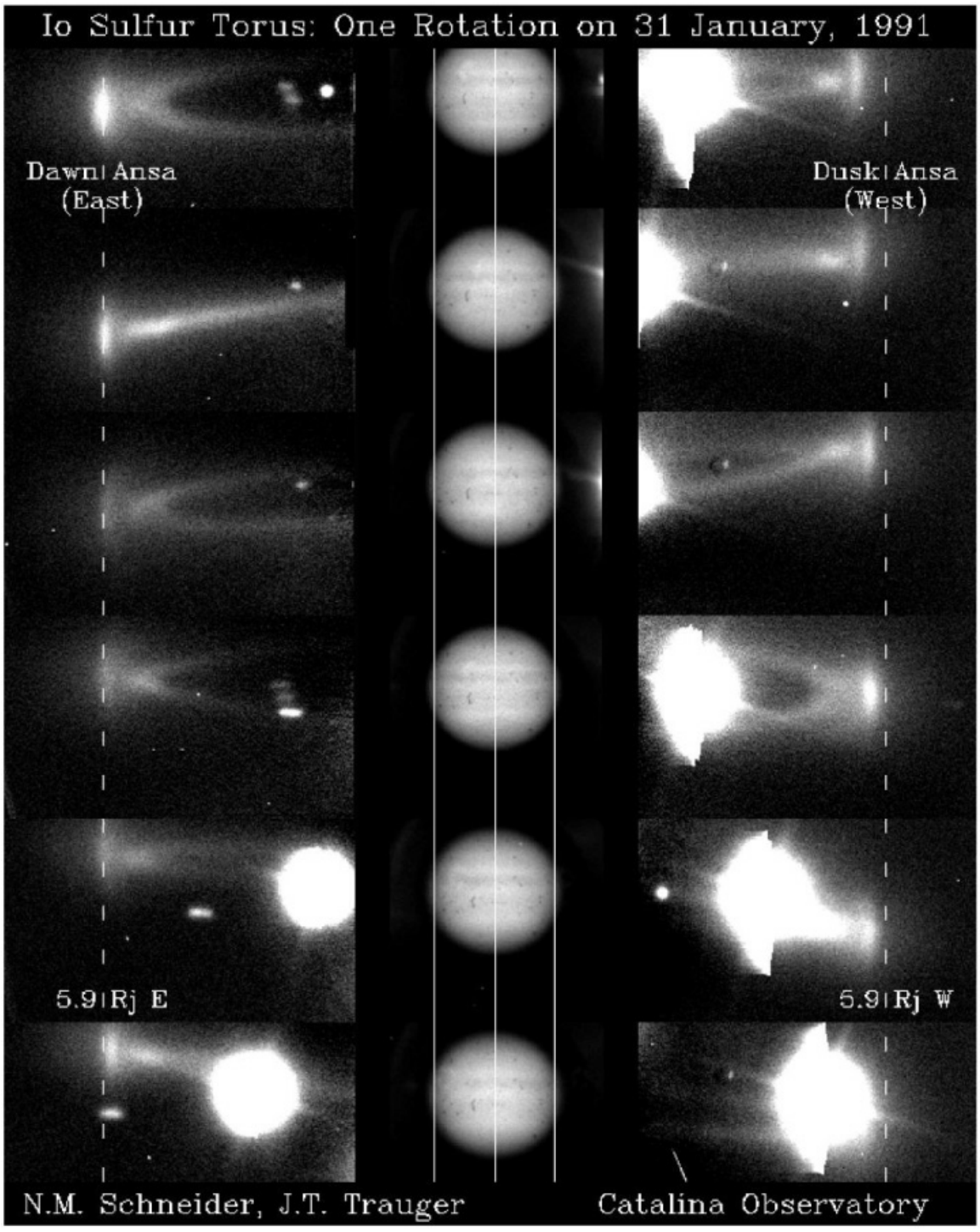

Figure 1.3: Io torus observed using sodium D line emissions from the Catalina Observatory [*Schneider and Trauer*, 1995].

While Jupiter's magnetosphere is quite large, the planet has a short rotation period of ~10 hrs. The plasma in the presence of the global magnetic field attempts to corotate with the planet, however, the mass loading from the Io plasma torus causes the magnetosphere to start noticeably lagging behind corotation between 15 and 20 R_J. The magnetosphere likely experiences slowing starting at the location of the plasma torus, but the amount is small and difficult to quantify due to uncertainties in measuring the flow speed. Due to the mass loading and rapid rotation of Jupiter's magnetosphere, the global dynamics are for the most part internally driven, with effects from the variable solar wind kept to minimum and having little to no influence within 20 R_J where Ganymede, Europa and Io are located. Hence Jupiter's magnetosphere shields these moons completely from the solar wind, while at the same time bombarding them with radiation and heavy magnetized plasma that sweeps past their orbital location at corotational speeds.

One last note on Jupiter's magnetosphere and the environment it provides for the moons embedded within: due to the 10° offset between the magnetic and rotation axis, Jupiter's plasma sheet wobbles relative to the orbital plane of the moons. That is, the plasma sheet periodically sweeps over the orbital location of each moon twice every 10 hours. Figure 1.4, significantly modified from *Bagenal et al.* [2004], illustrates this as well as the fact that due to the rapid rotation and mass loading, Jupiter's plasma sheet is relatively thin and high in density. Within the plasma sheet the moons experience an incident flow of high density magnetized plasma, whereas outside of the plasma sheet the plasma density decreases and magnetic field strength increases. This variability changes the characteristic Alfvén speed of the flow, which can change the interaction of the plasma flow with Ganymede's magnetosphere. The Alfvén speed plays an important role in governing the interaction of the magnetized plasma flow with the magnetosphere; it is the speed at which magnetic information can propagate in a medium. Objects experiencing a super-Alfvénic and supersonic flow will develop shocks, specifically a bow shock due to the fact that the speed of the flow is faster than plasma perturbations and magnetic information can propagate upstream to inform the flow of the magnetospheric obstruction. Every planet in the solar system experiences a super-

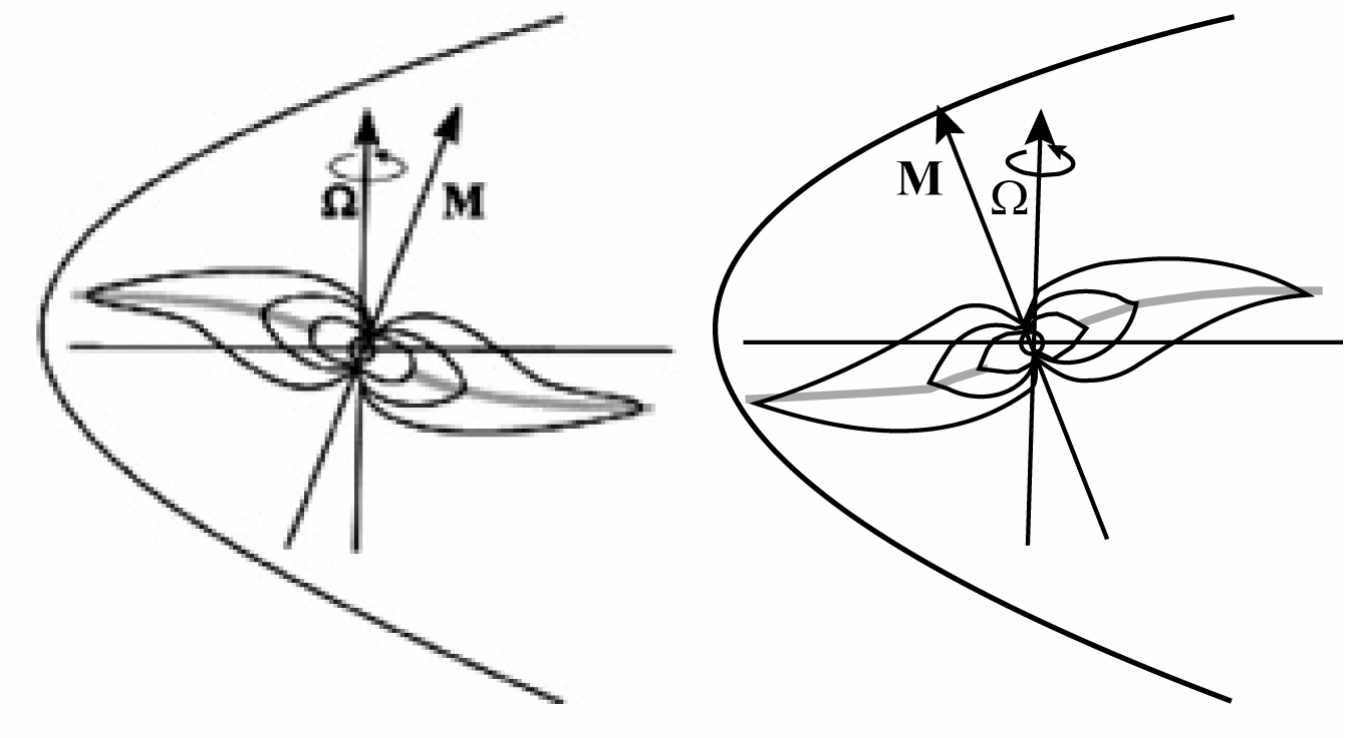

Figure 1.4: Modified from *Bagenal et al.* [2004], this figure shows the sweeping of the magnetic equator over the rotational equator where the moons orbit. This occurs twice every 10 hours at each of the moons, where their environment changes from the northern lobe, to the plasma sheet, to the southern lobe, back through the plasma sheet, and finally back to the northern lobe. This figure is not to scale.

Alfvénic solar wind flow, except sometimes after large storm events. The flow provided by the rotating Jovian magnetosphere at Ganymede is nearly always sub-Alfvénic, except at the center of the plasma sheet where it transitions to slightly super-Alfvénic. Hence Ganymede provides a unique opportunity to consistently study the how a sub-Alfvénic flow affects magnetospheric response to a magnetized plasma flow and how that response changes as the flow transitions to super-Alfvénic and back again.

1.2 Ganymede's Local Environment

Ganymede orbits Jupiter at approximately 15.1 R_J, or 1,070,000 km, and is face locked with Jupiter such that its rotation rate and orbital period are both 7.15 days. With a radius of 2634 km, Ganymede is the largest moon in the solar system and larger in fact than the planets Mercury and Pluto. The interior structure of Ganymede has been determined to be differentiated as illustrated in Figure 1.5, consisting of a high density iron (or iron mixed) core, possibly a silicate layer, and an outer frozen water shell that may contain a sub-surface liquid/slush conductive ocean [*Anderson et al.*, 1996; *Sohl et al.*, 2002; *Kivelson et al.*, 2002]. Ganymede's surface is composed mostly of ice and is covered in craters and large fracture features which indicate some form of complex ice tectonics, perhaps consistent with tidal forcing and a sub-surface ocean.

The surface of Ganymede is also altered via sputtering, or impact of energetic ions and electrons that liberate and eject surface water as hydrogen and O_2 molecules [*Johnson*, 1995; *Cooper et al.*, 2001]. A fraction of these ejected molecules will condense back onto the surface as frost, while the rest supply Ganymede's diffuse atmosphere [*Johnson*, 1995]. These atmospheric constituents may eventually become ionized via photoionization or further charge exchanging collisions, which enables them to be drawn into populating Ganymede's and Jupiter's magnetospheres. Surface sputtering along with surface sublimation are the major processes that supply Ganymede's atmosphere, along with molecular migration and diffusion from the surface regolith to a much lesser extent [*Alexander et al.*, 2000; *Cooper et al.*, 2001].

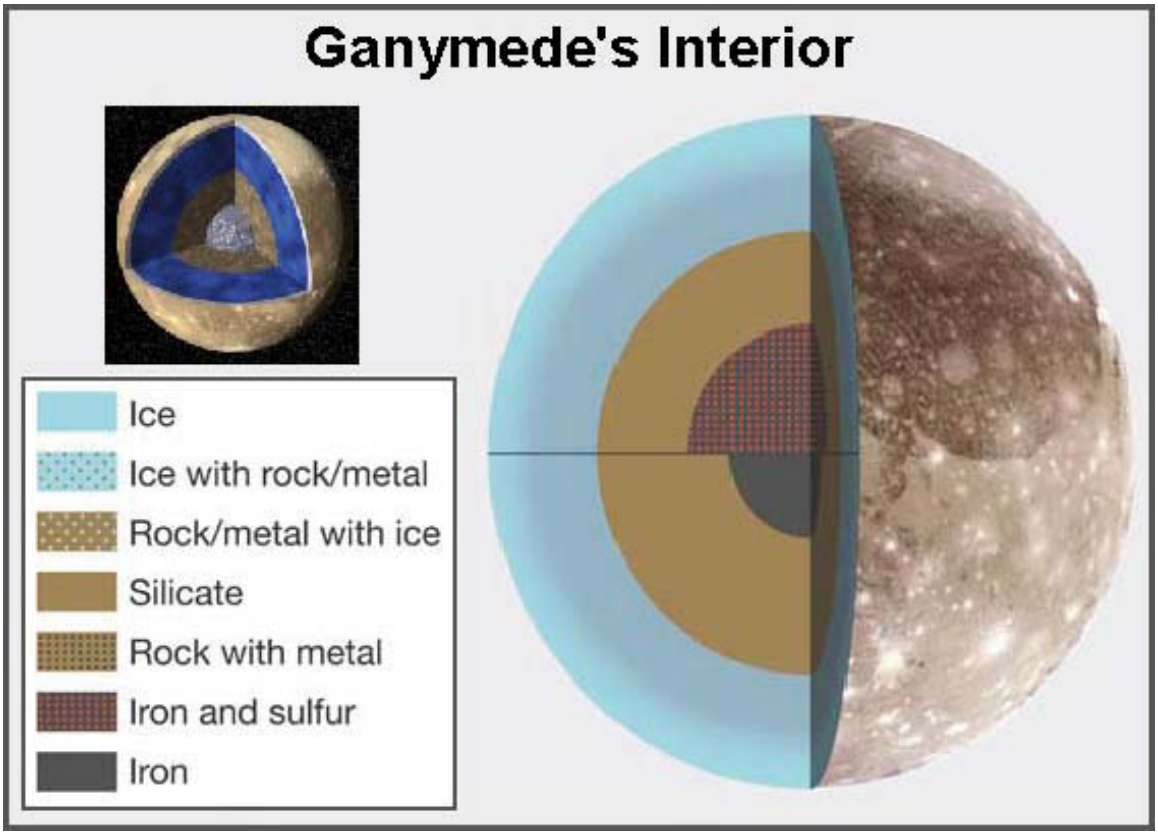

Figure 1.5: Schematic of Ganymede interior structure based on gravity data from multiple Galileo flybys. The three dimensional cartoon is courtesy of NASA/JPL Caltech and demonstrates the relative volumes of core, mantel and ice layer. The figure on the right hand side illustrates two interpretations of how Ganymede may be differentiated [modified from *Bagenal et al.*, 2004].

Ganymede's atmosphere is composed of the products of sputtering and surface ice sublimation, and varies with latitude in composition and density due to presence of its magnetosphere. The polar regions are composed of O_2 and O in a 2:1 ratio, whereas the equatorial region shielded by Ganymede's magnetosphere consists of mostly O [*Eviatar et al.*, 2001]. While there has been much debate over the composition of the ionosphere and the ionospheric polar outflow from interpretation of the Plasma Subsystem ion observations [see *Frank et al.*, 1997; *Vasyliunas and Eviatar.*, 2000], observations of Ganymede's aurora and atmospheric airglow clearly indicate the presence of both O^+ and H^+ [*Barth et al.*, 1997; *Hall et al.*, 1998; *Feldman et al.*, 2000]. In situ observations of the ion population and remote sensing of aurora and airglow will be discussed in detail in Chapter 2.

Ganymede is shielded from the solar wind due to its location embedded deep within the Jovian magnetosphere; however it still experiences a 'wind' in the form of Jupiter's corotational magnetosphere. The Jovian magnetosphere at Ganymede's orbital distance of 15.1 R_J has a velocity of ~190 km/s, which is in the same direction as Ganymede's orbital velocity of ~10 km/s. Subtracting out Ganymede's relative orbital speed yields an incident flow speed in Ganymede's reference frame of ~180 km/s. The plasma in Jupiter's magnetosphere local to Ganymede is composed of mostly O^+ and a few percent of H^+, with fractional percentages of heavier ions such as O_2^+, S^{++}, and S^+ sourced from the Io plasma torus [*Bagenal et al.*, 1994]. The average density of the incident flow is 3.7 ions/cm^3, with a mean mass of ~13.7 amu/ion [compiled by *Neubauer*, 1998]. The mean magnetic field strength in the incident magnetized plasma flow at Ganymede is ~110 nT. Of course, both the mean density and magnetic field strength vary local to Ganymede depending on its location to the Jovian plasma sheet; with higher densities and a weaker magnetic field strength inside the plasma sheet and lower densities and stronger fields outside of the plasma sheet [*Kivelson et al.*, 2002; *Paty and Winglee,* 2006].

As mentioned above, Ganymede is the only moon known to have an intrinsic dipole moment. Though the exact processes responsible for generating the magnetic field are not well understood, it is thought that tidal heating from orbital proximities to Jupiter and the

other Galilean satellites contributes enough heat energy to have a weak dynamo or allow for sub-surface melt for magneto-convection to occur [*Sarson et al.*, 1997]. Ganymede's magnetic moment is 1.83×10^{10} Tm^3 and the field is very nearly dipolar, which produces an equatorial surface field of ~720nT [*Kivelson et al.*, 2002].

In order to describe the orientation of the magnetic moment, it is first necessary to define a coordinate system for Ganymede that will hereto be referred to as GphiO coordinates (see Figure 1.6). GphiO coordinates are defined such that the x-axis points in the direction of the incident flow from the corotating Jovian magnetosphere, the y-axis points toward Jupiter, and the z-axis is the rotational axis (for both Ganymede and Jupiter). The alignment of Ganymede's dipole is about 176° from its rotational axis, almost completely anti-parallel to the Jovian magnetic moment [*Kivelson et al.*, 2002]. This causes the z-component of the magnetic field in the incident Jovian flow at Ganymede to be anti-parallel at all times, regardless of the position of the Jovian plasma sheet relative to Ganymede. Such a configuration creates ideal conditions for reconnection and plasma acceleration at the sub-flow point of Ganymede's magnetopause, which is similar to the Earth experiencing constant southward pointing magnetic field from the solar wind. The orientation and magnitude of the incident Jovian field does vary local to Ganymede depending on its location relative to the Jovian plasma sheet, however the z-component is always anti-parallel to Ganymede's magnetosphere and remains in the range of -80 ± 5 nT. Table 1.1 is adapted from *Kivelson et al.* [2002], and indicates the magnetic field strength and orientations for the Jovian magnetosphere local to Ganymede during the 6 Galileo flybys, along with the closest approach altitude and Ganymede's location relative to the plasma sheet during each flyby.

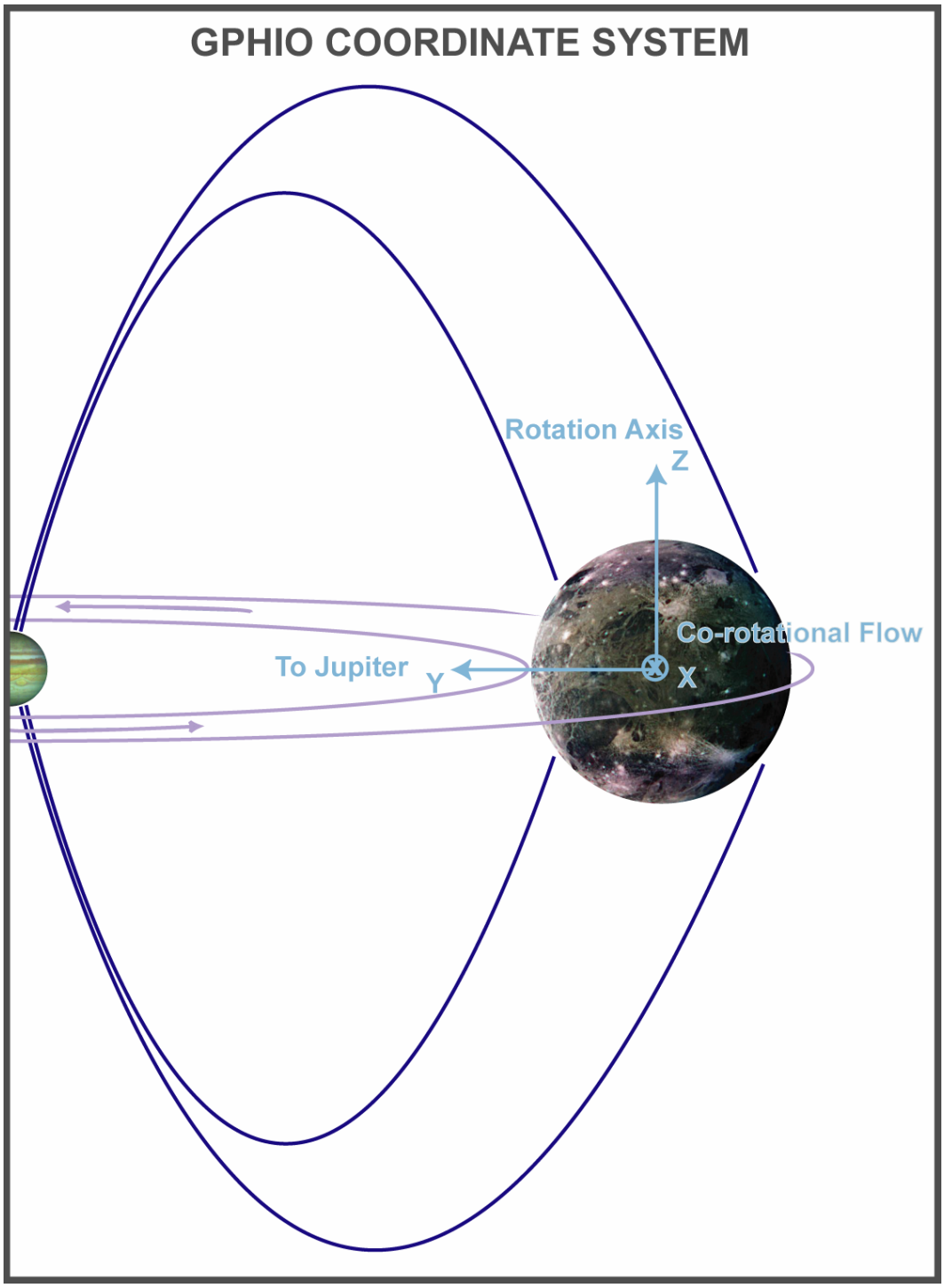

Figure 1.6: Illustration of GphiO coordinates (not to scale). X is in the direction of the flow, Y points towards Jupiter, and Z is in the direction of the rotation axis.

Table 1.1:

Galileo's Encounters with Ganymede: Local Jovian Magnetosphere Conditions

Flyby	|B| (nT)	B_x (nT)	B_y (nT)	B_z (nT)	Closest Approach (km)	Relative to Plasma sheet
G1	111.8	6	-79	-79	838	above
G2	113.3	17	-73	-85	264	above
G7	113.3	-3	84	-76	3105	below
G8	78.6	-11	11	-77	1606	Center
G28	109.1	-7	78	-76	900	Below
G29	114.9	-9	-83	-79	2320	Above

1.3 Combining Computer Modeling and Observations

In this thesis we study Ganymede's magnetospheric interactions using 3-dimensional modeling and several sets of observational data. The importance of this work is that it enables us to understand the 3-dimensional morphology of Ganymede's magnetosphere and local plasma environment along with the dynamic response and evolution of the system with respect to the variable plasma and magnetic environment provided by the Jovian magnetosphere. The rich data set existing for this system enables direct comparison and ground-truthing of the physical assumptions used in the model. The global perspective provided by the model can then be used to expand out ability to interpret remote sensing observations as well as some of the heavily debated Galileo data sets which have been interpreted in contradictory ways [see debate over Ganymede's polar ionospheric outflow *Frank et al.*, 1997; *Vasyliunas and Eviatar.*, 2000].

In situ satellite measurements provide essentially a 1-dimensional cut at an instant in time of the dynamic, 3-dimensional magnetosphere of Ganymede. Combining information collected by various instruments from multiple satellite trajectories we begin to understand the global morphology and plasma distribution of Ganymede's magnetosphere; however this is not straightforward due the dynamic response of the magnetosphere to the variable flow conditions provided by the wobble of the Jovian plasma sheet. Observations of Ganymede's aurora by the Hubble Space Telescope

[*Feldman et al.*, 2000] provides a 2-dimensional snapshot of energetic particle precipitation at Ganymede, indicative of the global dynamic response of Ganymede's magnetosphere to the flow conditions. While this can be extremely useful, the interpretation is difficult since there are no coincident flybys during remote Hubble Space Telescope auroral observations to characterize the Jovian magnetosphere environment local to Ganymede.

We have developed a self consistent 3-dimensional computer model of Ganymede's magnetosphere that is directly comparable to both in situ and remote sensing observations. It gives us the ability to piece together the wealth of information provided by these data sets in order to fully understand the dynamic response of Ganymede's magnetosphere. The model was tested and ground-truthed against the magnetometer data and then used to understand the 3-dimensional magnetic morphology along with the global dynamics of the system such as the distribution of various ion species, energization and acceleration of ions, and particle precipitation.

1.4 Comparative Planetology: Sub-Alfvénic Interactions and Heavy Ions

Ganymede's magnetospheric interaction with the sub-Alfvénic incident Jovian magnetosphere is unique when compared to every other planetary magnetosphere interacting with the solar wind in the solar system. However we can still use the knowledge garnered from the study of this system and apply it to understanding the Earth's magnetosphere after solar storms. For example, while the solar wind at Earth's orbital distance on average has a velocity of 400 km/s, a density of 5-10 protons/cm^3 and a magnetic field strength of 10 nT, during flares and coronal mass ejections (CMEs) those values can exceed 1800 km/s, 50 protons/cm^3 and 60 nT [cf. *Skoug et al.*, 2004]. After a CME, the solar wind has been known to 'turn off', or experience a period of rarefaction with extremely low plasma densities [*Ridley and Hansen*, 2005]. It is this period where the Earth's interaction with the solar wind is most similar to that of Ganymede's magnetospheric response to the Jovian magnetosphere. The characteristic

Alfvén speed of the flow is proportional to the magnetic field strength divided by the square root of the mass density of the incident flow. To obtain the Alfvén Mach number we divide the Alfvén speed into the flow speed, these flow conditions can drop the Alfvén Mach number from ~10 to near 1 or even sub-Alfvénic which is close to conditions at Ganymede. Every planet in the solar system experiences a super-Alfvénic solar wind flow for the most part, except during the above mentioned rarefaction events. Studying Ganymede's sub-Alfvénic interaction with Jupiter's magnetosphere as it moves in and out of the plasma sheet, transitioning from an Alfvén Mach number of nearly 1 to ~0.41 respectively, helps to understand the implications of a sub-Alfvénic flow and how transitioning into and out of such a flow regime can affect the overall magnetospheric dynamics.

The fact that the incident flow at Ganymede consists of heavy mass ions is also unique when compared to the solar wind, and provides the opportunity to study in detail the effects of heavy ions, stemming from their relatively large gyroradii, which lead to differential heating and acceleration experienced between heavy and light massed ion species. The radius of the ions gyro-orbit is determined by the local magnetic field, the ions mass to charge ratio as well as the magnitude of the ions velocity perpendicular to the local magnetic field, $r_{gyro} = \frac{m_i v_{i\perp}}{q_i |B|}$. Therefore accounting for the path of an ion throughout its gyro-orbit is important, especially when the ion encounters magnetic field gradients or crosses boundary layers such as the magnetopause that separate fundamentally different magnetic environments, in order to predict changes in ion drift motion and acceleration. The effects of relatively large ion gyroradii have been greatly ignored when studying the interaction of planetary magnetospheres with the solar wind, with the notable exception of *Winglee* [2004]. The physical assumptions used in the ideal Magnetohydrodynamic (MHD) formulation require that the ion cyclotron motion is small and plays little role in the overall dynamics of the system. While this holds true in environments where light ions interact with strong magnetic fields and small field gradients, the parameter space at Ganymede explicitly violates such assumptions. The

heavy ions and local weak field environment at Ganymede allow for ion gyroradii that are the same size or larger than relevant scale sizes in the system such as the ionospheric scale height, the radius of the planet and even the size of magnetosphere and altitude of the magnetopause.

1.5 Scope of Dissertation

This dissertation seeks to understand the interaction of Ganymede's and Jupiter's magnetospheres through a combination of multi-fluid simulations and observations. Chapter 2 will detail the *in situ* measurements and observations made by the Galileo spacecraft during its six flybys of Ganymede and the remote observations made by the Hubble Space Telescope. It will also discuss the important discoveries made and the questions raised by these observations, as well as some of the issues associated with interpreting Galileo's Plasma Experiment measurements.

In Chapter 3 we will discuss the modeling method implemented to study this system including the governing equations, how they differ from those used in previous magnetospheric models, boundary conditions, and numerical methods. Chapter 4 will quantify the effects from heavy ions, their gyromotion and the associated drift motions, in shaping Ganymede's magnetosphere via direct comparison to both Galileo magnetometer data and models that do not incorporate ion gyro- and drift motions. It will also illustrate the utility of ground-truthing the model from essentially 1-dimensional flybys, and then using the model to understand the 3-dimensional morphology of Ganymede's magnetosphere.

Chapter 5 examines the global distribution of plasma in Ganymede's magnetosphere, tracking the various plasma sources (i.e. the Jovian magnetospheric plasma versus the ionospheric species from Ganymede) using multi-fluid simulations. The model is used to interpret observations made by the Plasma Experiment on Galileo in order to better understand the process of ionospheric outflow and population of Ganymede's magnetosphere. This will be done by sampling the ion density, velocity and thermal

speed in order to generate synthetic ion energy spectrograms. Ion energy signatures are examined for various regions in Ganymede's near space environment. Chapter 6 examines acceleration and precipitation processes in Ganymede's magnetosphere using the multi-fluid simulations. The model predicted precipitation is compared with the auroral observations made by the Hubble Space Telescope. Differences in auroral morphologies between the flow facing and tail-side aurora are explored, and predictions are made for the tail-side aurora and the mechanism driving the precipitation. Lastly, Chapter 7 will include an overall discussion of results and future directions for this research project.

Chapter 2

OBSERVATIONS

While the Voyager spacecraft missions were instrumental in the initial characterization of the Jovian magnetosphere in the late 1970s and early 80s, much of what is currently known about Ganymede and its interaction with the Jovian magnetosphere has been learned in the last decade. The observations can be thought of in two categories; *in situ* observations made most recently by the suite of instruments on the Galileo spacecraft, and remote sensing observations made by the Hubble Space Telescope. This chapter will describe the key observations and discoveries made by these two spacecraft, and the questions raised by those observations that will be addressed by the modeling component of this dissertation.

2.1 In Situ Observations: Galileo Spacecraft

The Galileo spacecraft was launched on November 18, 1989 on board the Space Shuttle Atlantis, and arrived at Jupiter in December, 1995. During its 8 year tour of the Jovian system it made 34 elliptical orbits that included several flybys of each of the Galilean moons, Io, Europa, Ganymede, and Callisto before being de-orbited into Jupiter's atmosphere on September 21, 2003. The spacecraft had a suite of instruments dedicated to the study of the electric and magnetic fields and plasma in Jupiter's magnetosphere; these included the Plasma Wave Detector, Magnetometer, Energetic Particle Detector, and Plasma Science Experiment. These instruments were located on the spinning section of the Galileo spacecraft, which allowed for all-sky observations of fields and particles. Figure 2.1 is a schematic of instrumentation on the Galileo spacecraft, including the

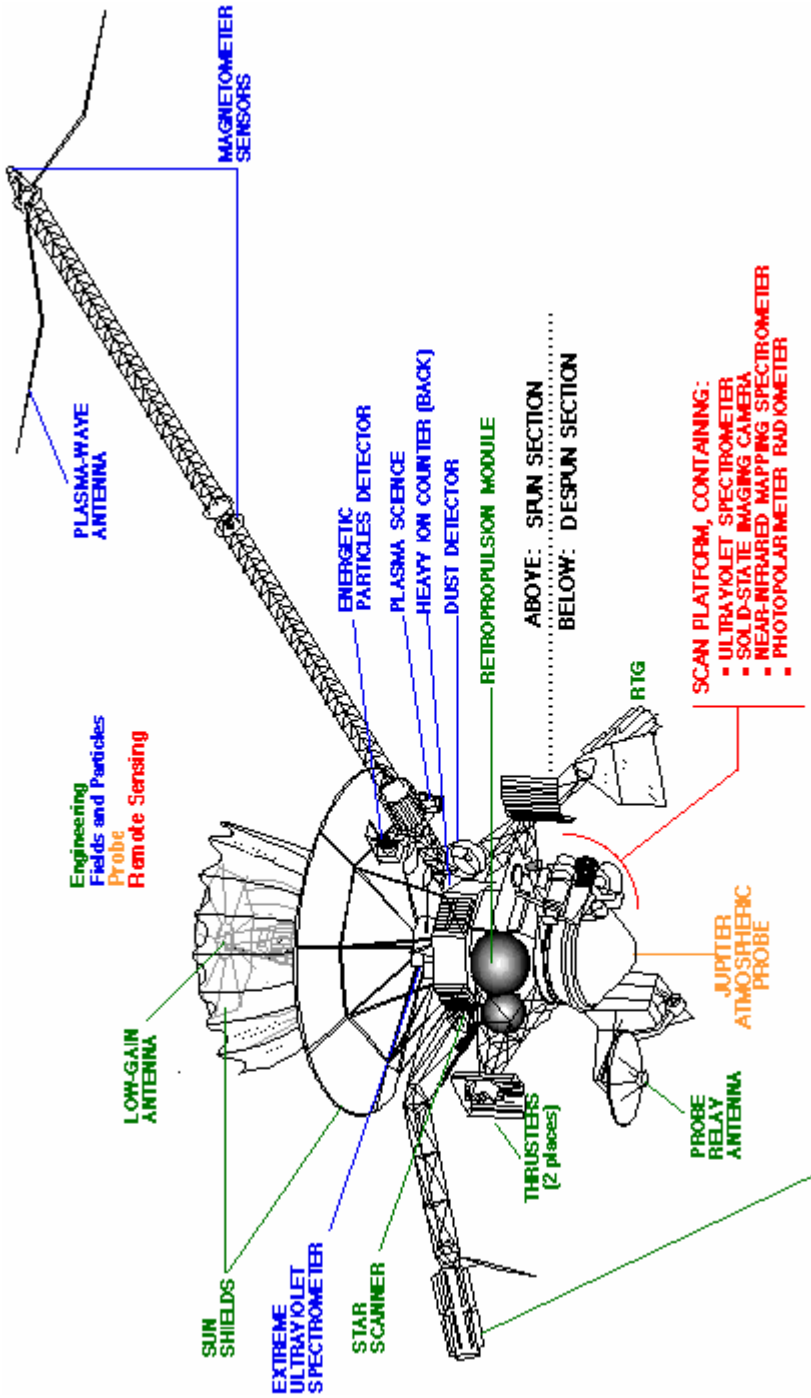

Figure 2.1: Schematic of the instrumentation on the Galileo spacecraft (courtesy NASA/JPL Galileo Legacy Archives).

Jupiter Atmospheric Probe. Most of the other observational instruments were included on the remote sensing platform, which contained spectrometers for a variety of wavelength increments, a visible light camera, and a radiometer. These instruments and the Dust Detector were dedicated to the study of Jupiter's atmosphere, the Io torus, the Jovian rings and the surfaces of the Jovian satellites.

There were 6 flybys of the moon Ganymede; Figure 2.2 illustrates the geometry of these flybys in GphiO coordinates. Notice that while there were only 6 close encounters, they provide reasonable coverage of Ganymede's near space environment. Figure 2.2a is a top down view that shows the scaled locations of the 2 upstream passes, 3 downstream passes, and the polar cap flyby. In Figure 2.2b the latitudinal coverage is illustrated. For reference, the naming convention used for the Galileo spacecraft orbits involved the first letter of the satellite encountered during the orbit and the total number of orbits made around Jupiter. Hence, the G28 orbit was Galileo's 28^{th} orbit around Jupiter, and it performed a close flyby of the satellite Ganymede (G) during the orbit.

2.1.1 Plasma Wave Instrument

The Plasma Wave Instrument measured both electric and magnetic field intensities. Figure 2.3 reproduces the spectrograms of the electric and magnetic field intensities from *Gurnett et al.* [1996] from the G1 flyby. On the G1 approach to Ganymede, the instrument observed electromagnetic waves well above the ion cyclotron wave frequencies and below the electron plasma frequency, indicating that they must be whistler mode emissions [*Gurnett et al.*, 1996]. This type of emission is generally associated with energetic radiation belt electrons [*Kennel and Petschek*, 1966], and no comparable emissions were observed before or after the Ganymede encounter, which led *Gurnett et al.* [1996] to believe the emissions to be associated with Ganymede and not the surrounding Jovian magnetosphere. Using the relationship that the electron cyclotron frequency f_e = 28B Hz (where B is in nanotesla, nT), and the generalization that whistler mode emissions are observed at frequencies ≤ half of f_e [*Burtis and Helliwell*, 1969], a

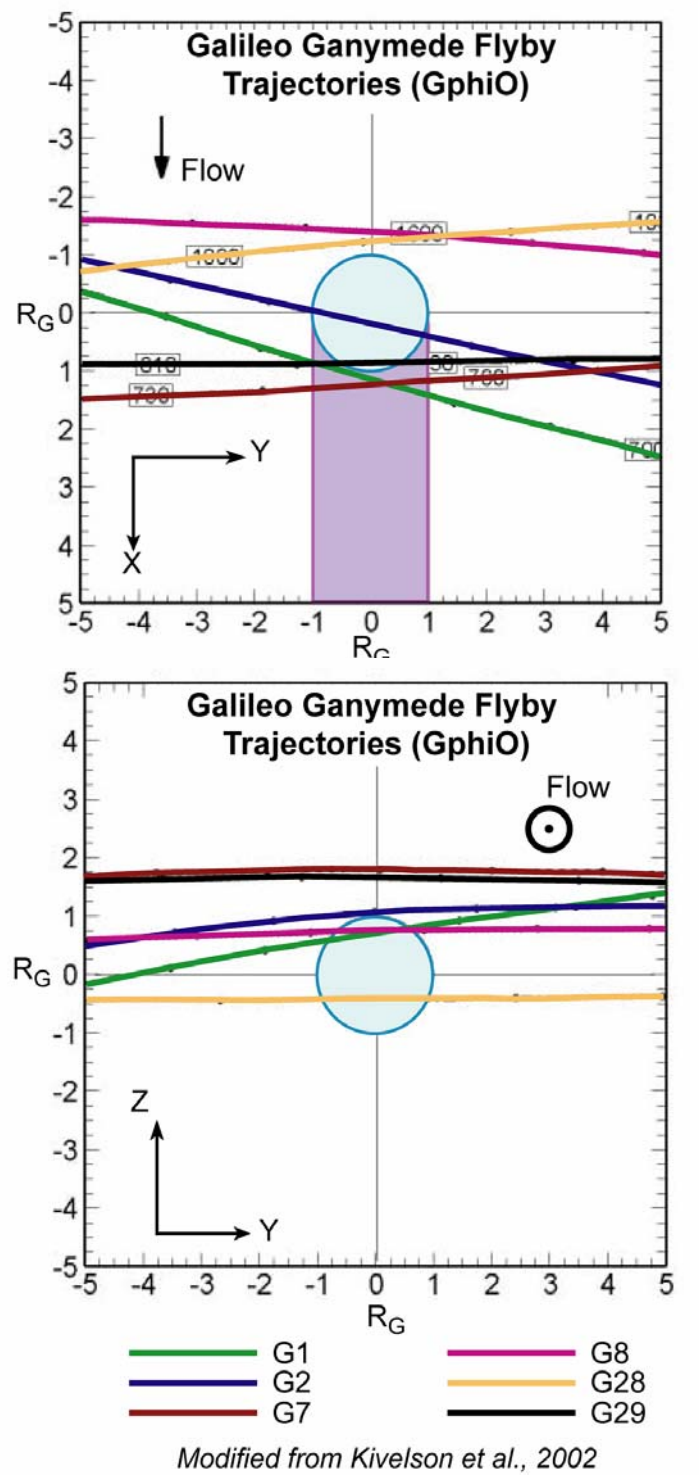

Figure 2.2a & 2.2b: Trajectories of the six Galileo flybys of Ganymede, looking down on the northern hemisphere and into the flow.

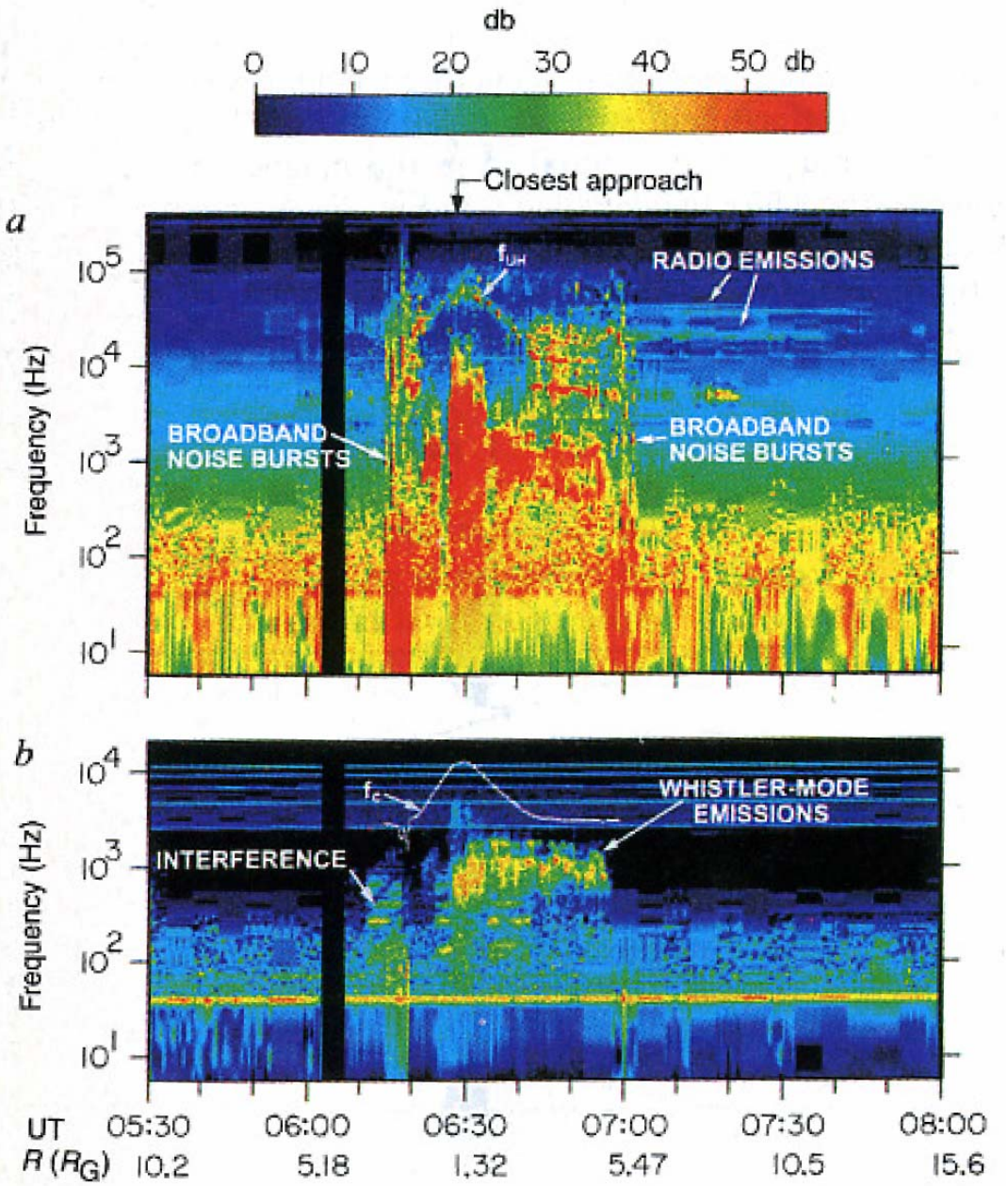

Figure 2.3: From *Gurnett et al*. [1996], the electric (a) and magnetic field (b) spectrograms.

local field strength of ~400nT was determined [*Gurnett et al.*, 1996]. Since this magnetic field strength was much greater than the 100 nT background field of Jupiter at Ganymede's orbital location it could not have been attributed to an induced magnetic field. Therefore, Ganymede was found to possess an intrinsic magnetic field, the first and so far only moon in the solar system with a magnetosphere.

Observations made by the Plasma Wave Instrument also defined magnetosphere boundary crossings and electron densities. This was accomplished through examining the electric field spectrum, where electrostatic emissions and waves were identified. They were identified as electrostatic since no comparable response was seen in the magnetic field (for reference, see Figure 2.3a and b for the electric and magnetic field spectrograms, respectively). Ganymede's magnetopause boundary crossings were identified from broadband electrostatic noise bursts. Such bursts are associated with bow shock and magnetopause crossings at Earth [*Scarf et al.*, 1981b; *Gurnett et al.*, 1979]. These boundary crossings were confirmed with the magnetometer data [*Kivelson et al.*, 1996]. Electron densities were determined from the narrow band emission identified as the upper hybrid frequency (f_{UH}) in Figure 2.3b, and found to be 43 cm^{-3} at the peak frequency [*Gurnett et al.*, 2006]. This high electron density at ~840 km above the surface of Ganymede required a substantial plasma source near the surface, and was indicative of a relatively substantial atmosphere that was not previously considered for the icy moon.

2.1.2 Magnetometer

The Magnetometer confirmed the discovery of Ganymede's magnetosphere and independently located the magnetopause crossings defined by the above mentioned Plasma Wave Instrument [*Kivelson et al.*, 1996]. Combining multiple flyby measurements of Ganymede's magnetic field signature, *Kivelson et al.* [1998] characterized the field strength at the surface of Ganymede and defined its magnetic moment by subtracting out the upstream Jovian magnetic field component and downward continuing the remaining fields from the first 4 Galileo flybys. This method did not take

into account the local plasma dynamic contributions to the observed magnetic field signatures (i.e. currents and induced magnetic fields), but served as a reasonable first order approach to solving for the magnetic moment. This modeled field was superposed with the Jovian upstream magnetic field for comparison to the actual observed signatures, and departures from this static superposition model were attributed to dynamic interactions with the Jovian magnetospheric plasma [*Kivelson et al.*, 1998].

The model of Ganymede's magnetic moment was further refined after the last two flybys, G28 and G29 [*Kivelson et al.*, 2002], with electron loss cones observed by the Energetic Particle Detector confirming the surface magnetic field strength [*Williams et al.*, 1997]. With the complete set of magnetometer data, *Kivelson et al.* [2002] determined that Ganymede's magnetic field signature contained both an intrinsic and an induced magnetic field component. The induced component was attributed to a sub-surface ocean, using the same methodology and reasoning as in the case of Europa [*Kivelson et al.*, 2000] and Callisto [*Khurana et al.*, 1998]. However, the methods used to obtain the size and strength of the induced field component still did not account for the dynamic plasma interactions driven by Jupiter's rotating magnetosphere, nor did they account for the induced response provided by Ganymede's ionosphere.

Several attempts have been made to model Ganymede's interaction with the Jovian magnetosphere in order to understand the field asymmetries and plasma dynamic perturbations found in the Galileo magnetometer data [cf. G8 magnetometer observations in *Kivelson et al.*, 1998]. Resistive MHD simulations by *Kopp and Ip* [2002] examined Ganymede's magnetic field and separatrix variability with respect to its location in and out of the Jovian plasma sheet, but still fell short of accurately predicting the observed perturbations. Models incorporating the effects of external field sources, such as those produced by magnetopause and magnetotail currents, were performed by *Stone and Armstrong* [2001] in order to refine magnetic moment calculations. However, these models required *a priori* assumptions of the current strength in the magnetopause and magnetotail and could not consistently predict the observed magnetic signature at Ganymede for more than a few of the Galileo flybys.

2.1.3 Energetic Particle Detector

The Energetic Particle Detector (EPD) was designed to measure the composition, intensity, energy, and angular distribution of ions with energies greater than approximately 20 keV, electrons with energies greater than 15 keV, and elemental species from protons through iron above ~10 keV/nucleon [*Williams et al.*, 1992]. These energy ranges were complimentary to the range of energies detectable by the Plasma Experiment described below. The EPD investigated many aspects of Ganymede's magnetosphere, including quantifying the amount of slowing experienced by the incident Jovian magnetospheric flow, the extent of the interaction region along Jupiter-Ganymede magnetic fieldlines, the presence of trapped ion and electron populations within Ganymede's magnetosphere, the existence of radiation belts, electron pitch angle diffusion within Ganymede's magnetosphere, and independent confirmation of Ganymede's surface magnetic field strength and magnetopause location [*Williams et al.*, 1997b; *Williams*, 2001; *Williams and Mauk*, 1997; *Williams et al.*, 1998; *Williams et al.*, 1997a]. The measurements were also used in conjunction with the Plasma Experiment observations to determine the amount of electron precipitation and power input to Ganymede's polar cap regions, and to determine sputtering rates from Ganymede's surface [*Ip et al.*, 1997; *Paranicas et al.*, 1999].

I will not go into all of the details associated with these observations other than to summarize the findings and the implications of those findings. *Williams et al.* [1997a] used measurements of electron pitch angle distributions to determine Ganymede's surface magnetic field strength at the magnetic footprints mapped from the spacecraft trajectory, and identified the magnetopause crossings as the locations where the Jovian corotational plasma signal disappeared and reappeared. The presence of so called 'butterfly' distributions from the electron pitch angle measurements in the G8 flyby were indicative of the spacecraft flying through fieldlines that closed to Ganymede on both ends (as opposed to fieldlines that connected to both Ganymede and Jupiter) and observing a

plasma trapped in Ganymede's magnetosphere [Williams et al., 1997b]. Figure 2.4 reproduces the G8 electron pitch angle distribution for two energy ranges, 15-29 keV and 304 to 527 keV respectively, from *Williams et al.* [1998]. The drop in counts per second (cps) at 0° and 180° are the double loss cone distributions expected for closed fieldline geometry, while the dip in cps at ~90° is thought to be resultant from gradient and curvature drift in a distorted magnetic field (i.e. magnetospheric shell-splitting) indicative of a trapped plasma population [*Williams et al.*, 1997b].

An understanding of the extent of Ganymede's influence on the incident Jovian magnetospheric flow was obtained via a thorough examination of the electron pitch angle diffusion and electron anisotropies on the G2 polar cap flyby [*Williams et al.*, 1998]. It was determined that the Jovian corotational flow is slowed by a factor of ~2/3rds at Ganymede, and this perturbed region extended several Jovian radii (R_J) along the Ganymede-Jupiter magnetic fieldlines to the plasma mirror points [*Williams et al.*, 1998]. Thus several bounce motions were observed by the spacecraft as it traversed the Ganymede-Jupiter fieldlines over Ganymede's polar cap, enabling a measurement of pitch angle diffusion and energy dependant electron scattering lifetimes. Based on these relationships ~10 hr old electron loss cone signatures were identified, indicating the perturbing effects from Ganymede are persistent throughout the entire orbital L shell (at 15 R_J) [*Williams et al.*, 1998]. The G28 flyby crossed Ganymede's upstream magnetopause and flew within 900 km of Ganymede's surface. This was Galileo's closest upstream encounter with Ganymede, and the EPD detected ion and electron populations with loss cones at 0° and 180°, with a peak cps at 90°. This indicated that not only did Ganymede have plasma trapped on closed fieldlines, but that its inner magnetosphere possessed a stably trapped population making up Ganymede's radiation belts [*Williams et al.*, 2001].

Not only did the EPD serve to characterize the energetic plasma environment of Ganymede's magnetosphere, it was also used to determine precipitation and sputtering rates. *Ip et al.* [1997] determined ion sputtering rates by using the ion intensity profile observed by the EPD during Galileo's G2 flyby and extrapolating it down to energies

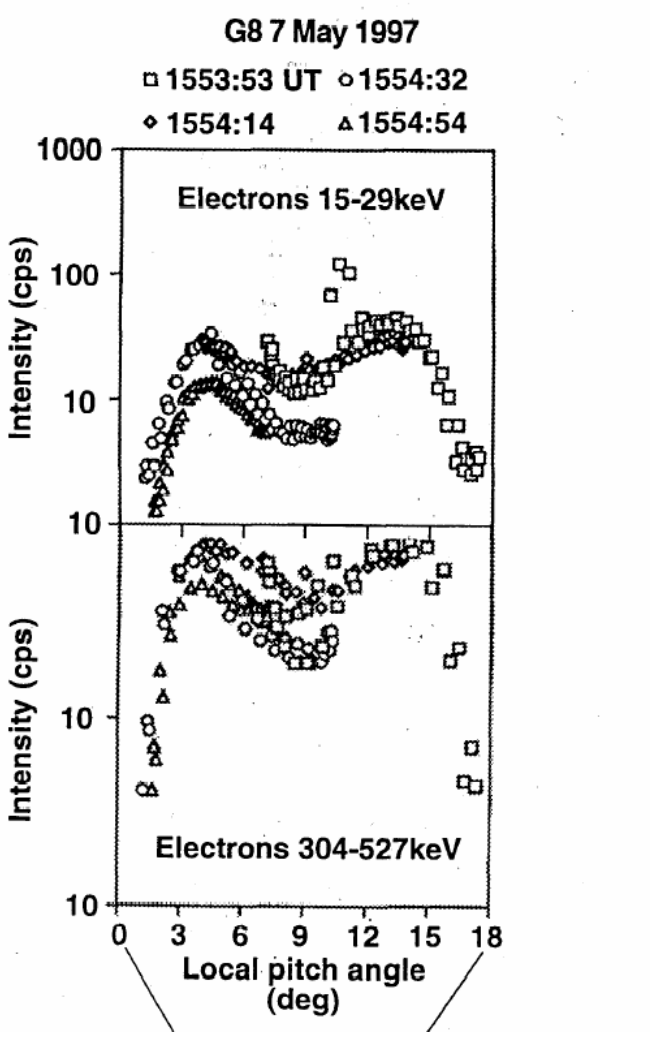

Figure 2.4: From *Williams et al.* [1998], the x-axis is the local pitch angle divided by 10.

below 20 keV. These rates were later revised by *Paranicas et al.* [1999] by incorporating the 1 eV to 20 keV ion energy data from the Plasma Experiment, which yielded sputtering rates of 2 x 10^{26} water molecules/s, or ~8 m/Gyr of surface erosion. *Paranicas et al.* [1999] also determine the power delivered to Ganymede from electron precipitation to be 3 x 10^{9} Watts.

2.1.4 Plasma Experiment

The Plasma Experiment was designed to observe the low energy plasma population, ranging from as low as ~1 eV up to ~50 keV; a complimentary and slightly overlapping range when compared to the EPD. It had the capacity to measure the temperature, density and bulk motion of the low energy ions and electrons. There were also three miniature mass spectrometers to assist in determining the composition of the ion population by measuring ion mass/unit charge. However, due to telemetry constraints only one was used at a given time. During the Galileo flybys the look direction of the 'in use' spectrometer was in the direction of the Jovian corotational flow.

The Plasma Experiment not only characterized the low energy plasma, but was pivotal in observing the polar ionospheric outflow at Ganymede [*Frank et al.*, 1997]. Due to the fact that the 'in use' mass spectrometer was pointed in the direction of corotation and not pointed towards Ganymede during the polar cap flyby, the composition of the ionospheric outflow remains a subject of much debate. Composition can not be directly inferred from the observed ion energy spectrograms. *Frank et al.* [1997] interpreted the cold population of ions flowing out of the polar cap as H^+, however, *Vasyliunas and Eviatar* [2000] found several flaws with that interpretation. They determined that no mechanism for H^+ ionization produced the numbers required to support the inferred outward flux. *Vasyliunas and Eviatar* [2000] interpreted the composition of the cold outflow as O^+, which was somewhat more consistent with the atmospheric models of *Eviatar et al.* [2001] but did not explain the observed Lyman alpha airglow emissions indicating a hydrogen exosphere [*Barth et al.*, 1997].

Figure 2.5 reproduces the Plasma Experiment observations for the G2 flyby of Ganymede's polar cap. The top panel is the ion energy spectrogram and the bottom is the electron energy spectrogram. The horizontal lines represent the 1 and 16 amu populations determined from the miniature mass spectrometer pointing into the Jovian magnetospheric plasma flow, and the vertical dashed lines represent the location of Ganymede's magnetopause. The low energy population in the center of the ion spectrogram was not measured by the mass spectrometer due to the geometry of the instrument, leaving open the debate of the composition of the outflow. [Figure 2.5 with permission from *Paterson*, personal communication of unpublished work.]

2.2 Remote Sensing Observations: Hubble Space Telescope

The Hubble Space Telescope was also used to observe Ganymede; two different types of observing instruments were used. The first was the Goddard High Resolution Spectrograph (GHRS) and the second was the Space Telescope Imaging Spectrograph (STIS). There were no observations that directly coincided with Galileo flybys of Ganymede.

2.2.1 Airglow Emissions

The far-UV spectrum of Ganymede was remotely observed by Hubble's GHRS. The reflected sunlight was isolated and subtracted from the observation, revealing an atmospheric airglow emission at 1304 and 1356 angstroms (Å). These emission lines correspond to Oxygen I lines, and the fact that the ratio of the flux of (1356 Å)/(1304 Å) was roughly 1-2 is diagnostic of dissociative electron impact excitation of molecular oxygen, O_2 [*Hall et al.*, 1998]. This observation was complimentary to the Galileo Ultraviolet Spectrometer (UVS) observation of an extended hydrogen exosphere [*Barth et al.*, 1997] from hydrogen Lyman alpha emissions; it supported the idea of sputtering and sublimation of surface ice supplying Ganymede's atmosphere. Both of these

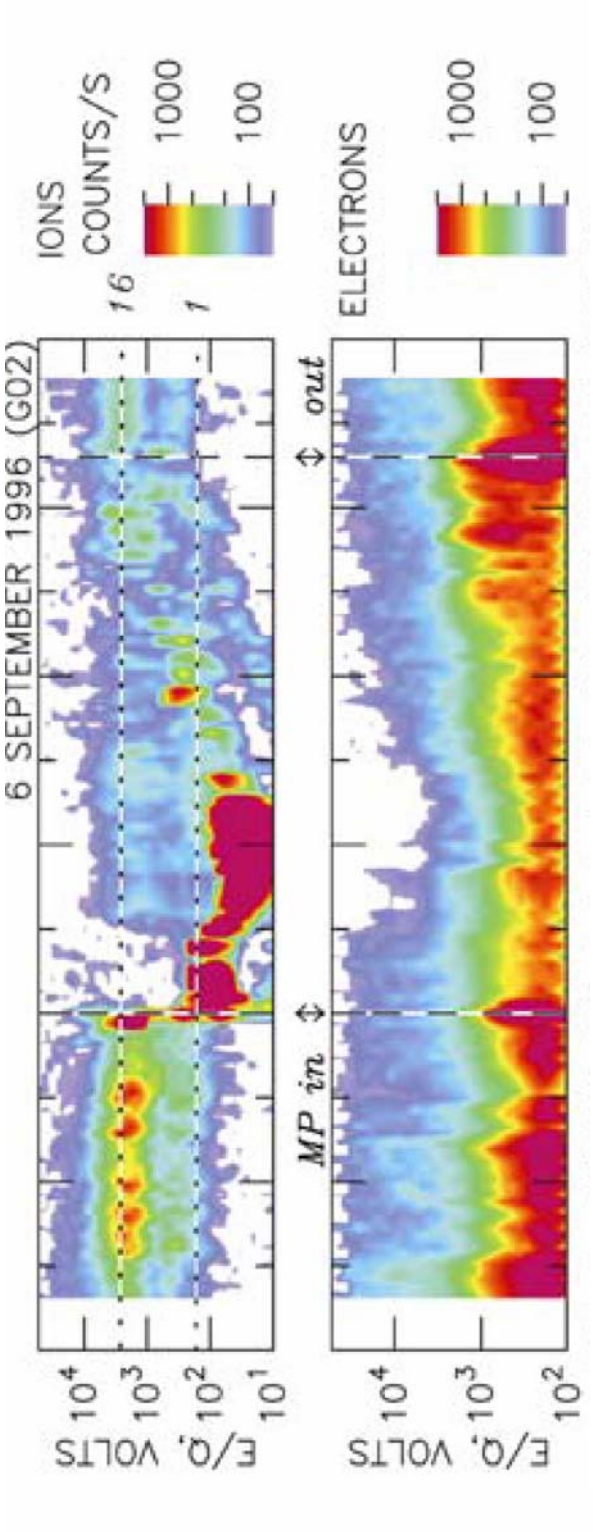

Figure 2.5: Ion and electron energy spectrograms from the Galileo Plasma Experiment (G2 flyby). Reproduced here with permission from *Paterson*, personal communication of unpublished work.

atmospheric airglow observations were used to yield the first approximations of Ganymede's atmospheric composition and density, and were later used in combination with the Plasma Experiment observations of *Frank et al.* [1997] to create chemistry driven atmospheric/ionospheric models for Ganymede [*Eviatar et al.*, 2001].

While there was no explicit spatial resolution for the Hubble GHRS observations of *Hall et al.* [1998], some spatial distribution information exists because the finite size of the observed object is convolved with the emission spectra. Hence, the double peaked distribution on the 1356 Å implied spatially confined emissions at Ganymede's poles [*Hall et al.*, 1998] as opposed to a uniform disk emission. A power of between 5 and 15 x 10^6 watts was determined from these emissions, which is well within the estimates of total power delivered to the system calculated by *Paranicas et al.* [1999].

2.2.2 Aurora at Ganymede

The spatially distinct emissions from the oxygen airglow in Ganymede's polar cap regions led several researchers to believe that these emissions were due to Jovian magnetospheric plasma gaining access to the poles along Jupiter-Ganymede fieldlines. However, further investigation and observations of the 1356 Å line with Hubble's STIS found that these emissions were much more confined in both latitude and longitude than originally thought [*Feldman et al.*, 2000]. There was a lack of limb brightening over the polar caps, which indicated that the entire cap was not illuminated by the flux of Jovian plasma along Ganymede's open fieldlines.

Also, the observations indicated that the emissions varied in time; Figure 2.6 reproduces the four observations of Ganymede's flow-facing hemisphere from *Feldman et al.* [2000]. The size and shape of the emissions varied significantly from one observation to the next, but the location of the emissions at > |40°| latitude remained constant. This was consistent with *Neubauer* [1998] and *Kopp and Ip* [2002], who both placed the location of Ganymede's separatrix at ~|40°|. The separatrix marks the boundary between Ganymede's closed magnetic fieldlines and those open to the Jovian

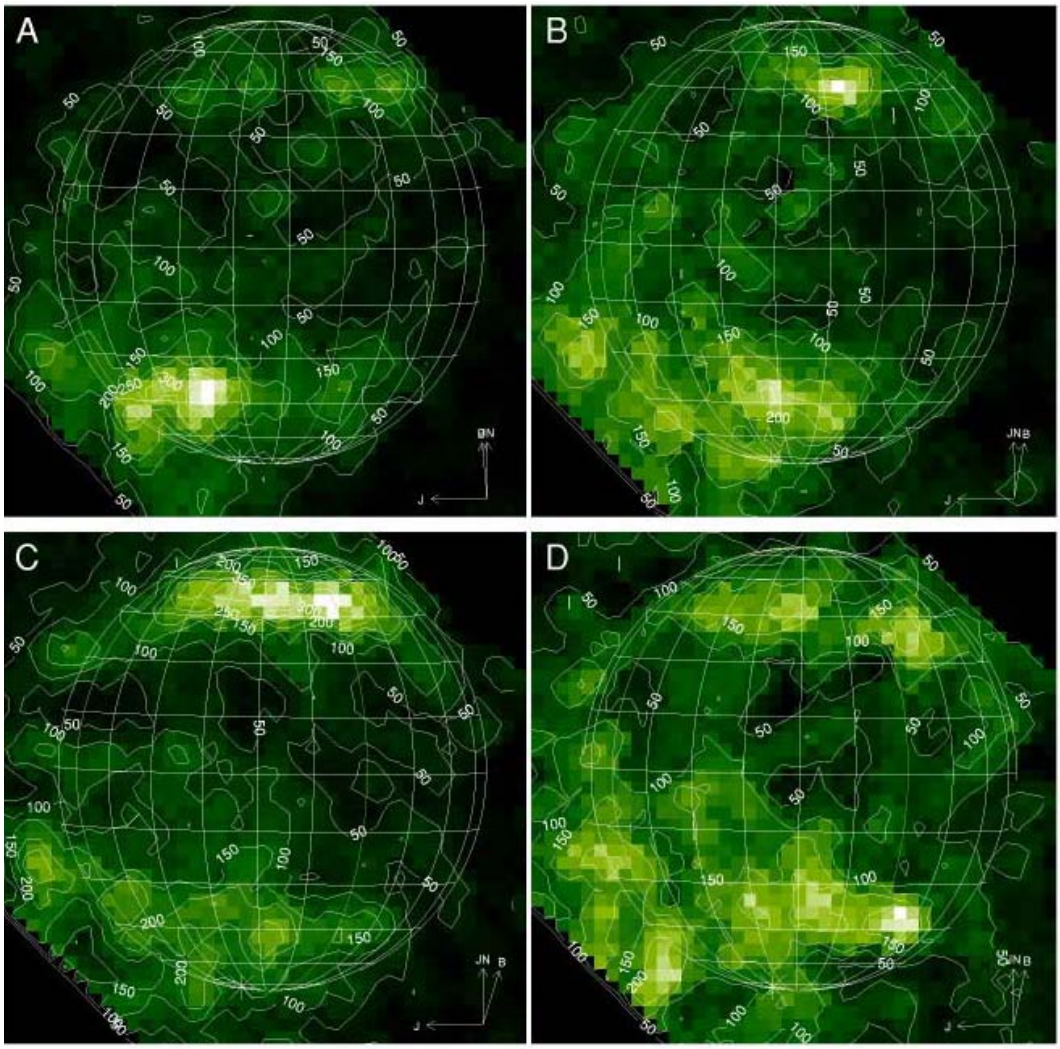

Figure 2.6: From Feldman et al. [2000], this figure illustrates the confinement of the auroral emissions in latitude and longitude as well as the temporal variability of the aurora. Note that the vectors in the lower right corners indicate the direction to Jupiter (J), the Jovian (and Ganymede) rotation axis (JN), and the anti-direction of estimated orientation of the incident Jovian magnetic field during the observation (B).

field; fieldlines undergoing reconnection at the magnetopause and the magnetotail map to this region. *Kopp and Ip* [2002] explored how variability in the orientation of the incident Jovian magnetic field and plasma density changed the location of the separatrix, however, this could not explain why the aurora were confined in longitude and appeared to wander. Much more than a passive airglow, uniform polar cap illumination, or even plasma accelerated by reconnection that mapped to the variable location of the separatrix, Ganymede's UV aurora required complex interactions between Ganymede's magnetosphere and the incident Jovian magnetized plasma.

2.2.3 Aurora at Jupiter

The polar UV aurora at Jupiter was discovered during the initial Voyager 1 encounter in 1979 [*Broadfoot et al.*, 1979]. This initial observation located UV aurora near ~65° latitude in both northern and southern hemispheres, and at the time it was believed that Jupiter's magnetospheric interaction with the Io plasma torus was directly responsible for the aurora. However, observations of Jupiter's aurora with the Wide Field Planetary Camera 2 on Hubble Space Telescope found a separation between the auroral oval and emissions associated with Io [*Clarke et al.*, 1996]. This indicated that Jupiter's auroral oval mapped to a region of the Jovian magnetosphere much further out than the radial distance to Io and the plasma torus. Further observations were made with the STIS on Hubble at even higher resolutions; these observations found distinct auroral footprints that magnetically mapped to the orbital locations of Io, Europa and Ganymede [*Clarke et al.*, 2002]. Figure 2.7 shows Jupiter's UV aurora, including the auroral footprints of Io, Europa, and Ganymede, originally from *Clarke et al*. [2002] and modified in *Bagenal et al.* [2004].

The discovery of the Ganymede and Europa's auroral footprints revealed the global influence of the icy moons on the Jovian magnetosphere, indicating strong coupling between the icy satellites and the Jovian magnetosphere and ionosphere not previously considered. For perspective, Jupiter's volume is ~20,000 times greater than that of

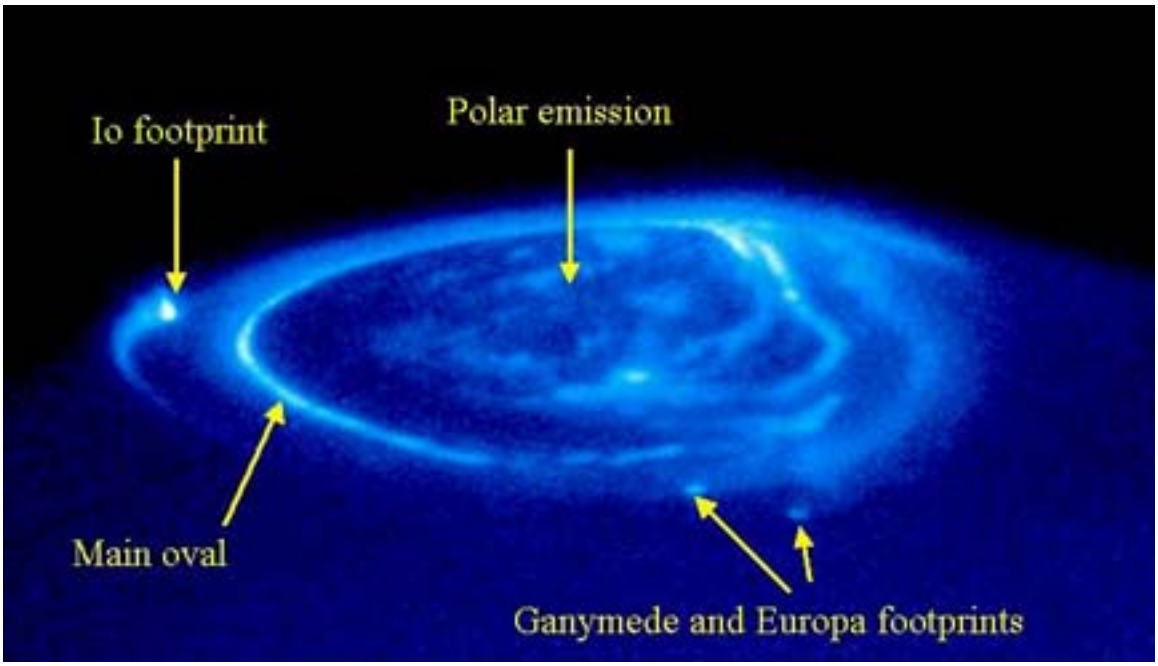

Figure 2.7: Jupiter's UV aurora observed by Hubble Space Telescopes Space Telescope Imaging Spectrograph. Notice that Jupiter has both an auroral oval and polar emissions, as well as the labeled auroral footprints of Io, Europa and Ganymede. [from *Bagenal et al*., 2004].

Ganymede and Ganymede orbits at 15.1 R_J or 407 R_G or 1,070,000 km from Jupiter. Local perturbations at Ganymede due to its interaction with the Jovian magnetosphere must be strong enough to travel millions of kilometers along the Jovian magnetosphere without significantly dissipating in order to reach Jupiter's atmosphere and generate an auroral footprint bright enough to be discernable from the reflected sunlight, atmospheric airglow, and main auroral oval of Jupiter.

2.3 Summary

The last decade has brought a wealth of information about the Jovian magnetospheric system and its interaction with the large icy moon Ganymede from both remote and *in situ* observations. Of course, these observations also brought forth many questions about this system. The questions to be addressed in dissertation through the combined use of computer simulations and observations are:

-What is the dynamic role of heavy ions in the Jovian magnetospheric plasma at Ganymede?

-How important is ion cyclotron motion in governing the Jupiter-Ganymede interaction?

-How do various ion species sourced from either the Jovian magnetospheric plasma or Ganymede's ionosphere populate Ganymede's magnetosphere?

-Can the simulations be used to help interpret the Plasma Experiment ion spectrograms as to the composition and mechanics of Ganymede's ionospheric outflow?

-Where does energization and precipitation of plasma occur? Can the model results combined with the observed aurora provide insight into Ganymede's global dynamics?

-How does Ganymede modify the Jovian magnetosphere both locally and distally?

Chapter 3

MULTI-FLUID SIMULATIONS

This and the following chapter discuss the role of ion cyclotron motion in shaping magnetospheres and governing magnetospheric dynamics, particularly in weakly magnetized systems such as the moons of outer planets. Since magnetohydrodynamic (MHD) modeling approaches explicitly neglect such effects, a multi-fluid modeling technique is used to study the interaction of Ganymede's magnetosphere with that of Jupiter. A detailed discussion of the multi-fluid method is presented in this chapter, along with the numerical algorithms implemented and the treatment of boundary conditions.

3.1 Justification for Including Ion Cyclotron Motion and Using a Multi-fluid Model

Plasma dynamics have been observed to play a large role in the coupled interaction of Ganymede's magnetosphere with the Jovian magnetosphere through the acceleration of electrons which generate the aurora both at Ganymede [*Feldman et al*., 2000] and Jupiter [*Clarke et al*., 2002]. Asymmetries in the magnetometer data and the presence of detectable plasma waves emanating from Ganymede are also indicators of the importance of plasma dynamics for understanding the interaction of Ganymede's magnetosphere with the magnetized plasma of the Jovian magnetosphere. Previously, resistive MHD simulations [*Kopp and Ip*, 2002] and models incorporating the effects of external field sources [*Stone and Armstrong*, 2001] have been performed to study Ganymede's magnetosphere. However, magnetic fields generated in those models did not contain the field asymmetries and plasma dynamic perturbations found in the Galileo magnetometer data [c.f. *Kivelson et al.*, 1998].

The pick-up of ionospheric ions by incident magnetized plasma flows are known to produce asymmetric flows and field morphologies, phenomenon that multi-fluid and hybrid simulations predict [*Harnett et al.*, 2005]. However, these effects are not included in MHD models because the MHD equations average over the gyromotion of the particles and sum together all of the ion components and the electrons into a single bulk fluid. Figure 3.1 schematically describes the conditions necessary for the MHD approximation of averaging over the gyromotion to be adequate, and illustrates the conditions under which this assumption breaks down. In Figure 3.1a the electron gyroradius is exaggerated 900 times relative to the gyroradius of the proton and O^+ ion in 3.1b. Hence, the gyromotion of an electron is sufficiently small that it does not detect the gradient in plasma quantity Q that would otherwise cause the electron to accelerate. This gradient in Q could represent a local change in electric field or pressure for example, or a boundary layer such as the bow shock or magnetopause where plasma parameters vary significantly across the region. As shown in Figure 3.1b, the gyroradii of the protons and heavy ions (O^+) for the same environment are large enough that through the course of their gyro-orbit the ions traverse and detect the gradient and will undergo the associated acceleration. Thus averaging over the ion gyromotion is only valid in settings where all scale lengths are larger than the ion gyroradius, which makes the associated ion drift motions and accelerations negligible. This is not the case in Ganymede's near space environment. In this system, the ion gyroradius of the major ion component O^+ can range from 400 km in the incident plasma flow to thousands of kilometers near the reconnection regions where the magnetic field becomes small. The size of the ion gyroradius is therefore larger than relevant scale sizes in the system such as the scale height of the ionosphere (125 km [*Eviatar et al.*, 2001]), Ganymede's radius (1 R_G = 2631 km), and the average altitude of the magnetopause (.85-1.82 R_G above the surface, based on the G28 flyby in *Kivelson et al*. [2002]).

The incident plasma from Jupiter's magnetosphere at Ganymede has an average mass per ion of 13.7 amu [*Neubauer*, 1998], and is composed of a variety of plasma species sourced from the Io plasma torus, Jupiter's ionosphere, and sputtering of the icy Galilean

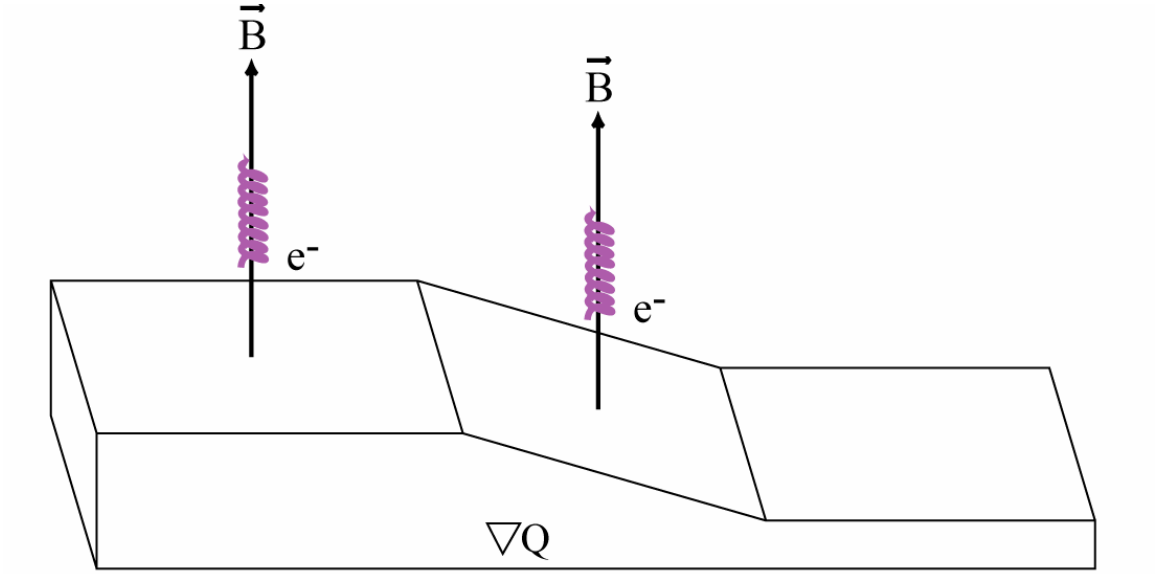

a.

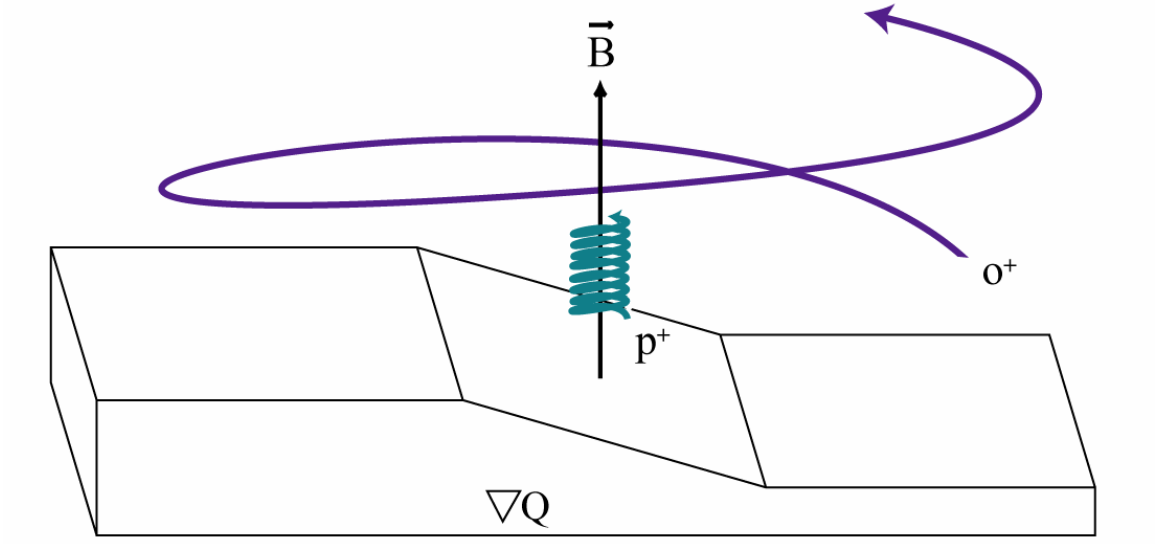

b.

Figure 3.1: A schematic of the gyromotion of an electron, a proton and an O^+ ion. The gyroradius of the electron is enlarged by a factor of 900 relative to the proton gyroradius, which is to scale with the O^+ gyroradius. Thus, the electrons gyro-orbit is very small and it does not detect the gradient in plasma quantity Q and does not experience the associated acceleration. In 3.1b, it is clear that the gyromotion of both ions depicted would detect the gradient in Q, and undergo the associated acceleration. Hence it is important to account for the gyromotion of ions in systems where the scales of gradients and boundary layers are similar to (or smaller than) the size of their gyroradius.

moons. Ganymede's ionosphere and exosphere are believed to be produced from sputtering of its icy surface by the incident Jovian magnetospheric plasma (JMP), causing it to be composed of neutral and ionized hydrogen and oxygen [*Ip et al.*, 1997; *Eviatar et al*., 2001], hence the importance of keeping track of the different ion species. In these simulations we consider three ion species: Ganymede's ionospheric H^+ and O^+ and the incident Jovian magnetospheric plasma. One limitation of the model, which is also present in MHD models, is that it assumes an isotropic temperature distribution and can not incorporate the high energy tails of the ion and electron distributions, though *Harnett et al.* [2005] shows these to be second order effects.

The multi-fluid treatment, explained at length for the context of Earth magnetospheric simulations by *Winglee* [2004] and below for the case of Ganymede, keeps track of the different ion species as separate fluids for which the ion gyromotion is not averaged out. A detailed comparison of the multi-fluid model to hybrid simulations for Pluto found that the ion drift motion due to explicitly modeled gyromotion in the hybrid case was comparable to the ion drift motion in the multi-fluid treatment [*Harnett et al*., 2005].

3.2 Multi-fluid Theory

In tracking electron and ion species the conservation of mass and momentum and pressure are calculated separately for each ion species; here α denotes the ion species, n is number density, $\vec{v}$ is velocity, q is ion charge, and ρ is mass density. γ is the ratio of specific heats and is set to $\frac{5}{3}$ for this 3-dimensional simulation.

$$\frac{\partial \rho_\alpha}{\partial t} + \nabla \cdot \left(\rho_\alpha \vec{v}_\alpha \right) = 0 \tag{1}$$

$$\rho_\alpha \frac{d \vec{v}_\alpha}{dt} = n_\alpha q_\alpha \left(\vec{E} + \vec{v}_\alpha \times \vec{B} \right) - \nabla P_\alpha - \left(\frac{GM_G}{R^2} \right) \rho_\alpha \hat{r} \tag{2}$$

$$\frac{\partial \mathrm{P}_{\alpha}}{\partial t} = -\gamma \nabla \cdot \left(\mathrm{P}_{\alpha} \vec{\mathrm{v}}_{\alpha} \right) + \left(\gamma - 1 \right) \vec{\mathrm{v}}_{\alpha} \cdot \nabla \mathrm{P}_{\alpha} . \tag{3}$$

Under conditions where the displacement current can be neglected, the plasma current, $\vec{\mathrm{J}}$, is

$$\vec{\mathrm{J}} = \mathrm{e}\left(\sum_{\alpha} \mathrm{n}_{\alpha} \vec{\mathrm{v}}_{\alpha} - \mathrm{n}_{\mathrm{e}} \vec{\mathrm{v}}_{\mathrm{e}} \right) = \frac{1}{\mu_o} \nabla \times \vec{\mathrm{B}} . \tag{4}$$

Equation (4) can be solved for the electron velocity, $\vec{\mathrm{v}}_{\mathrm{e}}$ to obtain the following expression

$$\vec{\mathrm{v}}_{\mathrm{e}} = \sum_{\alpha} \frac{\mathrm{n}_{\alpha} \vec{\mathrm{v}}_{\alpha}}{\mathrm{n}_{\mathrm{e}}} - \frac{\vec{\mathrm{J}}}{\mathrm{en}_{\mathrm{e}}} . \tag{5}$$

Assuming $\frac{d \vec{\mathrm{v}}_{\mathrm{e}}}{dt}$ is small on the ion cyclotron timescales and neglecting the gravitational term, the conservation of momentum equation of the electron population gives an electric field of the form:

$$\vec{\mathrm{E}} = -\mathrm{n}_{\mathrm{e}} \vec{\mathrm{v}}_{\mathrm{e}} \times \vec{\mathrm{B}} - \frac{\nabla \mathrm{P}_{\mathrm{e}}}{\mathrm{en}_{\mathrm{e}}} . \tag{6}$$

Substituting the formulations for $\vec{\mathrm{v}}_{\mathrm{e}}$ from equation (5) gives a modified Ohm's Law

$$\vec{\mathrm{E}} = -\sum_{\alpha} \frac{\mathrm{n}_{\alpha} \vec{\mathrm{v}}_{\alpha} \times \vec{\mathrm{B}}}{\mathrm{n}_{\mathrm{e}}} + \frac{\vec{\mathrm{J}} \times \vec{\mathrm{B}}}{\mathrm{en}_{\mathrm{e}}} - \frac{\nabla \mathrm{P}_{\mathrm{e}}}{\mathrm{en}_{\mathrm{e}}} + \eta \left(\vec{\mathrm{x}}_{\mathrm{i}} \right) \vec{\mathrm{J}} . \tag{7}$$

A resistivity term is added to the Ohm's Law in order to account for the collisional resistivity present in the ionosphere. The resistivity, $\eta(\vec{x}_i)$, is applied only in the ionosphere where collisions produce a finite conductivity, the rest of the simulation space is assumed to be a collisionless space plasma with η =0.

In dimensionless units, the ratio of the Hall and ∇P_e terms in equation (7) relative to the convection term is the order of the ratio of the ion skin depth, $d_i = \frac{c}{\omega_{pi}}$ where c is the speed of light and the ion plasma frequency $\omega_{pi} = \left(\frac{4\pi n_i q_i^2}{m_i}\right)^{\frac{1}{2}}$, to the grid spacing. Hence the MHD limit of these equations is obtained by setting this ratio to zero. For Ganymede the ratio is of order of unity for our model resolution, indicating the need for the full multi-fluid treatment.

Lastly, the evolution of the magnetic field is given by the induction equation,

$$\frac{\partial \vec{B}}{\partial t} = -\nabla \times \vec{E}\,. \tag{8}$$

3.3 Similar and Different From Ideal MHD

Of course, we should be able to recover the complete ideal MHD formulation by converting to a single fluid approach, averaging out the gyromotion, and assuming space plasmas have infinite conductivity. To start we sum together the conservation of mass equations for electrons,

$$\frac{\partial \rho_e}{\partial t} + \nabla \cdot (\rho_e \vec{v}_e) = 0 \tag{8}$$

and all ions,

$$\frac{\partial \rho_i}{\partial t} + \nabla \cdot \left(\rho_i \vec{\mathrm{v}}_i \right) = 0 \tag{9}$$

to obtain a single fluid conservation of mass

$$\frac{\partial \left(\rho_e + \rho_i \right)}{\partial t} + \nabla \cdot \left(\rho_i \vec{\mathrm{v}}_i + \rho_e \vec{\mathrm{v}}_e \right) = 0 . \tag{10}$$

We can define $\rho_{tot} = \rho_e + \rho_i$ and the net bulk velocity $\vec{\mathrm{V}} = \frac{\rho_e \vec{\mathrm{v}}_e + \rho_i \vec{\mathrm{v}}_i}{\rho_e + \rho_i}$ to obtain

$$\frac{\partial \rho_{tot}}{\partial t} + \nabla \cdot \left(\rho_{tot} \vec{\mathrm{V}} \right) = 0 . \tag{11}$$

Doing the same for the conservation of momentum equations, i.e. summing the expressions for ions and the electrons, we obtain

$$\frac{d \left(\rho_i \vec{\mathrm{v}}_i + \rho_e \vec{\mathrm{v}}_e \right)}{dt} = \left(\mathrm{n}_i \mathrm{q}_i + \mathrm{n}_e \mathrm{q}_e \right) \vec{\mathrm{E}} + \left(\mathrm{n}_i \mathrm{q}_i \vec{\mathrm{v}}_i + \mathrm{n}_e \mathrm{q}_e \vec{\mathrm{v}}_e \right) \times \vec{\mathrm{B}} - \nabla \mathrm{P}_{tot} - \left(\frac{\mathrm{GM_G}}{\mathrm{R}^2} \right) \rho_{tot} \hat{r} . \tag{12}$$

$\mathrm{P_{tot}}$ is the total pressure, or the sum of both the ion and electron pressures. Using the above mentioned definitions for ρ_{tot} and $\vec{\mathrm{V}}$, assuming quasi neutrality $\mathrm{n}_i \mathrm{q}_i + \mathrm{n}_e \mathrm{q}_e = 0$, and using the relationship from equation (4) for the current density, $\vec{\mathrm{J}}$, equation (12) reduces to

$$\rho_{tot} \frac{d \vec{\mathrm{V}}}{dt} = \vec{\mathrm{J}} \times \vec{\mathrm{B}} - \nabla \mathrm{P}_{tot} - \left(\frac{\mathrm{GM_G}}{\mathrm{R}^2} \right) \rho_{tot} \hat{r} . \tag{13}$$

The conservation of energy equation is used,

$$\frac{\partial e}{\partial t} + \nabla \cdot \left(\vec{\mathrm{V}} \left(e + \mathrm{P}_{\mathrm{tot}} \right) \right) = \vec{\mathrm{E}} \cdot \vec{\mathrm{J}} , \tag{14}$$

where

$$\mathrm{P}_{\mathrm{tot}} = \left(\gamma - 1 \right) \left[e - \frac{1}{2} \rho_{tot} \left| \vec{\mathrm{V}} \cdot \vec{\mathrm{V}} \right| \right]. \tag{15}$$

The induction equation for the changing magnetic field remains in the same form as equation (8), and Ampere's law remains the same as in equation (4) so that the current is obtained by taking the curl of the magnetic field. The ideal MHD equations are closed in the same way as the multi-fluid formulation, but with the *idealized* Ohm's law equation

$$\vec{\mathrm{E}} = -\vec{\mathrm{V}} \times \vec{\mathrm{B}} . \tag{16}$$

3.4 Numerical Methods

The 3D simulations incorporate a nested grid scheme, allowing for the highest resolution in areas of important boundary layers, and the coarsest resolution well outside the magnetopause, extending out to tens of Ganymede radii. A Cartesian coordinate system is used where x is in the direction of the Jupiter's corotational flow at Ganymede, y points in the Ganymede-to-Jupiter look direction, and z is along the rotational axis of Ganymede (GPHIO coordinates, see Figure 1.6). We solved the above equations using a 2nd order Runge-Kutta. This method estimates the derivatives in the above set of time dependant equations at the half-time-step, and implements those half-step estimates to solve the full time step for the time dependant quantities. Written generically for a quantity y whose

time derivative is a function of y and time, i.e. $\frac{d\,y}{dt} = f(y,t)$, this method determines the value of y at time t=n+1 from the value at t=n such that

$$y^{n+1} = y^n + \Delta t\left(f\left(y^n + \frac{1}{2}k_1, t + \frac{1}{2}\Delta t \right)\right) \tag{17}$$

where

$$k_1 = \Delta t\left(f\left(y^n, t\right)\right). \tag{18}$$

Flux correction was implemented at each time-step to reduce numerical grid point oscillations.

A nested grid system is implemented in the simulation such that the innermost box has a resolution of .045 R_G or about 120 km, and extends from approximately -3 to 3 R_G in x, -2 to 2 R_G in y and –2 to 2 R_G in z. The simulation has a grid spacing that increases by a factor of two between consecutive boxes, with the largest simulation volume of dimension 48 R_G in x and 32 R_G in y and z. Information from the inner boxes is passed to the outer boxes at a corresponding resolution, and information from the outer boxes is interpolated and passed inward along the inner box edges at every time-step. The time-step size, Δt, is determined after each time-step as a fraction of the time-scale prescribed by the Courant condition, which is based on the fastest speeds in highest resolution box and ensures that no information is lost when the boxes communicate. Therefore Δt varies for each time-step and is on the order of .01 s.

3.5 Boundary Conditions

There are both inner and outer boundary conditions to consider in this simulation. The outer boundary conditions involve the motion of the JMP from the corotational magnetosphere into the simulation volume along the upstream boundary. Our simulations

represented the bulk density of the JMP with mostly O^+ and a few percent H^+ based on the upstream plasma observations from *Frank et al.* [1997] and the mean mass per ion, speed and mach numbers compiled by *Neubauer* [1998], with the incident magnetic fields corresponding to the upstream Jovian field orientations for each of the Galileo flybys. The upstream Jovian field orientations used in the simulations and resultant sonic and Alfvén Mach conditions are determined from the magnetic field strengths and orientations observed by the Galileo magnetometer for each of the six Ganymede flybys. The other 5 sides of the simulation have open boundary conditions to allow the plasma to escape. The inner boundary lies along the base of the ionosphere and is set at 5,200 ions/cm^3, with a 4:1 ratio of O^+ to H^+ and a scale height of 125 km [*Eviatar et al*., 2001; *Herring-Captain et al.*, 2005]. The ionospheric density is held constant on the assumption of a constant source of ionospheric material [*Ip et al.*, 1997; *Paranicas et al*., 1999], and the resistivity $\eta(\vec{x}_i)$ is set to 3800 ohm-meters at the base of the ionosphere and zero everywhere else.

Chapter 4

CHARACTERIZING GANYMEDE'S MAGNETOSPHERE

Here we demonstrate the importance of ion cyclotron motion in the near space environment of Ganymede, using the 3-dimensional multi-fluid simulations discussed in the previous chapter. These simulations track several ion species, specifically Ganymede's ionospheric H^+ and O^+ and the Jovian magnetospheric plasma (JMP), and incorporate ion cyclotron effects through a comprehensive treatment of the plasma dynamics and the generalized Ohm's law equation. In order to better quantify the role of ion gyromotion, a set of simulations was conducted that explicitly neglected the effects, essentially assuming that the gyroradius was significantly small when compared to relevant length scales in Ganymede's near space environment. The model results for all simulations were compared to Galileo magnetometer data from several flybys through various regions of Ganymede's magnetosphere.

The following demonstrates that the multi-fluid simulations that fully incorporated the effects of ion gyromotion accurately predicted the Galileo magnetometer observations for several flybys and at various locations with a single, consistent model and set of parameters. The extent of the discrepancy between including the ion cyclotron terms and neglecting them was determined via examination of Ganymede's modeled global magnetospheric morphology, the size and altitude of the magnetopause, and by comparing both types of models to the magnetic signature observed by the Galileo spacecraft [results from *Paty and Winglee*, 2006].

4.1 Quantifying the Importance of Ion Cyclotron Motion

Two sets of simulations were performed; the first using a modified multi-fluid treatment where the ion gyromotion is neglected (hereafter referred to as the NG, or Non-Gyromotion, treatment), and the second using the full multi-fluid treatment which includes ion cyclotron effects. The NG treatment incorporates exactly the same boundary conditions and initializations as the full multi-fluid treatment, the difference is that the Hall term and ∇P_e term in the Ohm's law (7) are set to zero, i.e. the ion gyroradius is assumed to be small and the associated drifts negligible. Note that the NG treatment is not an MHD model since we still consider each ion species and the electrons to be separate fluids. The size and shape of the observed and modeled magnetospheres and the location of the magnetopauses are explored to determine the relative importance of ion cyclotron motion in governing Ganymede's magnetospheric dynamics.

We chose to compare these two treatments against the Galileo magnetometer data from the G8 flyby. We chose this flyby because the spacecraft was at low latitude, placing it within close proximity of the flow-side neutral point for the upstream field configuration at that time. This location should experience the greatest influence of ion cyclotron motion because of the extremely weak fields local to the spacecraft. Note also that at the time of the G8 flyby Ganymede was located in the center of the Jovian plasma sheet (see Table 1.1), which places it in a flow regime closer to an Alfvén Mach number of one due to the weaker magnetic field and enhanced density of the JMP in the plasma sheet.

Figure 4.1 illustrates the importance of fully treating the ion cyclotron motion. The full multi-fluid treatment simulation compares well with the observed magnetic field signature, while the NG treatment does not capture the observed field. Without the ion cyclotron motion, Ganymede's resultant magnetosphere is comparatively small to that observed by Galileo. This is due to the increased temperature, and therefore pressure, produced by the ion gyromotion terms on Ganymede's magnetospheric plasma. In the full multi-fluid treatment, the ionospheric H^+ and O^+ that support Ganymede's magnetosphere can exert more outward pressure to balance the incident flow of the Jovian magnetosphere, allowing the magnetopause to form further from Ganymede's

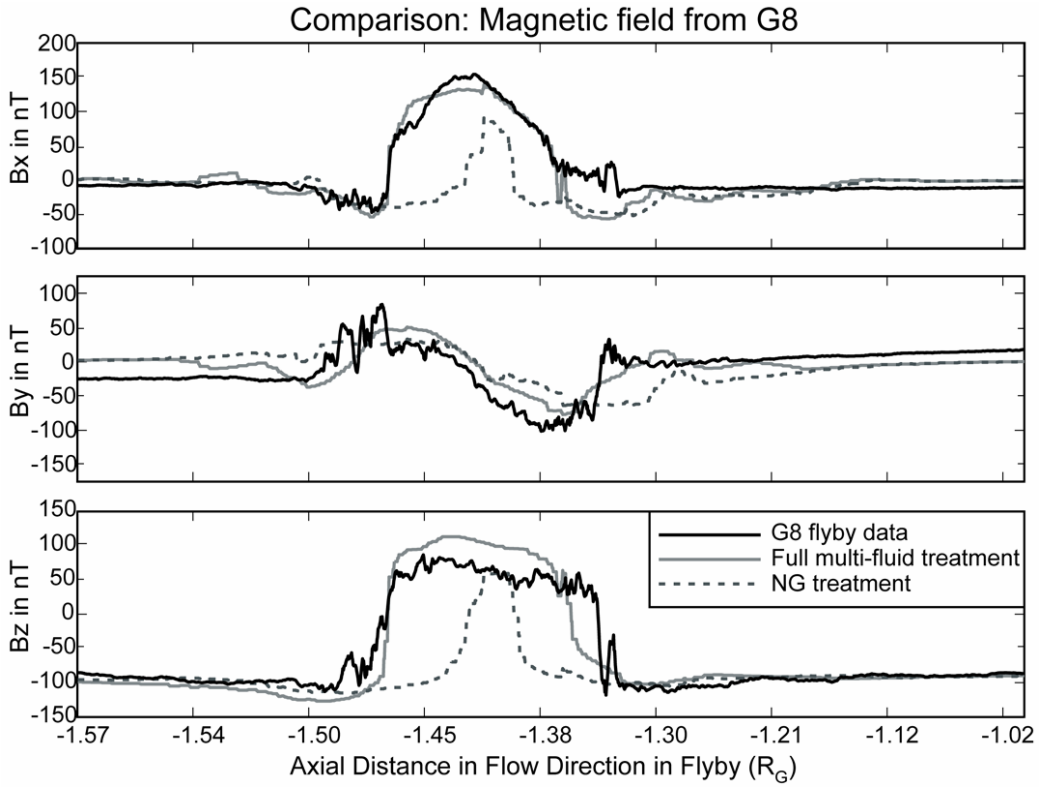

Figure 4.1: A comparison of the 3 components of the magnetic field measured by Galileo's magnetometer data from the G8 flyby (black) to the full multi-fluid treatment (grey) and the NG treatment (grey dashed). The axial distance in the flow direction is the x-direction in GPHIO coordinates [*Paty and Winglee*, 2006].

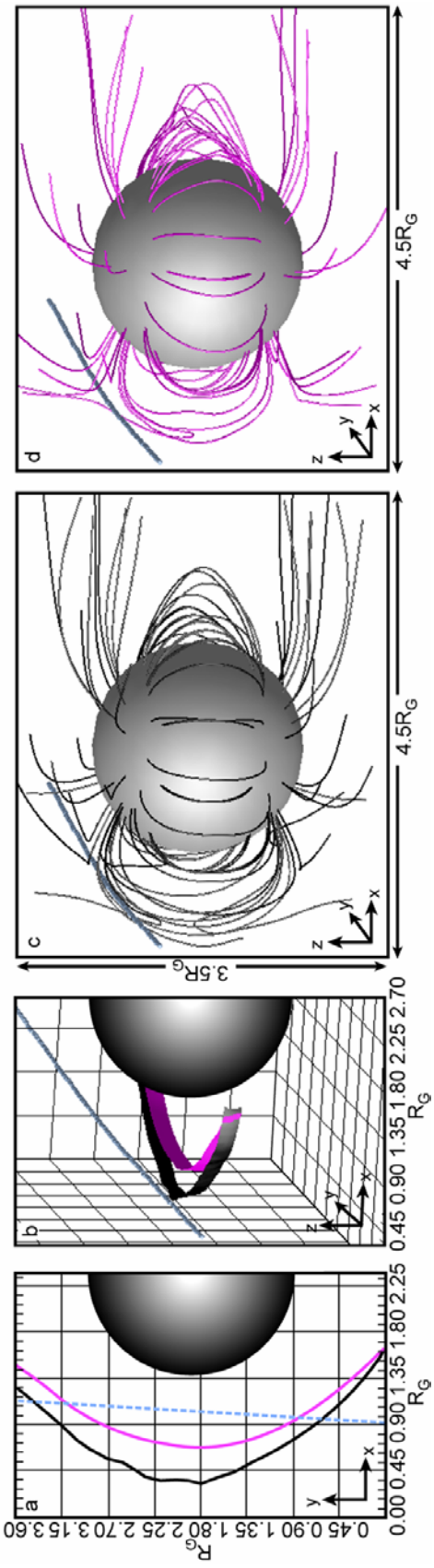

Figure 4.2(a-d): In 4.2a, a 2-dimensional projection in the x-y plane (GPHIO coordinates) of the equatorial magnetopause from the full multi-fluid (black) and the NG (magenta) treatments. The G8 spacecraft trajectory is projected into the plane in blue. Similarly in 4.2b, except the view is rotated to see all 3 dimensions and latitude information from the flyby. 4.2c & d show the magnetic field configuration for the multi-fluid and NG treatments respectively [*Paty and Winglee*, 2006].

surface on the flow facing hemisphere (see Figure 4.2). In Figure 4.1 it is clearly shown that in the NG simulation the spacecraft barely crossed into the magnetosphere, whereas in the actual flyby and in the full multi-fluid simulation the spacecraft spent a significant amount of time inside the magnetosphere. Note that during the G8 flyby the B_y component of the local Jovian magnetosphere varied from ~ -25 nT to 25 nT, so for this simulation the average (B_y= 0.0 nT) was used in order to run the simulation to a steady state. This produces the discrepancy in the simulated upstream conditions in Figure 1.

Figure 4.2a further illustrates the differences between the full multi-fluid and NG treatments by comparing the magnetopause locations in the x-y plane of the two simulations, black for the full multi-fluid treatment and magenta for the NG simulation. The magnetopause in 4.2a-b is determined by projecting the location where the B_z component of the magnetic field goes to zero in the equatorial plane; a reasonable approximation due to the fact that in the G8 flyby the orientation of the incident Jovian magnetic field and Ganymede's magnetosphere were anti-parallel in the z direction and nearly zero in x and y. Notice that the size and symmetry differ significantly, with the magnetopause altitude of the full multi-fluid treatment residing at an altitude of ~1.1R_G while the magnetopause in the NG simulation was at ~ 0.7 R_G. Since the full multi-fluid simulation was well correlated to the observed magnetic signature, the lower altitude modeled in the NG simulation corresponds to a 36% smaller magnetosphere than that observed by Galileo on the G8 encounter. Figures 4.2c and 4.2d demonstrate the 3-D shape of the modeled magnetospheres for the full multi-fluid treatment and NG treatment respectively. Again the spacecraft trajectory is mapped in blue. It is apparent that without the ion gyromotion effects included in the simulations (4.2d), the resultant magnetosphere is noticeably smaller than when fully treated (4.2c).

A more comprehensive test of the simulations is to investigate other flybys which provide different cuts through Ganymede's magnetosphere. At the time of the G2 flyby Ganymede was located well above the Jovian plasma sheet, and during the G28 flyby it was below the plasma sheet. Hence the upstream conditions for these two flybys consisted of slightly lower density plasma with stronger magnetic fields than was the case

for the G8 flyby which occurred while Ganymede was located in the Jovian plasma sheet. Figure 4.3 shows the results of the full multi-fluid simulations for the G2 and G28 flyby conditions and trajectories respectively. The only differences between these two simulations and the one performed and compared to the G8 flyby was the strength and orientation of the incident magnetic field from Jovian magnetosphere. Since the G2 flyby was located above the plasma sheet the B_y component of the Jovian magnetic field was negative; the G28 flyby occurred when Ganymede was located below the plasma sheet making the B_y component positive (see Table 1.1 for values). The density and possibly composition of the incident Jovian plasma could also be varied to represent Ganymede's location in the plasma sheet (G8) versus in the lobe (G2, G28) of Jupiter's magnetosphere, which could result in better correlation for the G28 flyby. However, the variability of these parameters are not well constrained so it was held constant so as not to introduce another free parameter.

For all three flybys shown here, the multi-fluid model accurately describes the three component magnetic field strengths and magnetopause crossings observed by the Galileo magnetometer. This indicates that the physics and assumptions included in the full multi-fluid treatment model are accurate for the weak field/heavy ion conditions present at Ganymede (and several other icy moons at Jupiter and Saturn). Simulations for the other three Galileo flybys (with Ganymede located similarly as in G2 and G28 relative to the Jovian plasma sheet) were also performed, all with comparably good correlations to the observed magnetic signatures. They will be discussed in detail in the context of magnetotail dynamics in Chapter 6.

4.2 Discussion of Multi-fluid Treatment vs. NG Treatment Results

The multi-fluid model containing the full treatment of the ion cyclotron motion was shown to consistently describe the magnetic field configuration detected by the Galileo magnetometer at the location of the Galileo spacecraft. This holds true for each of the possible incident Jovian field configurations, i.e. for Ganymede being located above

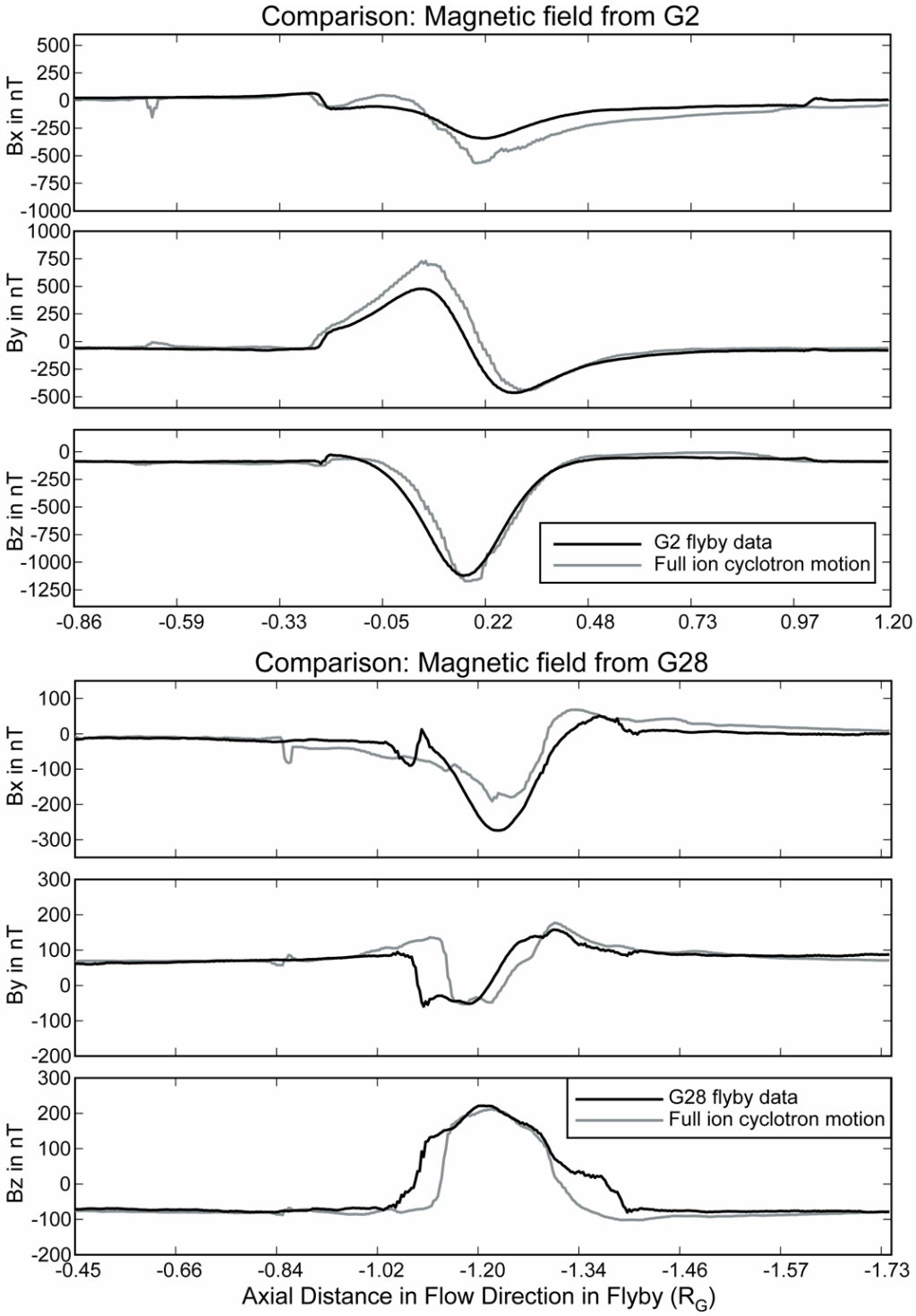

Figure 4.3: A comparison of the 3 components of magnetometer data from the G2 and G28 flybys (black) to multi-fluid simulations (grey) [*Paty and Winglee*, 2006].

(G2), below (G28) or inside (G8) the Jovian plasma sheet. This demonstrates the importance of treating the ion cyclotron motion when describing the Ganymede interaction with the surrounding Jovian magnetosphere.

The fact that the near space environment of Ganymede includes several heavy ion species and weak magnetic fields invalidates a general assumption for using ideal or resistive MHD models. Without including the physics associated with the gyromotion of these heavy ions, the simulated magnetosphere of Ganymede is significantly smaller than that observed by the Galileo spacecraft. That is to say that in the ideal MHD limit of the multi-fluid formulation the size of Ganymede's magnetosphere is underestimated, while the full multi-fluid simulation of the magnetosphere, which includes ion-cyclotron effects, predicts hotter ion populations relative to the NG simulations. The importance of treating the ion cyclotron motion is most noticeable near the magnetopause where magnetic field strengths approach zero. As a consequence, the predicted magnetopause is ~58% further from the surface than in the NG simulations and in good agreement to spacecraft observations. This multi-fluid model is the first simulation of Ganymede's magnetosphere that includes the ion gyromotion in the governing physical equations, and it consistently describes the field configuration observed by the Galileo spacecraft for several locations of Ganymede relative to the Jovian plasma sheet.

4.3 Sub-surface Oceans on Ganymede and Other Icy Moons

In *Kivelson et al.* [2002] much discussion came from the discrepancies between the magnetometer observations and the predicted field configurations from static superposition models. These models involved directly adding together the observed upstream Jovian field to the dipole field of Ganymede, which had been extrapolated using spherical harmonic reductions of Ganymede's magnetic perturbation to the local ambient Jovian field. It was proposed that the dynamic component of Ganymede's observed magnetic signature came from induced fields produced by induced currents in a sub-surface ocean. However, the effects from the interaction of Ganymede's magnetosphere

with the incident Jovian field were never quantified and assumed to be very small. While the astrobiological implications of a large sub-surface ocean at Ganymede shielded by a magnetosphere and a few kilometers of ice are enticing, the results from our complete treatment of the magnetic and plasma interaction show consistent agreement with the magnetometer observations from all six flybys. The possibility of an extant sub-surface ocean is not ruled out; however its effect on Ganymede's magnetic signature is small at spacecraft altitudes, which makes it impossible to infer characteristics such as size, depth and conductivity from the time variable magnetic field components.

Of course the same may not hold true for Jupiter's icy moon Europa or for Enceladus at Saturn, where the lack of an intrinsic magnetic field limits the magnitude of plasma dynamic effects responsible for observed magnetic signatures. *Schilling et al.* [2004] modeled the interaction of Europa with Jupiter's incident and variable magnetosphere and determined that the plasma dynamic effects were not large enough to account for the magnetic field magnitude and variations observed over the course of 5 Galileo flyby [*Kivelson et al.*, 2000]. As for Enceladus, the Cassini spacecraft is scheduled to make several more flybys over the life of its mission. To date it has been determined that plumes of water are spewing from the vicinity of the 'tiger stripes' on the southern pole [*Porco et al.*, 2006], and possibly the re-precipitation of some of that water as surface frost accounts for Enceladus having the highest reflective albedo of any object in the solar system. Whether these cryogenic volcanoes are indicative of a subsurface ocean or a localized heating phenomenon has yet to be determined.

Chapter 5

IONOSPHERIC PLASMA SOURCE AND ION DISTRIBUTIONS

Comparative studies of 3D multi-fluid simulations with Galileo magnetometer data were used in the previous chapter to develop a quantitative model of the currents and fields within Ganymede's magnetosphere as well as its bulk plasma environment. Comparisons between the magnetometer data and the simulation were shown to demonstrate good agreement for the strength and structure of Ganymede's magnetosphere. In order to understand the plasma population of Ganymede's magnetosphere it is important to account for the various sources of plasma into the system. The multi-fluid simulations explicitly track the various ion species, which enables examination of differential heating and acceleration of each ion species. It also allows us to determine which ion sources make up the population of a given region of the simulation. This chapter investigates the ion population of Ganymede's magnetosphere by examining Ganymede's ionospheric outflow as a source of heavy (O^+) and light (H^+) ions and the Jovian magnetospheric plasma as an external source of heavy ions. We develop a method for examining the energy distributions of each ion species in the simulation in a way directly comparable to the observations of the Plasma Experiment on the Galileo spacecraft. This is used to interpret the composition of Ganymede's ionospheric outflow shown in the ion spectrogram in Figure 2.5.

5.1 Ion Sources Populating Ganymede's Magnetosphere

The ions that populate Ganymede's magnetosphere come from two sources: the incident Jovian magnetospheric plasma (JMP) and Ganymede's ionosphere. The boundary

conditions used in the model for these parameters are described in detail in section 3.5. In brief, the JMP is composed of plasma from the Io plasma torus, Jupiter's ionosphere, and to a much lesser extent the solar wind. We chose to model the major constituents of the JMP (mostly O^+ and a few percent H^+) as determined by upstream observations [*Frank et al.*, 1997; *Neubauer*, 1998]. Ganymede's ionosphere was set with a density of 5,200 ions/cm^3, with a 4:1 ratio of O^+ to H^+ ions, and a scale height of 125 km based on the chemical models of *Eviatar et al*. [2001], sputtering rates of *Ip et al.* [1997] and *Paranicas et al*. [1999], and sputtering products of *Herring-Captain et al.* [2005].

In tracking the motion of these ion species as the system evolves toward steady state, the model demonstrated that Ganymede's magnetic field provides shielding from most of the bulk flow of the JMP. This leads to Ganymede's magnetosphere being primarily populated by Ganymede's ionospheric constituents. Figure 5.1 details the density distribution for each of the three modeled ion species throughout the system. In Figure 5.1 the first row illustrates the morphology of the magnetic field at Ganymede as it encounters the Jovian plasma in Jupiter's magnetospheric lobe as well as the density of each of the three modeled ion species in the x-z and x-y planes. Note that the color bar is consistent for all of the plots. At equatorial latitudes the bulk flow of the JMP is almost completely excluded from Ganymede's magnetosphere. However, on the flow facing side some of the bulk flow of the JMP can gain access to Ganymede's ionosphere and surface through the cusps. Ganymede's ionospheric H^+ and O^+ dominate the composition of Ganymede's magnetosphere, though the ionospheric O^+ is higher in density. This is due to both the ionospheric composition used in the simulation and the mass ratio of H^+ to O^+. H^+ is more easily accelerated to escape velocities, and hence more readily exits Ganymede's magnetosphere along the open polar magnetic field and is picked up by the Jovian magnetosphere.

Due to the continuum treatment used in the simulations only the bulk flow was modeled and the small fraction of the JMP at very high energies was not taken into account. JMP incident on Ganymede's magnetosphere with energies of 100s of keVs to MeVs will not be significantly deflected by Ganymede's magnetic field and will impact

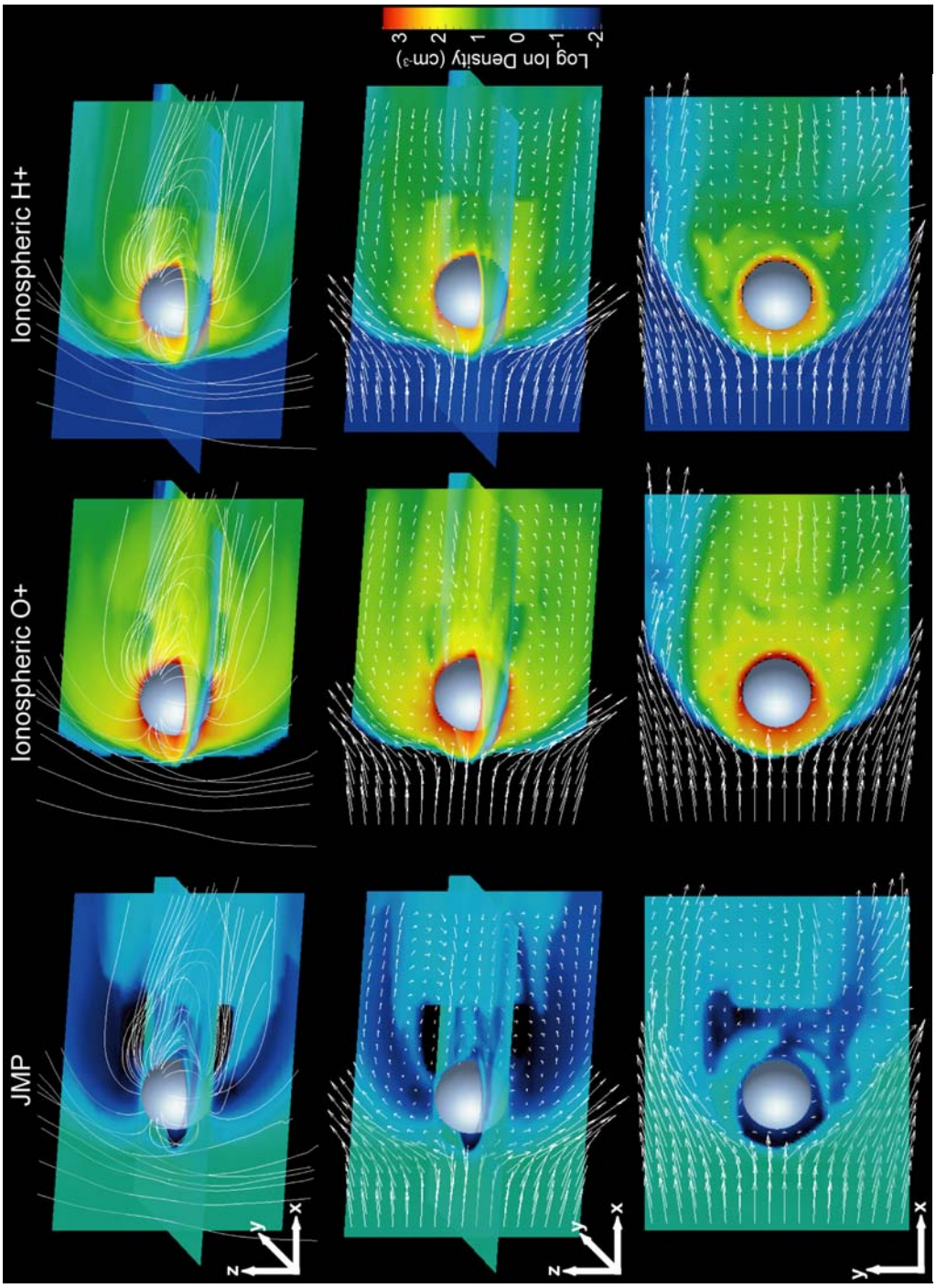

Figure 5.1: Discuss the field morphology, ion density and side/top down flow patterns for each ion species.

the surface at *all* latitudes. Implantation of such energetic and heavy ions from the Io plasma torus onto the flow facing hemisphere of Ganymede may be responsible for the darkened albedo observed via ground based telescopes as well as by Voyager and Galileo spacecrafts [*Morrison et al.*, 1974; *Millis and Thompson*, 1975]. However, the cause of the observed asymmetry in Ganymede's albedo is still heavily debated [cf. *Bagenal et al.*, 2004, and references therein for a detailed discussion].

The second row in Figure 5.1 pictures the ion density for each species, as well as the flow velocities projected in the x-z plane. The arrows show the direction of the flow and the size of the arrows scale relative to the magnitude of the velocity for each species. The deflection of the JMP in the upstream region where it approaches Ganymede's magnetopause is clearly illustrated. The convection of JMP over the poles and down tail can be seen along with the flow of the ionospheric H^+ and O^+ ions out of the poles being convected down tail. As the magnetic fields in the tail reconnect, the ion flow is redirected along closed field lines back toward Ganymede. It is through this process that the JMP gains access to Ganymede's magnetotail and the polar ionospheric outflow of O^+ and H^+ ions is trapped into populating Ganymede's magnetosphere. Ganymede's magnetic field configuration in the magnetotail and the location of reconnection is illustrated in Figure 5.2 and discussed further in the next section. The H^+ ion velocities track closely with the boundary between open and closed fieldlines leading to the tail reconnection region, while the heavy species flow down-tail and are redirected near the equatorial plane. This phenomenon was also noted by *Shay and Swisdak* [2004] when modeling the effects of the presence of heavy ions on reconnection.

In row three the view is shifted to look down upon the equatorial plane and show the density and flow for each modeled ion species. Again the deflection of the upstream JMP is noticeable as the arrows indicate the motion of the flow around Ganymede's magnetosphere. Ganymede's flow facing magnetosphere shields out the bulk JMP flow in the equatorial plane. In the magnetotail region the JMP gains access, and the flow of JMP appears quite asymmetric. Asymmetric flows in the equatorial magnetotail are visible in the ionospheric H^+ and O^+ as well, and are due to the ion cyclotron motion and finite

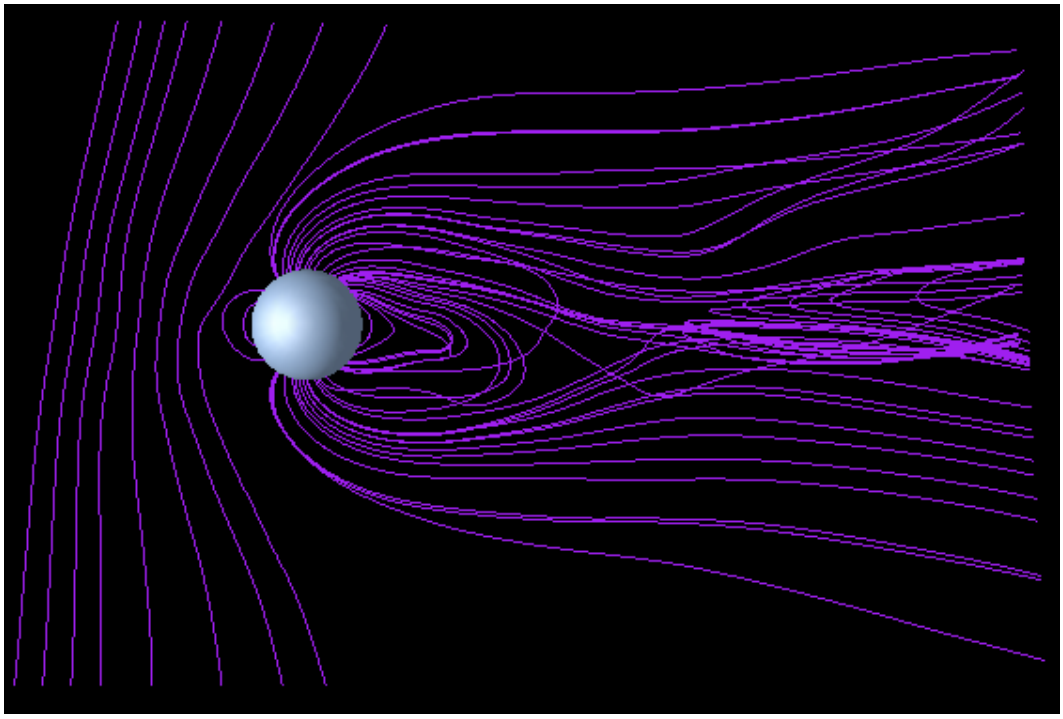

Figure 5.2: A schematic of Ganymede's magnetosphere illustrating the length of the magnetotail and location of reconnection in the magnetotail lies at ~7 R_G (+/- 2 R_G). The variability in this location is dependant on the upstream conditions, i.e. where Ganymede's location is with respect to the Jovian plasma sheet.

Larmor radius effects. The mass difference between the ionospheric H^+ and O^+ makes the O^+ Larmor radius a factor of 16 larger than that of H^+, and is responsible for the differences in flow asymmetries in the equatorial flow figures. Such flow asymmetries would not be present in an ideal MHD model where the ion cyclotron motion is averaged out.

5.2 Ionospheric Outflow

In order to better understand the flow of ionospheric ions away from Ganymede, the net flux of each ion species was determined. The flux of the ionospheric H^+ and O^+ ions was calculated at a distance of 24 R_G in order to determine the amount of ionospheric ions lost from the system and picked-up by the Jovian magnetosphere. This ensured that the flux was determined further down the magnetotail than the location of reconnection, and that the ions flowing out of the system would not become trapped on newly closed fieldlines and be redirected back towards Ganymede. Figure 5.2 illustrates Ganymede's magnetic field configuration, and indicates that the location of reconnection and the extent of Ganymede's closed magnetosphere lie at ~7 R_G (+/- 2 R_G as the upstream Jovian conditions vary). At this distance away, it was evident that Ganymede was losing on the order of 10^{26} ions/s of ionospheric O^+ as it was H^+. There were ~4 times more O^+ ions than H^+ ion exiting the system.

The flux of ionospheric H^+ and O^+ was also determined near the surface of Ganymede, at a distance of 3 R_G. The factor of ~4 difference between the rate of O^+ and H^+ ions flowing out of Ganymede's ionosphere was still present, however some of the outflow at this distance would become trapped in Ganymede's magnetosphere. The difference in outflow rates is evident when examining the ion population of Ganymede's magnetosphere in the first row of Figure 5.1, where the ionospheric O^+ density is shown to be the dominant species in Ganymede's magnetosphere by a factor of 2 to 8 (depending on the region of the magnetosphere). Since the ionospheric outflow supplies

Ganymede's magnetosphere with plasma, the difference in the outflow rates of O^+ and H^+ is represented in the ion density distribution.

While the net ionospheric loss was calculated to be on the order of 10^{26} O^+ and H^+ ions/s, these values were variable depending on the location of Ganymede with respect to the Jovian plasma sheet. Under Jovian plasma sheet upstream conditions, Ganymede's ionospheric outflow rates dropped by a factor of 2. Also note that the flux calculations from the simulation occur at instants in time, which cannot fully illustrate the loss due to quasi-periodic reconnection events driven in the magnetotail. An increase in the flux of ions is seen in the simulations during these events, with the above numbers representing a nominal loss flux. The average ionospheric outflow rate from the simulations can be compared to the sputtering rate independently determined from observations made by the Energetic Particle Detector and Plasma Experiment on Galileo. Since sputtering of surface ice is the main source for Ganymede's tenuous atmosphere, it is important to demonstrate agreement between source rates and the loss rates produced in our simulation. *Paranicas et al*. [1999] determined that the sputtering rate should be ~2 × 10^{26} water molecules/s in agreement with calculations by *Ip et al*. [1997]. Hence the multi-fluid simulations produce ionospheric outflows that are in good agreement with the sputtering rate.

The values calculated from the simulation for ionospheric loss are dependant on both the upstream flow conditions of the rotating Jovian magnetosphere (mentioned in the last paragraph) and the ion composition of Ganymede's ionosphere. The ionospheric composition used in the simulation will in part determine the relative fluxes of each of the ionospheric species. The reason the ionosphere was set with a 4:1 ratio of O^+ to H^+ is that much of the neutral H and H_2 will have enough energy from sputtering and dissociation that they will escape the system prior to being ionized [*Eviatar et al.*, 2001].

JMP ions lost to Ganymede were also calculated for the simulation, with ~ 2 × 10^{26} ions/s passing into the ionosphere. This value varies by nearly an order of magnitude depending on where Ganymede is located relative to the Jovian plasma sheet, with fluxes as small as 5 x 10^{25} in the lobe. This bulk flux into Ganymede is important for it drives

processes like sputtering, excitation of aurora and airglow. We do not expect this number to be exactly balanced by the net ionospheric loss rate, since not all sputtering products are lost or even populate the ionosphere. A fraction of sputtering related products recombines and precipitates back to the surface as a water frost layer. This result of surface processing has been observed in albedo variations between the well shielded equatorial latitudes compared to the less shielded polar latitudes [*Pappalardo et al.,* 1998; *Bagenal et al.,* 2004], where regions undergoing more sputtering and frost formation are brighter than shielded regions which appear darker. In addition, processes like sputtering and aurora are also driven by electron precipitation and the precipitation of the energetic tails of the ion distributions not incorporated in the above flux calculation. Keep in mind that ions and electrons that pass into the ionosphere are lost to the simulation; the physics and chemistry associated with generating aurora and producing surface sputtering are not yet included in the formulation driving the simulation.

5.3 Synthetic Spectrograms

Understanding the composition and energization of Ganymede's polar ionospheric outflow has been the subject of significant debate, as elaborated on in section 2.1. Note that the G2 flyby had the closest approach of all the Galileo flybys of Ganymede, passing 264 km from the surface while flying over the polar cap. This location enabled the spacecraft to observe the polar ionospheric outflow, however the lack of ion mass/species information on the observed outflow generated several interpretations of the observation [*Frank et al.*, 1997; *Vasyliunas and Eviatar*, 2000; *Eviatar et al.*, 2001]. The multi-fluid approach allows direct comparison of the above plasma flows with *in situ* observations made by the Plasma Experiment which measures particle fluxes versus energy. This comparison yields insight into Ganymede's ionospheric composition and atmospheric evolution by placing constraints on atmospheric/ionospheric models. As shown in the previous section, this outflow is also important for populating Ganymede's magnetosphere. Ions not trapped in Ganymede's magnetosphere are picked up by the

Jovian magnetosphere and may play a role in the local perturbation of Jupiter's magnetosphere expressed through the auroral footprint emissions [*Clarke et al.*, 2002].

In order to determine the energy distributions for each ion species in the simulation for this comparison, the density, temperature, and velocity for each ion species was sampled along the coordinates of the G2 flyby. Assuming a Maxwellian distribution for the ions, a probability distribution was determined over an energy (E) range of 10 eV to 10^5 eV (100 keV) to correspond to the sensitivity range of the Plasma Experiment such that

$$\mathcal{P}_i(\mathrm{E},\mathrm{x}) = \frac{e^{-\left(\left(\mathrm{V}\left(\mathrm{E},m_i\right)-\mathrm{V_i(x)}\right)^2/\left(2\mathrm{V_{Ti}(x)^2}\right)\right)}}{\mathrm{V_{Ti}}\left(\mathrm{x}\right)^3\left(2\pi\right)^{3/2}}. \tag{19}$$

Here x corresponds to positions along the spacecraft trajectory, V_{Ti} is the ion thermal velocity at each location (x) along the trajectory, and V_i is the magnitude of the ion velocity at each location. V is the velocity that corresponds to the energy in the range being integrated over and the mass of each ion species such that

$$\mathrm{V}\left(\mathrm{E},m_i\right) = \sqrt{\frac{2\mathrm{E}}{m_i}}. \tag{20}$$

To obtain the flux of particles per electron volt (N_i), which is in units of ions/s/eV/cm^2, the probability distribution was multiplied by the number density for each ion and the square of the velocity V, and divided by the ion mass. This expression

$$N_i(E,x) = \frac{n_i(x)V(E,m_i)^2}{m_i} \times \mathcal{P}_i(E,x) = \frac{1}{(2\pi)^{3/2}} \frac{1}{m_i V_{Ti}(x)^2} \frac{n_i(x)V(E,m_i)^2}{V_{Ti}(x)} e^{-\left(\left(V(E,m_i)-V_i(x)\right)^2/\left(2V_{Ti}(x)^2\right)\right)} \quad (21)$$

can then be summed over all the ion species to obtain an energy spectrogram that is directly comparable to the observation of the Galileo Plasma Experiment.

The simulations keep track of enough information to generate the above described synthetic spectrograms; they also enable us to split the full ion spectrogram into its individual ion components. Figure 5.3 illustrates this; the top figure reproduces the ion spectrogram from the Plasma Experiment during the G2 flyby (permission from *Paterson*), beneath it is the synthetic ion spectrogram determined using equation (21) along the G2 trajectory through the simulation. The bottom three figures split the full spectrogram into spectrograms for the JMP, ionospheric H^+ and ionospheric O^+ ions respectively. The y-axis plots is the log of the energy ranging from 10 eV up to 10^5 eV, and the x-axis is the radial distance from Ganymede through the G2 flyby. The color bar is the same for all of the model spectrograms, and maps the log of the ion flux per eV (or, ions/s/eV/cm^2).

Starting from the left hand side in Figure 5.3, the spacecraft is outside of Ganymede's magnetosphere and measures the upstream JMP conditions. The horizontal dotted black lines in the observed spectrogram represent the mean energies for two ion masses determined for the velocity of the Jovian rotational magnetosphere. The top line represents 16 amu O^+ ions, while the bottom line indicates the energy of 1 amu H^+ ions for a given velocity. These lines are meant as guides for interpreting the JMP composition and are not applicable when the spacecraft passes into Ganymede's magnetosphere. The vertical magenta lines represent the magnetopause boundary crossings as confirmed by the coincident magnetometer data. The low energy population in the center of the plot has contributed to the outflow debate; without also knowing the

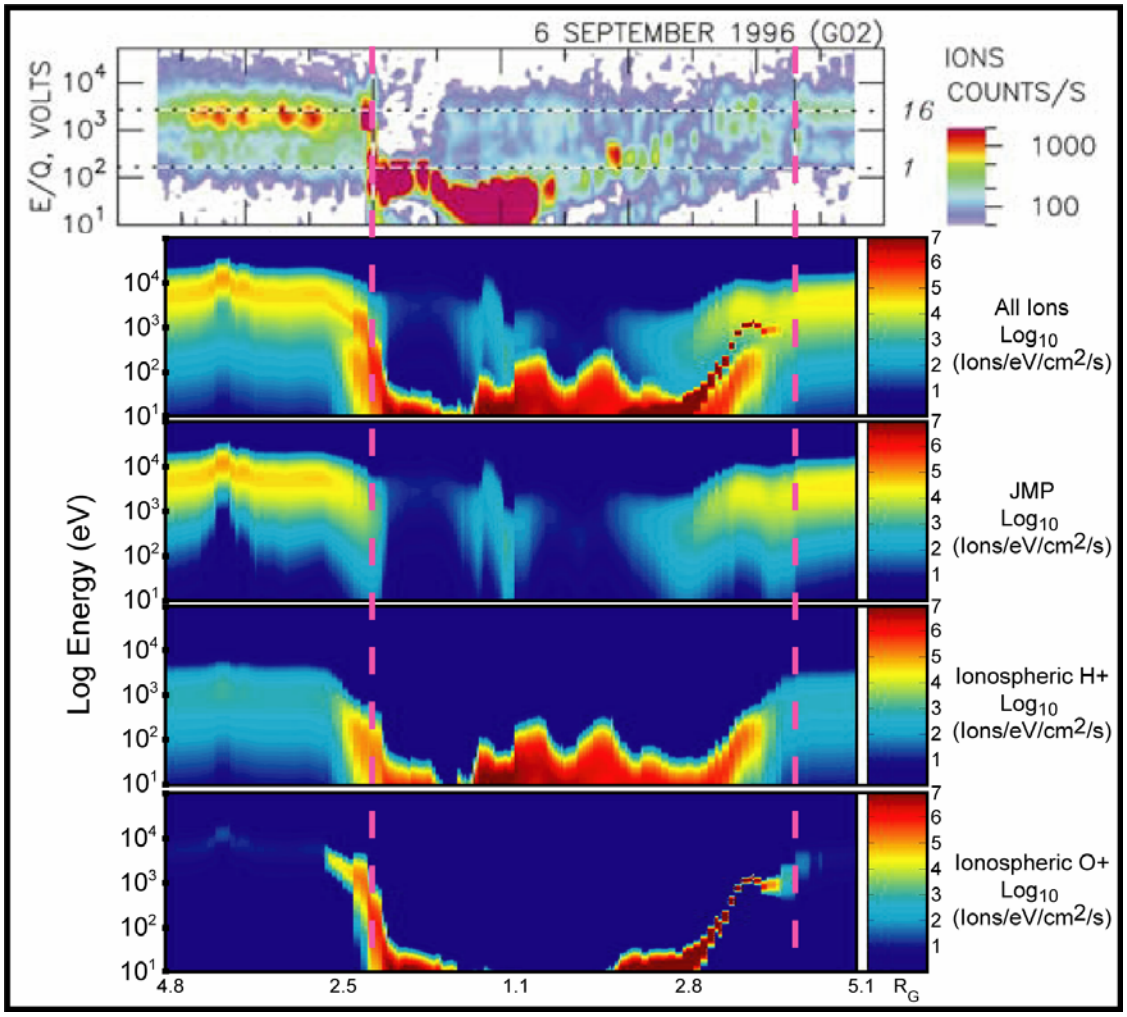

Figure 5.3: Comparison between the ion energy spectrogram observed by the Plasma Experiment on the G2 flyby and those predicted by the model.

mass or the velocity of the observed ion outflow, extrapolations to obtain ion composition from the energies in the spectrogram could not be uniquely interpreted [cf. *Frank et al.*, 1997; *Vasyliunas and Eviatar*, 2000]. Comparing the observed spectrogram to the full synthetic spectrogram, the simulation magnetopause crossings are well correlated to those observed by the Galileo spacecraft. The upstream population in the synthetic spectrograms is comparable to the observed upstream population, with the peak flux corresponding to energies defined by the modeled rotational flow velocity of the Jovian magnetosphere and the ion mass. The low energy population situated near the closest approach in the modeled spectrogram has the same energy range as the observed ionospheric outflow population.

Further examination of the low energy population is performed by examining the constituent ion species and their contribution to the ionospheric outflow, shown in Figure 5.3 in the bottom three plots. Notice that very little of the JMP is present over Ganymede's polar cap, the low energy population is entirely composed of ions sourced at the ionosphere. The ionospheric H^+ appears to makes up the bulk of the low energy population between 10 and 100 eV, however, most of the ionospheric O^+ is just below the threshold of the instrument's sensitivity (~10 eV). The simulation tracks the energy range of the ionospheric O^+ over the polar cap to be between 3 and 12 eV. This raises interesting possibilities for reinterpreting the ionospheric outflow which address some of the concerns raised in both *Frank et al.* [1997] and *Vasyliunas and Eviatar* [2000].

Some of the major concerns raised after and even in *Frank et al.'s* [1997] interpretation of the ionospheric outflow were due to the lack of O^+ detected in the outflow. The first concern raised was that ionization rate required to support the outflow of H^+ was not feasible, and the second dealt with oxygen accumulation at the surface *Vasyliunas and Eviatar* [2000]. The assumption that Ganymede's ionosphere is composed almost entirely of O^+ and O_2^+ ions comes from the hypothesis that sputtering of surface ice and dissociation of water group molecules imparts enough energy on neutral H and H_2 that it escapes before becoming ionized [*Eviatar et al.*, 2001], hence the concern over *Frank et al.'s* [1997] identification of the outflow as H^+. However, recent

laboratory studies have demonstrated that surface sputtering may produce more H^+ and H_2^+ than initially thought [*Herring-Captain et al.*, 2005], especially at the low temperatures present on Ganymede's surface. The second concern stated that if the outflow consisted of H^+ ions it would leave behind an accumulation of meters of oxygen on the surface, a feature not found in any surface spectral analysis. *Vasyliunas and Eviatar* [2000] argue that to solve both of these concerns the outflow population should be reinterpreted as a low energy population of O^+, moving at a quarter of the speed noted for the H^+ interpretation. This would keep with the observed energy range of the outflow population, solve the H^+ ionization rate issue and make sure that meters of oxygen were not left accumulating on Ganymede's surface.

However, the idea that O^+ could be flowing out of Ganymede's polar ionosphere at energies just below the threshold of the Plasma Experiment was not considered. The model predicts that O^+ ions are accelerated to energies of 3 to 12 eV over the polar cap (at G2 flyby altitudes), energies just at or below the detection threshold of the Plasma Experiment. H^+ ions from the ionosphere reach energies of 10 to 100 eV at the same altitudes and under the same model conditions. With this in mind, an alternate interpretation of the Plasma Experiment observation is presented. The ionosphere over Ganymede's polar cap, assumed to be composed of mostly O^+ ions and some H^+ ions, produces an ionospheric outflow of H^+ and lower energy O^+. The number fluxes of these species were calculated in the previous section, and it was determined that their relative abundance in the ionosphere was proportional to their relative outflow rates. While it appears necessary to have a measurable H^+ component in Ganymede's ionosphere to account for the ion energies observed by the Plasma Experiment, the ratio of H^+ relative to O^+ is not well constrained. More research is currently underway to determine to relative abundance of H^+ in Ganymede's ionosphere resultant from direct ionization from energetic particle interactions with the icy surface. However, regardless of the exact composition, the presence of a strong O^+ ionospheric population is generally agreed upon [*Eviatar et al.*, 2001; *Cooper et al.*, 2001] and the outflow of ionospheric O^+ helps in addressing the issue of oxygen building up on Ganymede's surface. H^+ may be escaping

in the observable range of 10 to 100 eV, but O^+ is also obtaining energies corresponding to velocities greater than escape velocity, where $v_{escape} = \sqrt{\frac{2GM_G}{R_G}}$. Hence oxygen is likely not building up on Ganymede's surface; it is escaping at energies just below the detection range of the Plasma Experiment.

5.4 Energy Distribution in the Rest of Ganymede's Magnetosphere

The energy distribution observed during the G2 flyby of Ganymede's polar cap was significantly different than that observed in the closed field region of Ganymede's flow facing magnetosphere. The energy distribution observed on the flow facing part of Ganymede's magnetosphere was also much different than that observed in the magnetotail (or wake) region. Figure 5.4 compares the G8 Plasma Experiment observation, which occurred on the upstream side of Ganymede at low latitudes, to model predicted energy spectrograms in the same manner as Figure 5.3 (cf. Figure 2.2 for flyby locations). The spacecraft observed enhancements in the ion counts per second around the keV energy range directly after crossing into Ganymede's magnetosphere and just before exiting. The central region of the spectrogram, which corresponds to the spacecrafts closest approach to Ganymede and is located well within Ganymede's magnetosphere, shows almost no ion counts in the $>$ 100 eV energy range. There appears to be some flux in the range of 10 to 100 eV near closest approach (~1.6 R_G), however that borders on the lower limit of the instruments sensitivity.

In the modeled spectrogram (second panel in Figure 5.4), there is a significant ion signature between the magnetopause crossings. In the bottom three panels it is shown that the modeled signature at closest approach is representative of ionospheric H^+ and O^+ ions trapped along closed fieldlines in Ganymede's magnetosphere. The energy of the ionospheric O^+ in this region is at higher energies than the ionospheric H^+, and the ratio of energies implies that they have similar velocities. The energies of the ionospheric O^+ and H^+ just inside the magnetopause crossings are consistent in energy with the observed

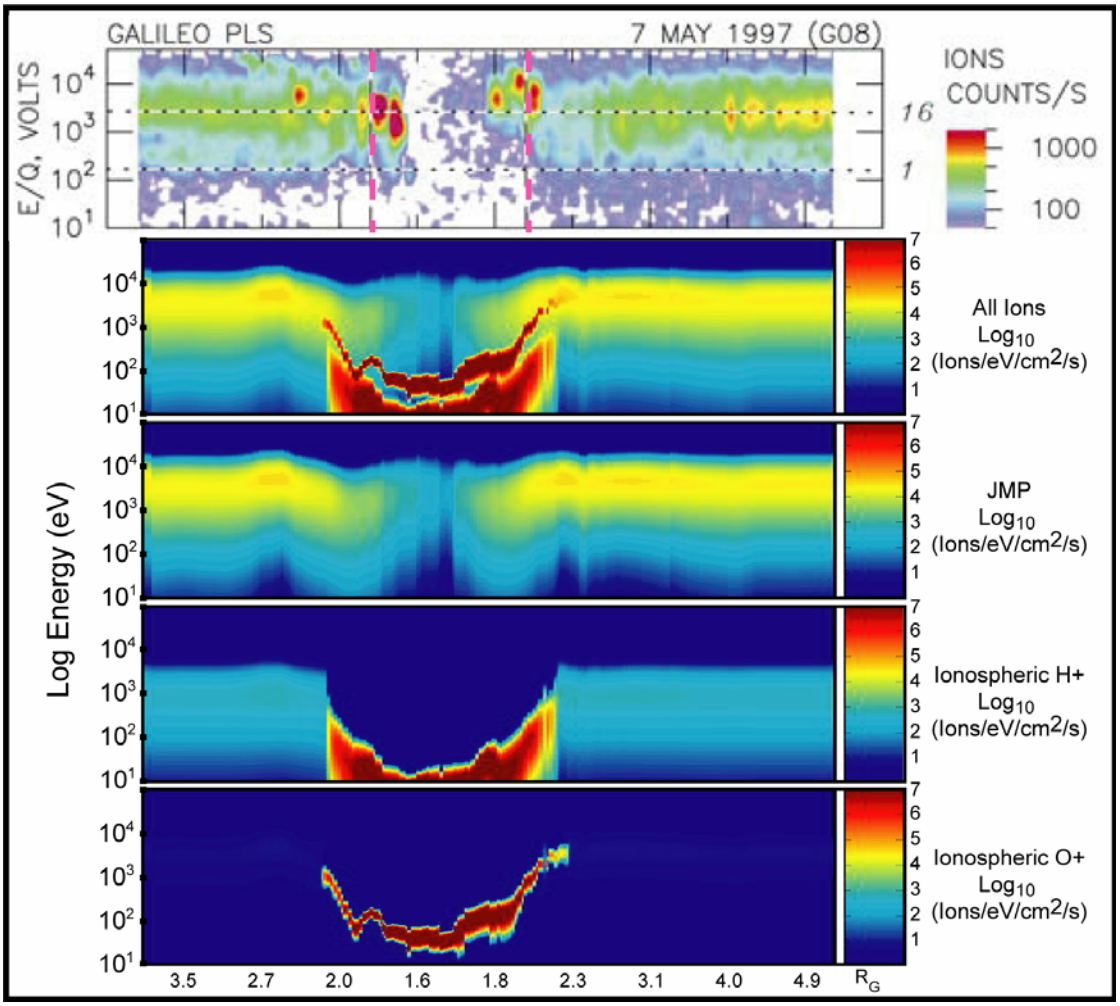

Figure 5.4: Comparison between the ion energy spectrogram observed by the Plasma Experiment on the G8 flyby and those predicted by the model.

enhancements, on the order of keV. The lack of high energy ions near closest approach is also predicted by the model, with the O^+ and H^+ energies lower than 100 eV near closest approach. Even though there appears to be a drop out of observational data inside Ganymede's magnetosphere for this particular flyby, the model provides information on the bulk energies of the various ion species as the spacecraft makes its closest approach. Simply stated, the model predicts that the energies of the ions near closest approach will be lower than 100 eV, and possibly below the detection threshold for this particular flyby.

Figure 5.5 compares the observed ion energies from the G7 flyby to those derived from the model along the same trajectory. It is first evident when comparing the G7 and G8 (Figure 5.4) observations that the ion energy distributions are significantly different in the magnetotail versus on the flow facing side. The ions in Ganymede's magnetotail are observed to have much higher energies than the trapped ions in the flow facing magnetosphere (G8). Also the morphology of the energy distribution during the G7 flyby changes while the spacecraft resides in Ganymede's magnetosphere, i.e. between the magnetopause crossings. After the first magnetopause crossing the ion flux appears to have a consistent energy at ~100 eV until the spacecraft reaches 2.8 R_G. Then the signature changes, the ions start increasing in energy as the spacecraft approaches the magnetopause and crosses back out into the Jovian magnetosphere. Two ion populations are clearly visible between 4 and 6 R_G; the ratio of their mean energies corresponds approximately to a factor of 16 difference in mass given that they are moving at the same velocity. Another interesting feature observed in this flyby was that a small flux of ions was observed at similar energies as the incident JMP within Ganymede's magnetosphere.

The modeled energy distributions are well correlated to the G7 observations. The structure of the modeled spectrogram also appears to be divided into two regions within the magnetopause crossings. Moving from left to right, the first region resembles the signature of the ions over the ionospheric outflow in the G2 flyby (see Figure 5.3). That is, the model predicts the region after the first magnetopause crossing will have an ion population with a constant energy in the 10s to 100 eV range until about 2.2 R_G. The second half of the modeled spectrogram appears similar to the ions modeled in the flow

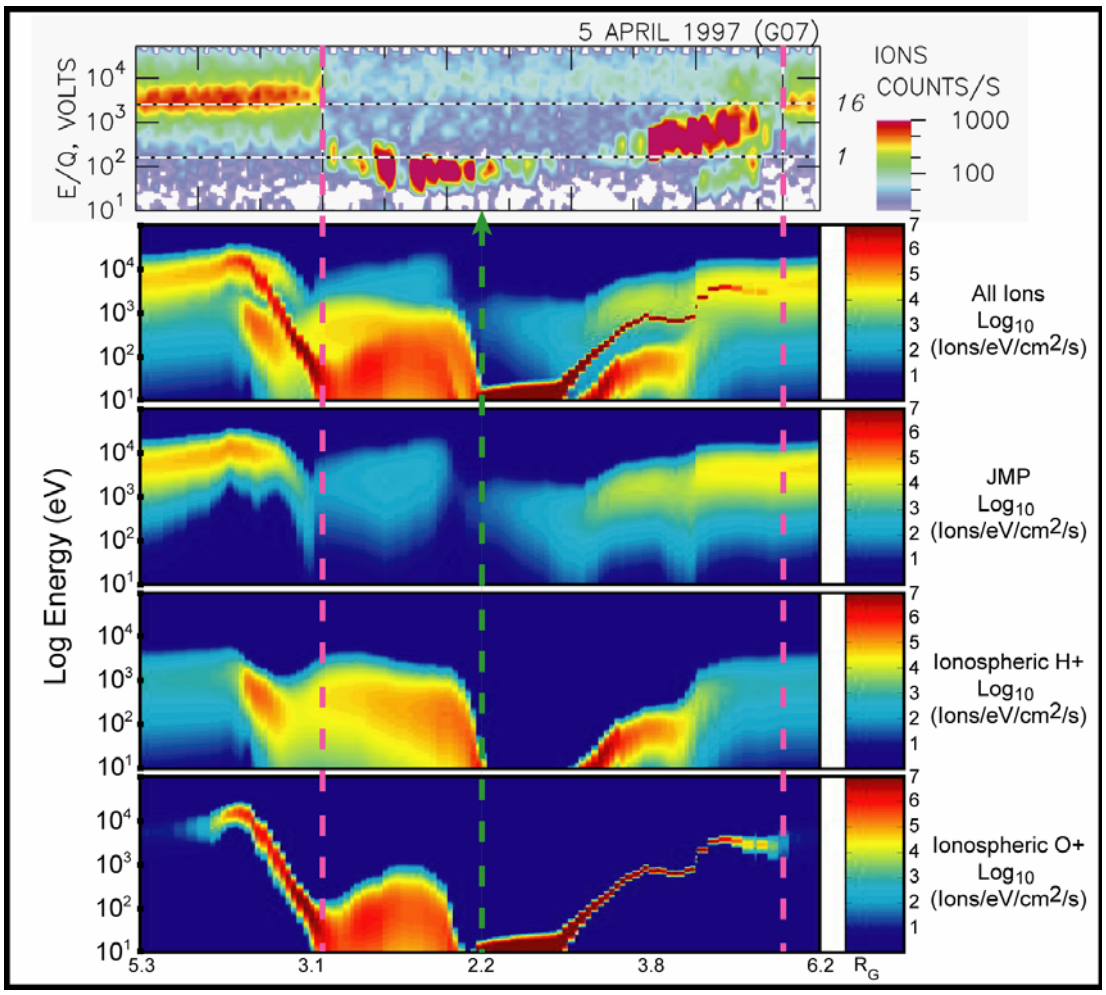

Figure 5.5: Comparison between the ion energy spectrogram observed by the Plasma Experiment on the G7 flyby and those predicted by the model.

facing hemisphere (see Figure 5.4). In this region a second ion population can be seen at lower energies, and the energies for both ion species are rising as the spacecraft moves further away from Ganymede and approaches the magnetopause. The higher energies found in ions in the first region of Ganymede's magnetotail region are likely due to acceleration process resultant from ionospheric outflow and convection and reconnection in the tail. The spacecraft appears to transition from a region of fieldlines being convected down-tail, to a region of reconnected fieldlines with ion energy signatures consistent with those of closed fieldlines (similar to those found in the modeled G8 flyby). Also, the spectrogram for the modeled JMP (the third panel in Figure 5.5) shows that a fraction of the JMP is present within Ganymede's magnetosphere at the high latitudes of this flyby.

5.5 Discussion

This chapter addressed the ion population, ionospheric outflow and ion energy distributions within Ganymede's magnetosphere. In order to understand the plasma population and distribution within Ganymede's magnetosphere, it was important to account for the various sources of plasma into the system. While Ganymede's magnetosphere is small in size and strength relative to the magnetic field of the rotating Jovian magnetosphere, it still provides enough shielding to exclude much of the JMP at low latitudes (< 45°). The JMP gains access through two processes: some precipitates through Ganymede's cusps and some convects down tail and becomes trapped along reconnected fieldlines. Ganymede's magnetospheric plasma is composed of mostly ionospheric O^+ and H^+ ions. These ions are sourced at the ionosphere, flow out at the polar cap regions, and are convected down tail and eventually trapped on reconnected fieldlines. The flux rate of the ionospheric O^+ and H^+ was calculated to be on the order of 10^{26} ions/s for the simulation, which is well correlated to the independently determined sputtering rate for the surface of Ganymede that actively supplies the atmosphere and ionosphere [*Ip et al.*, 1997; *Paranicas et al*. 1999].

While examining the density distribution and flow of ions in Ganymede's near space environment was useful, it was not comparable to observational data. A method for comparing the model to the observations of the Plasma Experiment was developed, which examined the ion energy distributions for 3 of the Galileo flybys. This provided a means for reinterpreting the ionospheric outflow observed on the G2 flyby. We found that likely both ionospheric H^+ and O^+ were flowing out of the polar caps. However the O^+ outflow was at energies below the detection threshold of the Plasma Experiment. This technique was also used to examine both upstream (G8) and magnetotail (G7) flybys. The predicted energy spectrograms were well correlated to the observed spectrograms, and enabled the identification of ion species and representative energy signatures for different regions of Ganymede's magnetosphere.

Chapter 6

AURORA/PRECIPITATION PHENOMENON

The previous chapter examined the ionospheric outflow, the distribution of various ion populations within Ganymede's magnetosphere, and the ion energy distributions for various regions within Ganymede's magnetosphere. In this chapter, plasma acceleration due to reconnection is examined, with particular attention to energetic particle precipitation and the generation of aurora. Qualitative comparisons are made between the Hubble Space Telescope observations of Ganymede's UV aurora and the model predicted aurora. Included is discussion of differences between the aurora morphology on the flow facing (or upstream) hemisphere versus the downstream hemisphere, the role of Ganymede's cusps in generating aurora, and the global picture of ion acceleration in Ganymede's magnetosphere.

6.1 Ganymede's Upstream Facing Hemisphere Aurora

Another way to check the validity of the model and understand the global structure and dynamic nature of Ganymede's magnetosphere is to examine the position and variability of the aurora. This can be performed by qualitatively comparing the model to auroral observations and examining the role of variations in the incident Jovian magnetospheric conditions on auroral morphology. While auroral chemistry is not incorporated into the multi-fluid simulations, the location that aurora would likely occur is determined by examining the energy of ions moving through the inner (ionospheric) boundary. The location of energetic plasma penetrating through the ionosphere in the model should correspond to plasma precipitation events. Again, fluid simulations only directly model

the bulk or average properties of the plasma with protons obtaining a few keV bulk energies and heavy ions a few 10's of keV.

Figure 6.1 illustrates the temperature (in log eV) for each of the ion species mapped at the altitude of the ionosphere on the upstream (or *flow*) facing hemisphere of Ganymede compared to the *Feldman et al*. [2000] auroral observation. All of the auroral observations from *Feldman et al.* [2000] were of the upstream facing hemisphere [cf. Figure 2.6]. The incident JMP experiences heating to the keV range associated with flow side reconnection. This corresponds to an increase in incident JMP energy of between a factor of five and an order of magnitude. The JMP is then funneled to the cusps where it gains access down through the ionosphere. Ganymede's cusps are visible in Figure 6.1, and are significantly larger relative to the size of the satellite than those at the Earth or Jupiter. This is due to comparable strengths of the incident Jovian magnetic field and Ganymede's surface field as well as the shock free sub-Alfvénic interaction. The cusps are located at ~ 45° latitude for the modeled orientation of the Jovian magnetic field, and this orientation corresponds to Ganymede being located in the southern lobe. In general cusps occur at high latitudes and have significant latitudinal and longitudinal extent. Their exact location is dependant on the orientation of the incident Jovian magnetic field.

Though the JMP is heated through magnetic reconnection and permitted to penetrate down through the cusps, relatively little heating was observed in either of the ionospheric plasma species on the flow side of Ganymede. Both the ionospheric O^+ and H^+ appear warmer in the closed field line region than in the open ones. This is due to the processes described in the previous chapter, namely, that the ionosphere of Ganymede is initially cold and is accelerated as it flows out of the poles, is convected down tail, and trapped along reconnected fieldlines. Hence the ionospheric plasma trapped in the closed fieldline region is warmer and more energetic and a fraction can precipitate down to the altitude of the ionosphere, whereas over the poles on open fieldlines the ionospheric plasma is flowing out and being accelerated away from the ionosphere (cf. Figure 5.1).

The HST aurora observations [*Feldman et al*., 2000] allow for a qualitative comparison between remote measurements and the simulation, as shown in Figure 6.1.

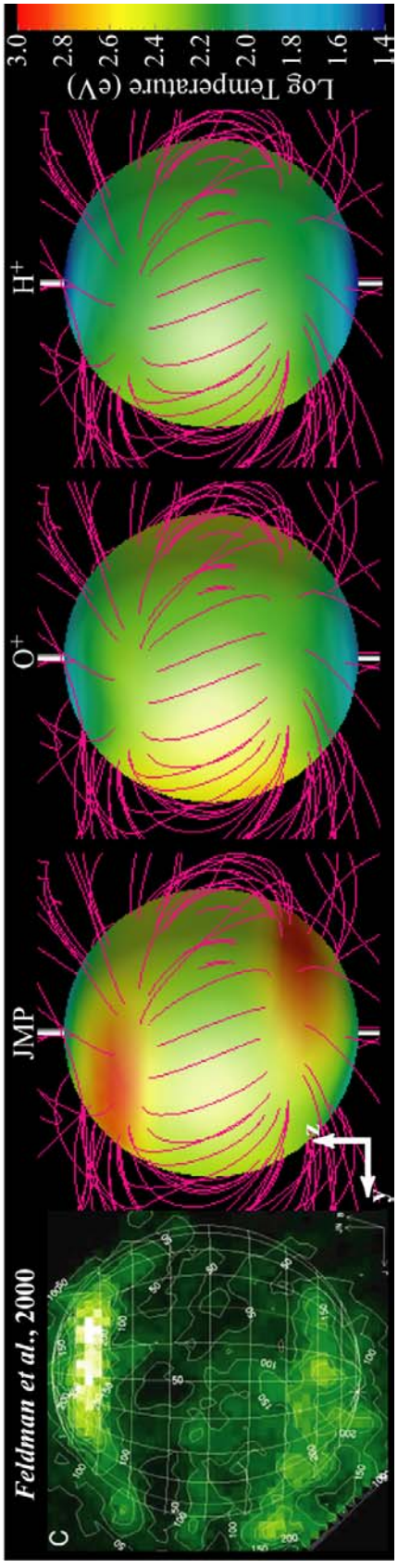

Figure 6.1: An HST observation of Ganymede's UV aurora [*Feldman et al.*, 2000] (left hand-side) compared to the temperature of each ion species for the trailing hemisphere of Ganymede; magnetic field line configuration is included to demonstrate the shape of the magnetosphere and location and size of the cusps [*Paty and Winglee*, 2004].

Since there was not a coincident measurement of the upstream conditions at Ganymede during the HST observation, the orientation of the Jovian magnetic field could only be estimated. Hence, while the orientation of the Jovian magnetic field in the simulation was likely not exactly consistent with that in the observation, the simulation produces key characteristics in agreement with those observed with HST. Namely, the longitudinal variability and a lack of limb brightening over the poles indicated by *Feldman et al*. [2000] are present in the simulation. While it was originally thought that both polar caps would be completely illuminated by aurora due to open field lines allowing direct access of JMP, Ganymede's magnetospheric behavior restricts the region of acceleration and access for precipitation.

Changing the orientation of the incident Jovian magnetic field in the simulation within the range provided by the tilt of the magnetic axis with respect to the spin axis of Jupiter, allows the location of the cusps to move and change shape as shown in Figure 6.2. The orientation and magnitude of the incident Jovian magnetic field (B_J) is labeled with the blue arrow in each image, representing Ganymede's location above, in and below the Jovian plasma sheet, respectively. The cusps wander due to periodic variations in the orientation and strength of the magnetic field in the incident flow of Jupiter's magnetosphere, whereas the sizes of the cusps vary due to the magnetic field strength and the plasma density of the incident flow. For example, when Ganymede is located within the Jovian plasma sheet the orientation of the incident magnetic field is anti-parallel to Ganymede's dipole field, which places both cusps at the sub-flow longitude (270° longitude, using left-handed spherical coordinates where 0° faces Jupiter). This is shown in the second view in Figure 6.2, where the high temperature regions appear at higher latitudes. The Jovian plasma sheet is also higher in density than the lobes and weaker in magnetic field strength, thus the Alfvén speed of the incident flow, where $V_A = \frac{|\mathrm{B}|}{\sqrt{\mu_o \rho_{tot}}}$, drops and the characteristic Alfvén Mach number approaches unity. This change in the characteristic flow properties is responsible for the cusps appearing smaller and at higher latitudes while in the Jovian plasma sheet. The periodic variability of not only the

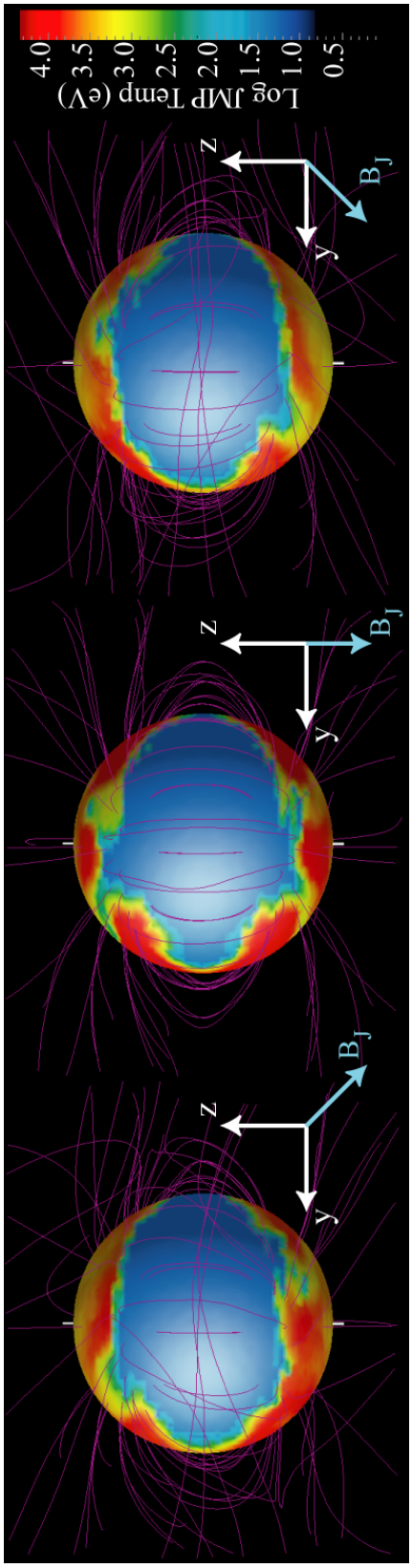

Figure 6.2: The modeled flow facing aurora of Ganymede for locations above, in, and below the Jovian plasma sheet, respectively. The color bar is log scaled to indicate the temperature in eV of the precipitating JMP. The blue arrows indicate the orientation and relative magnitude of the Jovian magnetic field (B_J) for each image.

incident magnetic field orientation, but also the incident magnetic field strength and the flow plasma density are responsible for the variability in longitude and size of the aurora between Hubble observations which spanned several hours [*Feldman et al*., 2000], enough time for significant variability in the Jovian magnetosphere local to Ganymede. It is shown in Figure 6.2 that when Ganymede is located far within the northern and southern lobes, the cusps become broadened in both latitude and longitude relative to when it is located in the plasma sheet.

6.2 Ganymede's Downstream Facing Hemisphere Aurora

There have been few Hubble Space Telescope observations of Ganymede's downstream hemisphere aurora, and to date none have been published. For this reason we chose to do a predictive study for the tail-side (downstream hemisphere) aurora. Later the actual HST image was provided for comparison, which is detailed in the end of this section.

The tail-side aurora is fundamentally different from the flow facing (upstream hemisphere) aurora in both form and generation process. The flow facing aurora involved plasma accelerated through flow side reconnection being funneled to the cusps, while the tail-side aurora occurs through the acceleration of plasma convected from the incident flow over the poles via reconnection in the tail. The convected fieldlines undergo reconnection in the tail, approximately 7 R_G downstream, and the associated JMP either returns to the Jovian magnetosphere or is trapped along newly closed fieldlines and accelerated as they 'snap' back toward Ganymede. This phenomenon is illustrated by the generic reconnection cartoon in Figure 6.3 as well as for Ganymede's magnetotail in Figure 5.2. The associated flow patterns calculated in the simulation are show for each of the plasma species in Figure 5.1 and discussed in detail in the previous chapter.

While density of the JMP entering Ganymede's magnetosphere is low when compared to the density of the ionospheric species populating the magnetosphere, Figure 6.4 shows the temperatures of each ion species looking the x-z plane and mapped onto the ionosphere. The accelerated JMP is greater than an order of magnitude more energetic

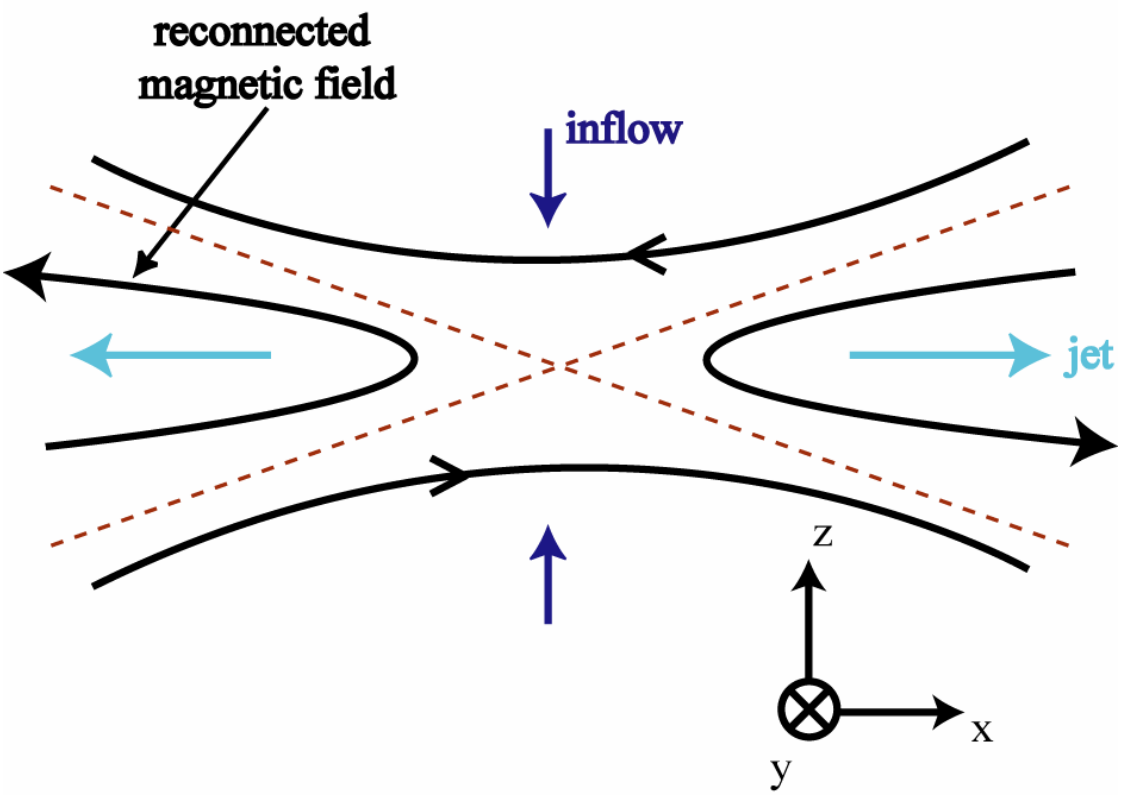

Figure 6.3: Schematic of reconnection in Ganymede's magnetotail.

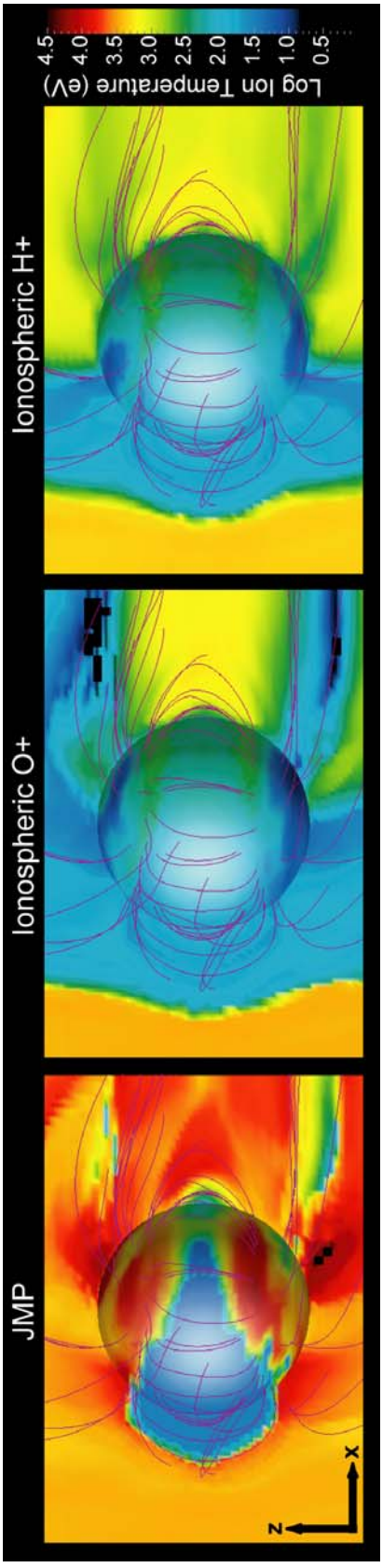

Figure 6.4: Discuss the energization of the various ion species, as well as precipitation as it pertains to the ionosphere and magnetospheric shielding.

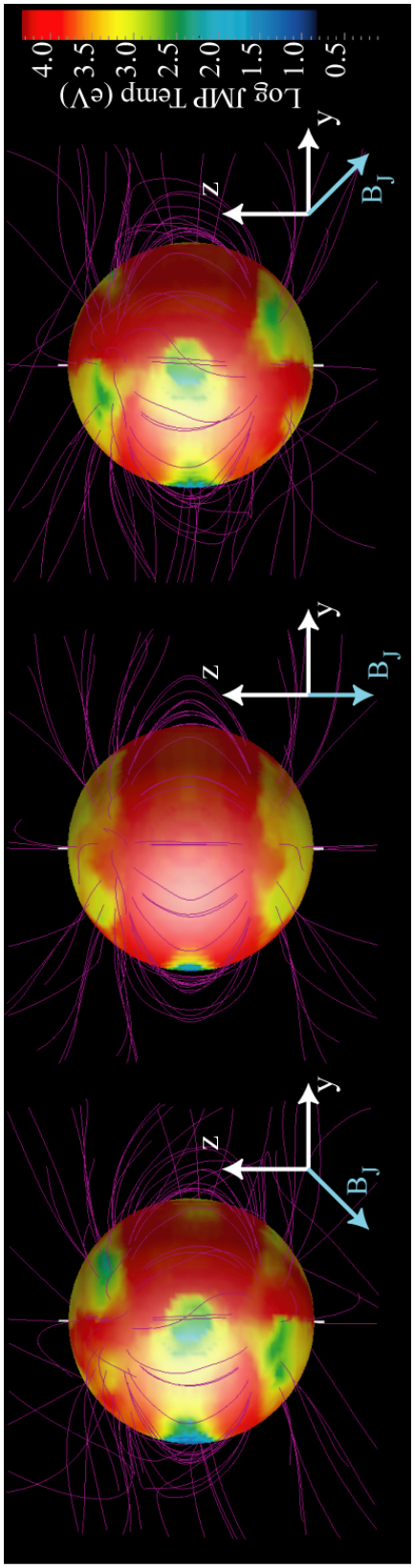

Figure 6.5: The modeled tail-side aurora of Ganymede for locations above, in, and below the Jovian plasma sheet, respectively. The color bar is log scaled to indicate the temperature in eV of the precipitating JMP.

that the ionospheric H^+ and O^+. We also can see the upstream acceleration of JMP and the funneling to the cusps that generate the flow facing aurora.

Rotating the view from Figure 6.4 and examining the flux of energetic JMP ions through the ionospheric boundary, we demonstrate predictions for aurora in the downstream hemisphere which are shown in Figure 6.5 for various orientations of the incident Jovian magnetic field (arranged similarly to Figure 6.2). The morphology of these tail-side aurora is much different from the flow facing aurora; these aurora seem to follow along the separatrix, which is the boundary between open and closed fieldlines. The most recently closed fieldlines from the tail reconnection process map to this region, and the newly trapped and heated JMP travels down those fieldlines and precipitates into the ionosphere. High latitude aurora is predicted when Ganymede is located in Jupiter's magnetospheric lobe, which appear to move relative to the orientation of the incident Jovian magnetic field. The color bar in Figures 6.2 and 6.5 was kept consistent between the images for comparison, however some of the features in individual figures were lost on this scale. The central image in Figure 6.5 was reproduced in Figure 6.6 with a scaled color bar to better examine the features of Ganymede's tail-side aurora. It is shown that when Ganymede is located within the Jovian plasma sheet, the banded structure of the separatrix is most apparent. Again note that since this is a continuum treatment of the ion species, only the bulk properties are modeled. Therefore, there will be JMP ions of even higher energies than modeled in this fluid approach that reach the surface of Ganymede, which further enable sputtering and aurora generation.

While Hubble observation of the tail-side aurora have yet to be formally published, they have been presented at meetings and the images have been granted for the use of comparison in this thesis. This study was completed before the tail-side auroral images were released; it was only *after* the completion of this work that the image was shared for comparison to the model. Figure 6.7 shows a comparison of one of the flow facing aurora images to the observation of the tail-side aurora. It is clear that the morphology of aurora is significantly different from hemisphere to hemisphere, and that the simulation accurately predicts this morphological difference. Also, the integrated brightness of the

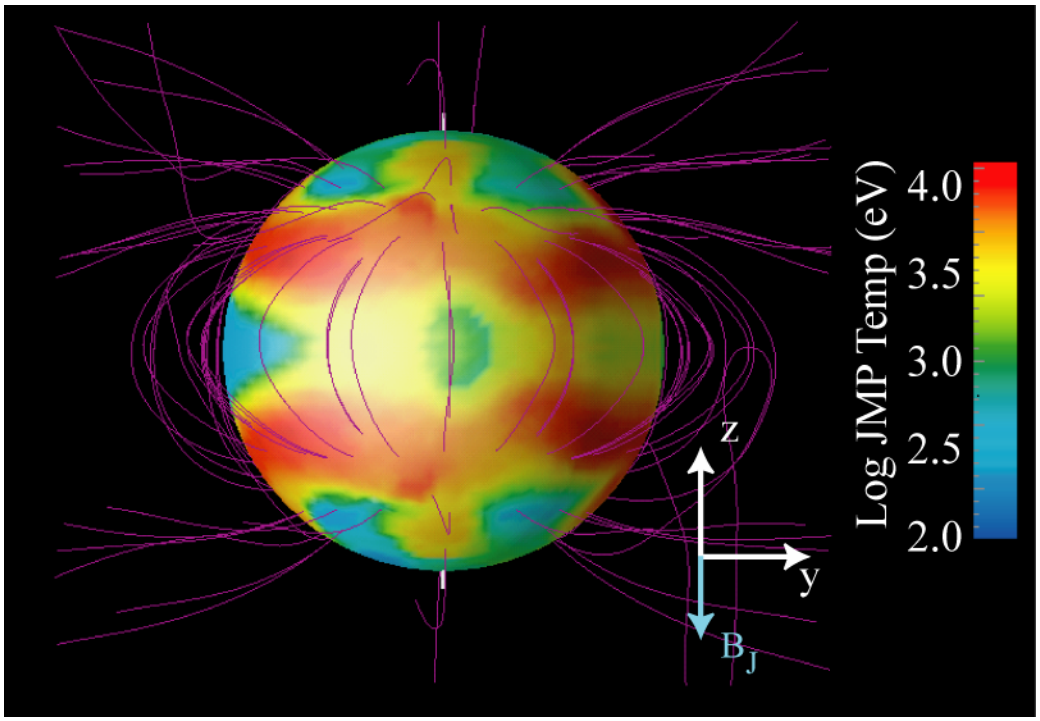

Figure 6.6: Ganymede's tail-side aurora reproduced from Figure 6.5 with a color scheme that better matches the maximum and minimum temperatures for this particular plot.

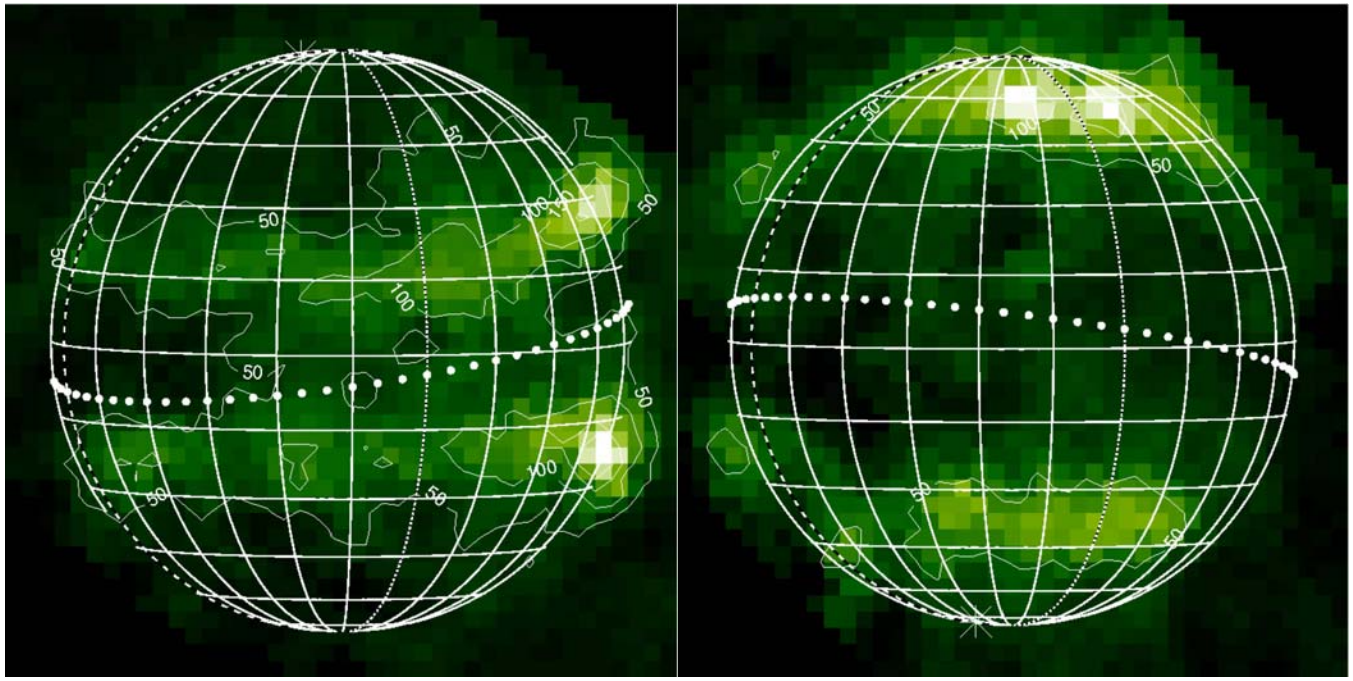

Figure 6.7: Comparison of the tail-side (a) and flow-facing (b) aurora as imaged by the Hubble Space Telescope [McGrath et al., 2002]. The asterisks represent the location of Ganymede's magnetic pole, while the dotted white line represents the magnetic equator. Both images were adjusted from their original form by subtracting out the reflected solar spectrum [*Retherford*, 2006, personal communication; *McGrath*, 2002].

tail-side aurora was observed to be brighter than the flow facing aurora, which is also consistent with the model predictions. The use of remotely observed aurora as a means to demonstrate the validity of the model is a first for global magnetospheric simulations. The scarcity of in situ data for this system makes it otherwise difficult to verify the model outside of the vicinity of the 6 Galileo flybys, but having this means for comparing aurora observations which are indicative of global processes in Ganymede's magnetosphere speaks to the overall accuracy of the ability of the model. This is especially true in this scenario where the model predictions were made without a priori assumptions of what the tail-side aurora would look like.

6.3 Summary of Plasma Precipitation and Aurora Results

This chapter discussed the characteristics of plasma acceleration and precipitation at Ganymede, specifically pertaining to the generation of aurora and surface processing through sputtering. The size and location of regions of Jovian magnetospheric plasma precipitation on Ganymede's flow facing hemisphere predicted by the model are similar in size, shape and variability to the observed UV emissions from *Feldman et al.* [2000], and appear to be linked to the size and location of Ganymede's cusps. Examining the distribution and the flow of all three modeled ion species, it was shown how JMP gains access to Ganymede's magnetosphere, and where it is heated and accelerated to higher energies than the plasma sourced from Ganymede's ionosphere. The morphology and process behind the generation of tail-side aurora was vastly different from that of the flow facing aurora. Predictions of the tail-side aurora were made, without prior knowledge of Hubble observations, and eventually compared to the unpublished observations, demonstrating excellent qualitative agreement in size, shape and integrated brightness.

Chapter 7

SUMMARY AND FUTURE WORK

The goal of this dissertation has been to examine the interaction of Ganymede's and Jupiter's magnetospheres using a combination of 3-dimensional multi-fluid simulations and the *in situ* and remote sensing data from the Galileo spacecraft and the Hubble Space Telescope. First, we examined the role of ion cyclotron motion in governing the magnetic morphology and dynamic response of Ganymede's magnetosphere through the development and implementation of a multi-fluid model. After benchmarking the model against the Galileo magnetometer data, it was then used to study the composition and distribution of the ion population in Ganymede's magnetosphere. A comprehensive study of the ion sources and sinks was performed, which led to a new self-consistent interpretation of the ionospheric outflow observations. Lastly, the model was used to predict the location of Ganymede's aurora by tracking the flux and energy of ions through the ionospheric boundary. The predicted auroral morphology was shown to be in agreement with that observed by the Hubble Space Telescope.

The findings presented in the previous chapters represent significant gains in understanding the Ganymede-Jupiter magnetospheric interaction; however several questions remain pertaining to the coupling of Ganymede into the larger Jovian magnetospheric system. This work should prove a useful platform for launching further investigations into this and other coupled magnetosphere systems. It also lends strong support to the continued incorporation of ion cyclotron motion in models and the use and further development of multi-fluid simulations for space physics applications.

7.1 Summary and Discussion

The major findings of this dissertation pertain to the influence of the rotating Jovian magnetosphere on Ganymede, the response of Ganymede's magnetosphere and ionosphere to the periodic variations in the upstream flow of Jovian magnetospheric plasma (JMP), and the acceleration of the JMP that leads to precipitation and generation of aurora.

We find that ion cyclotron motion plays an important role in influencing the size and shape of Ganymede's magnetosphere. This is due to the fact that the ion gyroradius in Ganymede's near space environment is on the order of 400 km in the incident JMP and varies up to thousands of kilometers near Ganymede's sub-flow magnetopause where the magnetic field strength approaches zero. Such large gyro-orbits enable the ions to sample across boundary layers and gradients, and the associated drift motions and accelerations prove to be important for the size and shape of Ganymede's magnetosphere. Neglecting such effects in the physical formulation of the model resulted in a predicted magnetopause location that was only two-thirds the altitude of Ganymede's magnetopause. In other words, without the associated ion gyro-physics the size of the magnetosphere is under predicted. Including the ion gyromotion also allows for asymmetries in the ion flow and shape of Ganymede's magnetosphere, asymmetries which are explicitly indicated in the Magnetometer [*Kivelson et al.*, 1998] and Energetic Particle Detector observations [*Williams et al.*, 1997b]. This is the first simulation that has consistently and accurately modeled Ganymede's magnetosphere for all of the Galileo magnetometer observations.

The multi-fluid model enables us to track the differential motion and acceleration of multiple ion species from multiple ion sources. By tracking the two major plasma sources (JMP and Ganymede's ionospheric ions) we determined that Ganymede's magnetosphere is primarily composed of ions sourced from its ionosphere. Ganymede's magnetosphere shields out most of the bulk JMP flow, especially at low (< 45°) latitudes on the flow facing hemisphere. However some JMP gains access to Ganymede's magnetosphere.

This occurs in two ways: on the flow (or upstream) facing hemisphere some JMP is funneled to and gains access through Ganymede's magnetospheric cusps, whereas on the downstream facing hemisphere some of the JMP becomes trapped along reconnected fieldlines that convect over Ganymede's polar caps back to Ganymede's magnetotail.

It is through the process of reconnection in the flow facing magnetopause and in Ganymede's magnetotail that the JMP gains the energy needed to precipitate down to Ganymede's ionosphere and generate the observed aurora. The process differs between hemispheres in that on the flow facing hemisphere the JMP is funneled to the cusps where it gains access to the ionosphere, whereas in the magnetotail the JMP flows along recently reconnected fieldlines and thus gains access to Ganymede's ionosphere along the separatrix (or boundary between open and closed fieldlines). The model was well correlated to the observations of Ganymede's flow facing hemisphere aurora [*Feldman et al.*, 2000], and described a mechanism that allowed the aurora to be variable in size, shape and location. The shape, size, and location of Ganymede's cusps are dependant on the upstream Jovian magnetospheric conditions, which are variable over the ~10 hour rotation period due to the Jovian plasma sheet essentially sweeping over Ganymede's orbital location. Hence Ganymede's flow facing hemisphere aurora is also subject to variabilities throughout the Jovian rotational period.

There are no published observations of Ganymede's tail-side aurora, so the modeled aurora for the downstream hemisphere are in fact predictions of the process generating the aurora as well as their morphology. It was only *after* this work was completed that the tail-side aurora observation was made available for comparison. The observed aurora has several features in common with the model predicted aurora, including the banded emission morphology that appears to be located along the separatrix. Hence the multi-fluid model was able to predict the tail-side aurora without *a priori* knowledge of the auroral morphology or generation process.

We found that in studying the flow of ions sourced from Ganymede's ionosphere along with their energy distributions it was possible to bring a new interpretation to the existing ionospheric outflow debate. By sampling the ion densities, velocities, and

thermal speeds along the G2 trajectory through the simulation, it was possible to generate synthetic ion energy spectrograms directly comparable to those observed by the Galileo spacecraft's Plasma Experiment. We found that the ionospheric H^+ ions at the location of the G2 flyby had been accelerated to energies of between 10 and 100 eV, whereas the ionospheric O^+ ions were less energetic, in the range of 3 to 12 eV. Therefore, the O^+ ions were at energies just below the detection threshold of the instrument at the location of the G2 flyby. The observed outflow population was in the same energy range as that predicted for the ionospheric H^+ ions in the model [*Frank et al.*, 1997; *Paterson personal comm.*, 2005], which led us to interpret the outflow population in the observation as H^+ ions. However, the ionospheric O^+ ions were also part of the modeled ionospheric outflow, just not in the observable range. Hence we found that the ionospheric outflow consisted of both H^+ and O^+ ions, an interpretation that satisfied many of the debated issues presented by *Frank et al.* [1997], *Vasyliunas and Eviatar* [2000], and *Eviatar et al.* [2001].

An enhanced understanding of the interaction between Ganymede's and Jupiter's magnetospheres has been obtained through the use of multi-fluid modeling techniques in combinations with several observational data sets. We have further established a physics driven model that both accurately describes the ion dynamics in a magnetospheric system and is capable of being used to decipher previously controversial observations.

7.2 Continuing Work for Ganymede

The bulk of this work has focused on understanding the influence of the variable Jovian magnetosphere on Ganymede; however significant questions remain in understanding how Ganymede couples into the larger Jovian magnetosphere. Some continuing work on this system involves coupling the model developed for studying the local Ganymede interaction into an existing large-scale Jovian magnetospheric model. There are several observations that indicate the long range extent of Ganymede's influence on Jupiter's magnetosphere, including the auroral footprint observation [*Clarke et al.*, 2002] and the

Energetic Particle Detector observation of long lasting perturbed plasma above Ganymede's polar cap [*Williams et al.*, 1998]. Applying further nested grids in a Jupiter magnetospheric model will enable us to incorporate the Ganymede magnetospheric model with high enough resolution to track the perturbations to the Jovian magnetosphere. This will further our understanding of the acceleration processes, propagation, and mass loading provided by Ganymede to the Jovian system and provide a template for studying other coupled systems (described in the next section).

Further work on understanding Ganymede's ionosphere is also required. Researchers are currently adding to the understanding of the process and products of sputtering ice. As better estimates of the ionospheric composition are made possible, they can be implemented into the model in order to more completely understand how various ratios of atmospheric and ionospheric components contribute to Ganymede's magnetospheric population as well as to Jupiter's magnetospheric population. Observations of a neutral torus located between the orbital locations of Ganymede and Europa were recently made as Cassini flew by the Jovian system en route to Saturn, the source of which is undoubtedly the icy surfaces of these to Galilean satellites [*Mauk et al.*, 2003]. The sputtering of the surfaces of these moons is important to understanding both the ionized and neutral populations of Jupiter's magnetosphere.

Another means for continuing work on the Jupiter-Ganymede interaction involves understanding how ion energy distributions change throughout the system. We currently model the bulk flow and estimate the energy distribution assuming a Maxwellian distribution. However, integrating lagrangian particles into the modeled fields and gradients would enable us to examine the evolution of a prescribed ion energy distribution as well as to track the motion of ions with a range of initial energies. In this way the model could be more directly compared with observations from the Energetic Particle Detector, which is not possible while modeling only the bulk flow. Lagrangian particle trackers could also be used to study the trajectories of high energy ions as they exit Ganymede's magnetosphere and are picked up by the Jovian magnetosphere.

7.3 Future Work for Other Systems

The Ganymede-Jupiter interaction is unique in several ways: it is the first known lunar magnetosphere embedded within a large planetary magnetosphere, Ganymede's magnetosphere is the only magnetosphere known to exist consistently within a sub-Alfvénic flow, and Jupiter's magnetosphere is the largest planetary magnetosphere in the solar system and is fed heavy ions from the volcanic moon Io. However, this interaction is also a member of a family of coupled magnetospheric interactions. Applying and expanding on the techniques developed for the Ganymede-Jupiter interaction will be beneficial to understanding several other interesting coupled interactions in space physics.

Both Jupiter and Saturn have several moons that orbit within their magnetospheres; the modeling techniques used to study the influence of the Jovian magnetosphere on Ganymede are directly applicable to studying those interactions. For example, though Io likely does not possess an intrinsic magnetic field [*Kivelson et al.*, 2001], the thick atmosphere and ionosphere provided by active volcanism creates an induced magnetosphere in response to the variable Jovian magnetosphere. Aurora have also been observed at Io [*Roesler et al.*, 1999] as well as at Io's magnetic footprint on Jupiter [*Clarke et al.*, 1998], so a coupled interaction is present at Io as well as at Ganymede. Similarly Europa, while it lacks an intrinsic magnetic field and a substantial atmosphere, has a weak induced magnetosphere from currents induced in a sub-surface layer [*Shilling et al.*, 2005]. The coupled interaction is again observed in aurora at Europa [*Bagenal et al.*, 2004] and its magnetic footprint [*Clarke et al.*, 2002]. There are currently few observations of Saturn's moons interaction with its magnetosphere, however, several flyby's of Titan and now Enceladus indicate that complex coupled interactions are indeed present in Saturn's magnetosphere.

Studying interactions such as those occurring at Io and Enceladus require advancement of the current modeling method. The high densities of ions and neutrals in these systems require further treatment of charge-neutral interactions. This can be

accomplished by essentially adding a neutral population or 'fluid' to the multi-fluid model. The neutral fluid would not be influenced by electric and magnetic fields, but rather would behave as a gas with source and loss terms governing the neutral population's charge exchanging interactions with the ion species. Likewise, source and loss terms would be incorporated into the ion formulation to conserve mass and explicitly couple the charge and neutral populations.

Once neutrals are fully integrated into the modeling method, it becomes possible to more accurately study the process of mass loading in the large magnetospheres of Jupiter and Saturn due to interactions with moons, rings, and torii. Both Io and Enceladus provide mass on the order of tons of ions per second to their near space environments and the rings of Saturn have an observed atmosphere [*Hall et al.*, 1996] and are much larger in spacial extent than any of the orbiting satellites. Incorporating neutrals into the model will also significantly advance the understanding of the moon Titan, which possesses the thickest atmosphere of any moon in the solar system and may even spend part of its orbit located outside Saturn's magnetopause. Similarly, studying the Venusian response to the variable solar wind will be significantly aided by applying a multi-fluid simulation that takes into consideration the neutral-charge interactions.

The multi-fluid model is based on the physics that govern the interaction of charged particles with electric and magnetic fields. These small scale interactions drive each of the above mentioned systems, as well as several others including the Earth's magnetospheric interaction with the solar wind and the Sun's heliospheric interaction with the interstellar wind. Hence this type of modeling method should be applicable to many case studies in order to understand the role each system's unique characteristics (such as a magnetosphere, thick atmosphere, or orbiting satellites) play in governing the system's dynamic interaction with a variable flow of magnetized plasma.

BIBLIOGRAPHY

Alexander, L., et al. (2000), Spatial and temporal modeling of the exosphere of Ganymede using sputtering, sublimation and molecule migration, AAS, DPS Meeting #32, #35.02, *Bull. of the AAS, 32*, p.1057.

Anderson, J.D., et al. (1996), Gravitational constraints on the internal structure of Ganymede, *Nature, 384*, 541-3.

Bagenal, F., et al. (2004), *Jupiter: The Planet, Satellites and Magnetosphere.* Cambridge University Press.

Barth, C.A., et al. (1997), Galileo ultraviolet spectrometer observations of atomic hydrogen in the atmosphere of Ganymede, *Geophys. Res. Lett.*, *24*, 2147-2150.

Broadfoot, A.L., et al. (1979), Extreme ultraviolet observations from *Voyager 1*: Encounter with Jupiter, *Science, 204*, 979-982.

Burtis, W.J. and R.A. Helliwell (1969), Banded chorus – A new type of VLF radiation observed in the magnetosphere by OGO 1 and OGO 3, *J. Geophys. Res.*, *74*, 3002-10.

Clarke, J.T., et al. (1996), Far-ultraviolet imaging of Jupiter's aurora and the Io "Footprint," *Science, 274*, 404-409.

Clarke, J.T., et al. (2002), Ultraviolet emissions from the magnetic footprints of Io, Ganymede and Europa on Jupiter, *Nature, 415*, 997-9.

Cooper, J.F., et al. (2001), Energetic ion and electron irradiation of the icy Galilean satellites, *Icarus*, *149*, 133.

Durran, D.R. (1999), *Numerical Methods for Wave Equations in Geophysical Fluid Dynamics*. Springer-Verlag.

Eviatar, A., et al. (2001), The ionosphere of Ganymede, *Planet. Space Sci.*, *49*, 327-36.

Eviatar, A., et al. (2001b), Excitation of the Ganymede ultraviolet aurora, *Astrophys. J., 555*, 1013-9.

Feldman, P. D., et al. (2000), HST/STIS ultraviolet imaging of polar aurora on Ganymede, *Astrophys. J., 535*, 1085-90.

Frank, L. A., et al. (1997), Outflow of hydrogen ions from Ganymede, *Geophys. Res. Lett. 24*, 2151-4.

Gurnett, D.A., et al. (1996), Evidence for a magnetosphere at Ganymede from plasma-wave observations by the Galileo spacecraft, *Nature*, *384*, 535-7.

Hall, D.T, et al. (1996), Fluorescent hydroxyl emissions from Saturn's ring atmosphere, *Science, 272*, 516-18.

Hall, D.T., et al. (1998), The far-ultraviolet oxygen airglow of Europa and Ganymede, *Astrophys. J.*, *499*, 475-81.

Harnett, E. M., et al. (2005), Three-dimensional multi-fluid simulations of Pluto's magnetosphere: A comparison to 3D hybrid simulations, *Geophys. Res. Lett.*, 32, L19104, doi:10.1029/2005GL023178.

Herring-Captain, J., et al. (2005), Low-energy (5-250 eV) electron-stimulated desorption of H^+, H_2^+, and $H^+(H_2O)_n$ from low-temperature water ice surfaces, *Phys. Rev. B, 72*, doi:10.1103PhysRevB.72.035431, 1-10.

Ip, W.-H., et al. (1997), Energetic ion sputtering effects at Ganymede, *Geophys. Res. Lett., 24*, 2461-34.

Johnson, R.E., (1995), Sputtering of ices in the outer Solar System, *Rev. Mod. Phys., 68*, 305-312.

Kennel, C.F. and H.E. Petschek (1966), Limit on stably trapped particle fluxes, *J. Geophys. Res., 71*, 1-28.

Khurana, K.K., et al. (1998), Induced magnetic fields as evidence for subsurface oceans in Europa and Callisto, *Nature, 395*, 777-780.

Kivelson, M.G., et al. (1998), Ganymede's magnetosphere: Magnetometer overview, *J. Geophys. Res.*, *103(E9)*, 19963-72, 10.1029/98JE00227.

Kivelson, M.G., et al. (2000), Galileo magnetometer measurements: A stronger case for a subsurface ocean on Europa, *Science, 289*, 1340-3.

Kivelson, M.G., et al. (2001), Magnetized or unmagnetized: Ambiguity persists following Galileo's encounters with Io in 1999 and 2000, *J. Geophys. Res., 106(E11)*, doi: 10.1029/2000JA002510, 26121-26136.

Kivelson, M.G., et al. (2002), The permanent and Inductive Magnetic Moments of Ganymede, *Icarus*, *157*, 507-22.

Kopp, A. and W.-H. Ip (2002), Resistive MHD simulations of Ganymede's magnetosphere 1. Time variabilities of the magnetic field topology, *J. Geophys. Res., 107*, 12, 1490.

Kurth, W.S., et al. (1982), Detection of nonthermal continuum radiation in Saturn's magnetosphere, *Geophys. Res. Lett., 9*, 889-892.

Mauk, B.H., et al. (2004), Energetic neutral atoms from a trans-Europa gas torus at Jupiter, *Nature, 412*, 920-22.

McGrath, M.A. (2002), Hubble Space Telescope observations of Europa and Ganymede, *Eos Trans. AGU, 83(47)*, Fall Meet. Suppl., Abstract P52C-05.

Merrill, R.T., et al. (1998), The Magnetic Field of the Earth: Paleomagnetism, the Core, and the Deep Mantle. Academic Press.

Millis, R.L., and D.T. Thompson (1975), UBV photometery of the Galilean satellites, *Icarus, 26*,408-419.

Morrison, D., et al. (1974), Four-color photometry of the Galilean satellites, *Icarus, 23*, 399-416.

Mozer, F.S., et al. (2002), Evidence for diffusion regions at a sub-solar magnetopause crossing, *Phys. Rev. Lett., 89*, doi:10.1103/PhysRevLett.89.015002, 1-4.

Ness, N.F. (1994), Intrinsic magnetic fields of the planets: Mercury to Neptune, *Phil. Trans. R. Soc. Lond.* A, 349, 249-260.

Neubauer, F.M. (1998), The sub-Alfvén is interaction of the Galilean satellites with the Jovian magnetosphere, *J. Geophys. Res.*, *103*, 9, 19843-66.

Pappalardo, R.T., et al. (1998), A comparison of the plasma bombardment boundary on Ganymede's surface to Galileo imaging data, AAS, DPS meeting #30, #54.01, *Bull. of the AAS, 30*, p.1120.

Paranicas, C., et al. (1999), Energetic particle observations near Ganymede, *J. Geophys. Res.*, *104*, 17,459-69.

Paterson, W. (2005), personal communication of unpublished work.

Paty, C., and R. Winglee (2004), Multi-fluid simulations of Ganymede's magnetosphere, *Geophys. Res. Lett., 31*, L24806, doi:10.1029/2004GL021220.

Paty, C., and R. Winglee (2006), The role of ion cyclotron motion at Ganymede: Magnetic field morphology and magnetospheric dynamics, *Geophys. Res. Lett., 33*, L10106, doi:10.1029/2005GL025273.

Porco, C.C., et al. (2006), Cassini observes the active south pole of Enceladus, *Science, 311*, 1393-1401.

Retherford, K. (2006), personal communication of unpublished work.

Ridley, A.J., and K. Hansen (2005), Alfvén wing formation at the magnetosphere and the saturation of the ionospheric potential, *Eos Trans. AGU, 86(52)*, Fall Meet. Supp., Abstract SM53A-07.

Roesler, F.L., et al. (1999), Far-UV imaging spectroscopy of Io's atmosphere with HST/STIS, *Science, 283*, 353-7.

Sarson, G.R., et al. (1997), Magnetoconvection dynamos and the magnetic fields of Io and Ganymede, *Science, 276*, 1106-9.

Scarf, F.L., et al. (1981), Jupiter tail phenomena upstream from Saturn, *Nature, 292*, 585-6.

Scarf, F.L., et al. (1981b), Plasma wave turbulence at planetary bow shocks, *Nature, 292*, 747-750.

Schneider, N.M., and J.T. Trauer (1995), The structure of the Io torus, *Astrophys. J., 450*, 450-462.

Shay, M.A., and M. Swisdak (2004), Three-species collisionless Reconnection: Effect of O^+ on magnetotail reconnection, *Phys. Rev. Lett., 93*, doi:10.1103/PhysRevLett.93.175001, 1-4.

Shilling, N., et al. (2004), Limits on an intrinsic dipole moment in Europa, *J. Geophys. Res., 109*, E05006, doi:10.1029/2003JE002166.

Skoug, R.M., et al. (2004), Extremely high speed solar wind: October 29-30, 2003, *J. Geophys. Res., 109*, A09102, doi:10.1029/2004JA010494.

Sohl, F., et al. (2002), Implications from Galileo observations on the interior structure and chemistry of the Galilean satellites, *Icarus, 157*, 104-119.

Stone, S.M., and T.P. Armstrong (2001), Three-dimensional magnetopause and tail current model of the magnetosphere of Ganymede, *J. Geophys. Res., 106*, 10, 21263-75.

Vasyliunas, V., and A. Eviatar (2000), The outflow of ions from Ganymede: a reinterpretation, *Geophys. Res. Lett. 27*, 1347-50.

Williams, D.J., et al. (1992), The Galileo energetic particles detector, *Space Sci. Rev., 60*, 385-412.

Williams, D.J., and B. Mauk (1997), Pitch angle diffusion at Jupiter's moon Ganymede, *J. Geophys. Res., 102*, 24,283-7.

Williams, D.J., et al. (1997), Energetic particle signatures at Ganymede: Indications for Ganymede's magnetic field, *Geophys. Res. Lett. 24*, 2163-6.

Williams, D.J., et al. (1997b), Trapped electrons in Ganymede's magnetic field, *Geophys. Res. Lett. 24*, 2953-6.

Williams, D.J., et al. (1998), Properties of Ganymede's magnetosphere as revealed by energetic particle observations, *J. Geophys. Res.*, *103*, 8, 17523-34.

Williams, D.J. (2001), Ganymede's ionic radiation belts, *Geophys. Res. Lett. 28*, 3793-6.

Winglee, R.M. (2004), Ion cyclotron and heavy ion effects on reconnection in a global magnetotail, *J. Geophys. Res.*, *109*, 9, 10.1929/2004JA010385.

VITA

Carol Paty was born and grew up in a small town in upstate NY, where her desire to study the planets and physics began at a very early age. From trips to the Natural History Museum in Manhattan, to the spring board at gymnastics practice, to the hours drawing a bow across the strings of her violin, to back yard telescope sessions with her dad, physics played both underlying and obvious roles in her first 18 years. After finishing at Monticello High School, she left to study physics and astronomy at Bryn Mawr College and Haverford College outside Philadelphia, PA. She first experienced space plasma physics research while studying abroad at the University of St. Andrews in Scotland and taking a solar physics class, and found herself immediately hooked. In 2001 she received her B.A. and promptly set off for the UW to pursue a graduate degree under the guidance of Professor Robert Winglee studying planetary magnetospheres in the Dept. of Earth and Space Sciences.